ANALYZING THE INFLUENCE OF A SWIRL BRAKE ON A SMOOTH LIQUID ANNULAR SEAL THROUGH MEASURING STATIC AND ROTORDYNAMIC CHARACTERISTICS

A Thesis

By

NATHAN EDWARD BALKE

Submitted to the Office of Graduate and Professional Studies of
Texas A&M University
in partial fulfillment of the requirements for the degree of

MASTER OF SCIENCE

Chair of Committee,   Dara W. Childs
Committee Members,   Luis San Andrés
                      Lynn Beason
Head of Department,   Andreas Polycarpou

December 2017

Major Subject: Mechanical Engineering

ABSTRACT

Data are available for a previously tested annular seal with no swirl brakes (NSB). The NSB seal design was modified by adding slots at the inlet to produce a swirl brake (SB) seal. Tests were conducted to evaluate the static and dynamic characteristics of the modified SB seal. The SB data was then compared to the NSB data to understand how the seal rotordynamic coefficients are affected when swirl brakes are added.

The SB and NSB seals had a radial clearance (C_r) of 203.2 μm with the diameter of the seals (D) being 102 mm. The length to diameter ratio (L/D) of the NSB seal was 0.50, while the SB seal had an L/D of 0.45 due to the addition of swirl brakes.

The SB seal was tested at three different inlet pre-swirl ratios (PSR): high pre-swirl, medium pre-swirl, and radial injection. During testing, operational conditions were varied by changing differential pressure (ΔP), running speed (ω), and eccentricity ratio (ε_0). The test points were at $\omega = 2, 4, 6, 8$ krpm, $\Delta P = 2.07, 4.14, 6.21, 8.27$ bar and $\varepsilon_0 = 0.00, 0.27, 0.53, 0.80$. The test fluid was ISO VG 2 oil.

The static data for SB showed that the flow rate ($\dot{Q}$) increased as the imposed PSR increased, meaning the high pre-swirl case produced the highest $\dot{Q}$ values. Swirl brakes deliver the greatest reduction in PSR compared to that of NSB seals at high ΔP, low ω, and toward the centered position (ε_0=0.00). A vector Reynolds number was produced over the range of 1300 to 4400. The flow through the test stand was predicted to be transitional and turbulent.

Results show that varying inlet PSR on a SB seal has little effect on the seals dynamic performance characteristics. Providing a swirl brake to a seal modestly increases direct stiffness, decreases cross-coupled stiffness, modestly increases direct damping, reduces cross-coupled damping, decreases direct virtual mass and reduces the cross-coupled virtual mass. These dynamic results show why swirl brakes are effective in remedying rotordynamic instabilities and provide a clearer understanding as to the effects upon the rotordynamic coefficients when adding swirl brakes to a smooth liquid annular seal in turbulent and transitional flow.

A notable phenomenon was observed with the direct stiffness. At certain test points the direct stiffness would abruptly increase and decrease when increasing either ΔP and ω. The behavior could be explained largely by being on the laminar/transitional/turbulent boundaries.

ACKNOWLEDGEMENTS

will continue to be. You taught me much when it comes to challenging problem solving. Without your daily support, I never would have gained a greater understanding of the test stand and applied engineering principles. Jose Torres, I extend thanks for an outgoing, welcoming attitude which helped to smooth my transition process into graduate school. The enthusiasm you brought every day to work and fun made my experience at TAMU that much better. I know you're going to do great things in the future! Jimmy McLean, thank you for being the paternal figure in the lab my first year there. Without your vast knowledge this place wouldn't have been the same. Andrew Crandall, you are still the smartest person I know. Your support while writing my thesis was invaluable. I wish you best with whatever your endeavors are now. Tommy Kerr, thank you for the laughs and encouragement, I wish you and Hannah the best! Joshua Bullock, thank you for setting me straight on a good path while keeping me humble. Clay Norrbin, Travis Cable, Mauricio Ramirez, Keith Gary, Ovais, and others. Thank you guys so much for your friendship, help and support. Brian Hausman, Patricio Ramirez and Connor Morrow; you guys supported us in the cell and helped complete many important projects. My goal is that you were able to take valuable experience from the lab, hope you had fun too! To everyone else in the lab thank you so much! It was an amazing experience because of all of you!

To my parents, Trent Balke and Dr. Janet Balke, not much needs to be said because you already know. Without your support and love all of my life I would have never made it this far. I know I'm a knucklehead, but you taught me attitude is everything and life balance is important. I hope that you continue to look on with pride

v

at my accomplishments, because they would have never begun without you two. Love you guys! To my brother, Ryan, you know.

Thanks are also in order to my grandfather, Thomas Edward Ahart. Thank you so much for being my inspiration for going into engineering. I loved going to the flight museums, listening to all of your stories of agricultural equipment on the farm, and riding around on the lawn mower. Without that, you would have never put the spark of inquiry and creativeness into my spirit. If I can live with half of your integrity, kindness, persistence and intelligence I will consider my life to be one of worth. I hope I made you and grandma proud!

I would also like to thank Sarah Vaughan who provided support, inspiration, and happiness during graduate school despite long hours in the lab and studying. Your encouragement and love will always be appreciated. You are the A to my M.

To all of my numerous friends, colleagues and other influential figures in my life not mentioned here; thank you. A man is not made by one, but by many. You are the driving force which supported my completion of this project. I hope to continue to remain friends and keep in contact with all of you. Especially Marlos Cartinez, K. Lambert, Garth, Ross, Kelsey, Kimberla, Austin, other Southwestern friends, WAIS friends, A&M friends, coaches, teammates, workout partners, and so many others… Thanks and Gig'em!

With gratitude,

Nathan Edward Balke

NOMENCLATURE

A	Cross sectional area [L^2]
$\boldsymbol{A_X, A_Y}$	Frequency domain stator acceleration components [L/T^2]
C_{ij}	Seal damping coefficients [FT/L]
C_r	Seal radial clearance [L]
C_{eff}	Seal effective damping, defined in Eq. (24) [FT/L]
D	Seal outer diameter [L]
$\boldsymbol{D_{ij}}$	Frequency domain stator displacement components [L]
e_0	Rotor static eccentricity [L]
e_{X0}, e_{Y0}	Static eccentricity components in X and Y directions [L]
F_r	Fluid-film static reaction force magnitude [F]
f_{rX}, f_{rY}	Seal reaction force components in the X and Y, defined in Eq. (1) [F]
F_s	Applied static load magnitude [F]
$\boldsymbol{F_X, F_Y}$	Applied dynamic load in X and Y directions, defined in Eq. (17) [F]
$\boldsymbol{H_{ij}}$	Frequency domain dynamic stiffness coefficients[F/L]
$\boldsymbol{j}$	Complex operator [-]
K_{ij}	Seal stiffness coefficients [F/L]
L	Seal axial length [L]

M_{ij}	Seal virtual mass coefficients [M]
M_s	Stator mass [M]
$\dot{Q}$	Seal volumetric leakage rate [L^3/T]
R	Shaft radius [L]
Re_z	Reynolds Number in axial direction, defined in Eq. (10) [-]
Re_θ	Reynolds Number in circumferential direction, defined in Eq. (11) [-]
Re	Vector Reynolds Number, defined in Eq. (12) [-]
u	Swirl Ratio (inlet and outlet), defined in Eq. (7) [-]
v	Circumferential Fluid Velocity [L/T]
W	Average axial flow velocity [L/T]
$\ddot{X}_s, \ddot{Y}_s$	Stator acceleration components in the X and Y directions [-]

Greek symbols

ΔP	Seal differential pressure [F/L^2]
ΔP_u	Pitot Tube Pressure measurement
$\Delta X, \Delta Y$	Rotor-stator relative displacement components[L]
$\varepsilon_0 = e_0/C_r$	Static eccentricity ratio [-]
μ	Fluid dynamic viscosity [FT/L^2]
ρ	Fluid density [M/L^3]
ω	Rotor speed [1/T]
ω_n	Natural Frequency [1/T]

Ω	Excitation frequency [1/T]

Subscripts

i,j	Interchangeable X and Y directions
X,Y	X and Y directions

Abbreviations

CFD	Computational Fluid Dynamics
DAQ	Computer Data Acquisition System
ESP	Electrical Submersible Pump
NSB	No Swirl Brake Configuration
OSR	Outlet Swirl Ratio
PSR	Pre-Swirl ratio
SB	Swirl Brake Configuration
TAMUTL	Texas A&M University Turbomachinery Laboratory
WFR	Whirl Frequency Ratio, defined in Eq. (23)

TABLE OF CONTENTS

Page

LIST OF FIGURES

Page

LIST OF TABLES

CONTRIBUTORS AND FUNDING SOURCES

Contributors

This work was supported by a thesis committee consisting of Professor Dara W. Childs and Luis San Andrès of the Department of Mechanical Engineering and Professor Lynn Beason of the Department of Civil Engineering.

All other work conducted for the thesis was completed by the student independently.

Funding Sources

1. INTRODUCTION

An annular seal is an annular clearance between a rotor and a stator within a turbomachine that restricts leakage flow ($\dot{Q}$), arising due to a pressure differential (ΔP) across the seal. As described by Baldassarre et al. [1] swirl brakes are widely applied in centrifugal compressors to improve their rotordynamic stability. Swirl brakes have also been used in centrifugal pumps. An example of a swirl brake from a centrifugal pump can be observed in Fig. 1. A swirl brake consists of radial or axial slots machined into an annular seal stator. They are placed upstream of the seal inlet to reduce the inlet fluid swirl, also commonly referred to as the "pre-swirl," of the inlet flow. Pre-swirl is a central contributor to developing destabilizing forces in annular seals. Scant literature is available to address swirl brakes used in liquid annular seals for pumps. The existing literature only provides case studies for their successful application. Currently, no paper offers a complete set of static and rotordynamic data before and after modifying a seal to add a swirl brake.
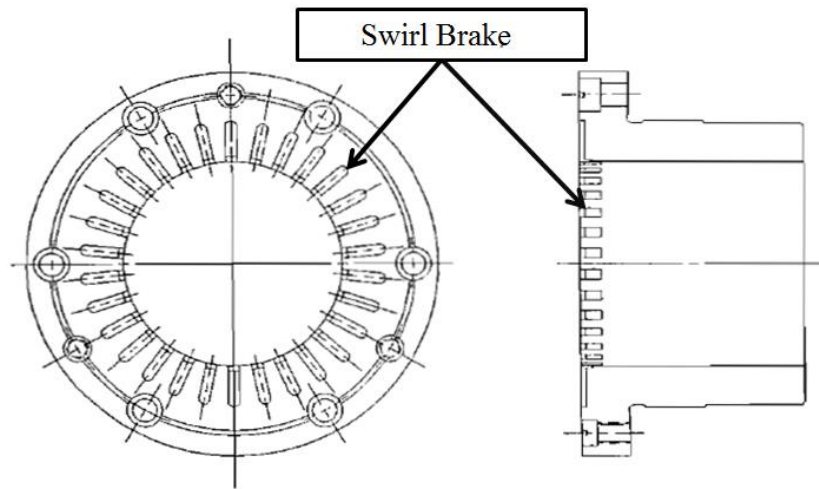
Figure 1. Example of swirl brakes on a balance-piston seal in a centrifugal pump, adapted from Massey [2]

For this thesis, the focus will be on swirl brake applications for annular seals in Electrical Submersible Pumps (ESPs). ESPs [3] are used to extract hydrocarbons potentially containing a high concentration of solids from oil wells. A typical ESP has the following key elements: a housing with head and base, a shaft, stages of impellers on the shaft, and annular seals. For pumps, annular seals have clearance-to-radius ratios (C_r/R) typically ranging from 0.003 to 0.005, where C_r is the radial clearance and R is the radius of the shaft rotating within the seal. Figure 2 represents various annular seal locations within an ESP.
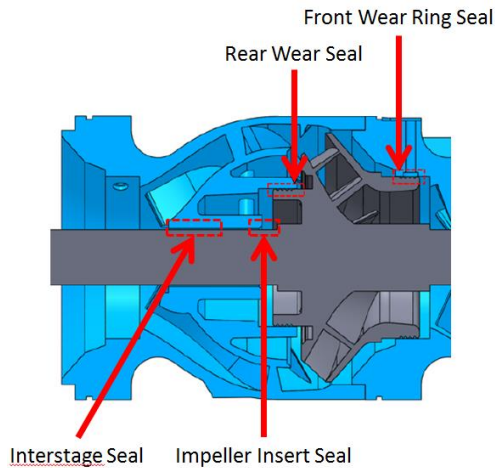
Figure 2. Cross-section view of an ESP pump stage with seal locations. Modified from original work by Norrbin et al. [4]

Henry Black [5] established in 1969 that seals were critical in rotordynamic calculations for pumps. Black's [6] work paved the way for understanding the impact that annular seals have on pump rotordynamics. Black passed away in 1980, but his last contribution was subsequently published by Allaire and Barret [7]. Their paper showed that inlet circumferential flow had a significant impact on seal rotordynamics and suggested that if inlet swirl was reduced, the destabilizing forces in a machine would also be reduced. All of these factors proved to be critical in modelling and understanding the effects of seals on pump rotordynamics.

In 1983, Childs [8] adapted Hirs [9] turbulent lubrication model for turbulent-flow annular seals. Following this paper, Childs [10] used a bulk-flow Navier Stokes model to develop the following reaction force model for small motion about a centered position

$$-\begin{Bmatrix} f_{rX} \\ f_{rY} \end{Bmatrix} = \begin{bmatrix} K & k \\ -k & K \end{bmatrix} \begin{Bmatrix} \Delta X \\ \Delta Y \end{Bmatrix} + \begin{bmatrix} C & c \\ -c & C \end{bmatrix} \begin{Bmatrix} \Delta \dot{X} \\ \Delta \dot{Y} \end{Bmatrix} + \begin{bmatrix} M & m \\ -m & M \end{bmatrix} \begin{Bmatrix} \Delta \ddot{X} \\ \Delta \ddot{Y} \end{Bmatrix} \qquad (1)$$

In Eq. (1), ΔX and ΔY terms are the relative displacement components of the rotor-stator system, $\Delta \dot{X}$ and $\Delta \dot{Y}$ are the relative velocity components, and $\Delta \ddot{X}$ and $\Delta \ddot{Y}$ are the relative acceleration components. Seal reaction-force components in the X and Y directions are f_{rX} and f_{rY}, respectively.

In 1988, Nelson and Nguyen [11] developed a rotordynamic model that was valid for seals at arbitrary eccentricity ratios $(\varepsilon_0 = e_0/C_r)$, where e_0 is the seal rotor's displacement from the seals center.

$$-\begin{Bmatrix} f_{rX} \\ f_{rY} \end{Bmatrix} = \begin{bmatrix} K_{XX}(e_0) & K_{XY}(e_0) \\ K_{YX}(e_0) & K_{YY}(e_0) \end{bmatrix} \begin{Bmatrix} \Delta X \\ \Delta Y \end{Bmatrix} + \begin{bmatrix} C_{XX}(e_0) & C_{XY}(e_0) \\ C_{YX}(e_0) & C_{YY}(e_0) \end{bmatrix} \begin{Bmatrix} \Delta \dot{X} \\ \Delta \dot{Y} \end{Bmatrix} +$$

$$\begin{bmatrix} M_{XX}(e_0) & M_{XY}(e_0) \\ M_{YX}(e_0) & M_{YY}(e_0) \end{bmatrix} \begin{Bmatrix} \Delta \ddot{X} \\ \Delta \ddot{Y} \end{Bmatrix} \qquad (2)$$

K_{XX} and K_{YY} are the direct stiffness terms. K_{XY} and K_{YX} are the cross coupled stiffness terms. C_{XX} and C_{YY} are the direct damping terms, and C_{XY}, C_{YX} are the cross coupled damping terms. M_{XX} and M_{YY} are the direct virtual mass terms. The cross coupled virtual mass terms are M_{XY} and M_{YX}.

When the signs of $K_{XY} > 0$ and $K_{YX} < 0$ these terms can produce destabilizing forces due to fluid rotation within the seal. The reduction of the magnitude of K_{XY}, K_{YX} enhances rotordynamic stability. Swirl brakes act to reduce the magnitudes of K_{XY} and K_{YX} by reducing fluid inlet pre-swirl.

The reaction force vector ($\boldsymbol{f_r}$) developed by an annular seal is generated by (a) the hydrodynamic effect and (b) the Lomakin effect. Pinkus and Sternlicht [12] state in 1961 that the hydrodynamic effect in journal bearings is created by the shear flow of the fluid film due to shaft rotation. As the rotor is displaced from the centered position, a higher pressure region develops on the converging clearance region. A lower-pressure region develops in the diverging region. The hydrodynamic effect is displayed in Fig. 3. For hydrodynamic bearings, cavitation largely eliminates the negative-pressure region, and a centering force is developed. In pumps, the ambient pressure suppresses cavitation, and the induced negative pressure persists.
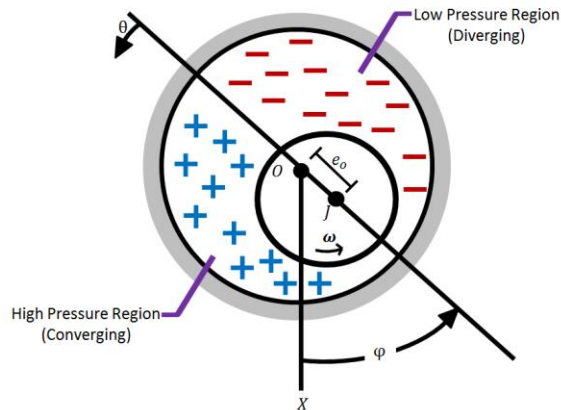
Figure 3. Depiction of the hydrodynamic effect adapted from Childs [13]

In 1958, Lomakin [14] explained how the axial pressure gradient in annular seals could develop a centering force. The fluid accelerates as it enters the annular clearance of the seal, leading to an inlet pressure drop. Displacement of the rotor to higher e_0

produces a larger clearance on one side of the seal while producing a smaller clearance on the other. The larger clearance has higher $\dot{Q}$, higher Reynolds numbers, and lower wall friction factors. The smaller clearance side displays lower $\dot{Q}$, lower Reynolds numbers, and higher wall friction factors. The pressure distribution generates a restoring reaction force caused by the changing clearance. An axial view of the Lomakin effect is displayed in Fig. 4.
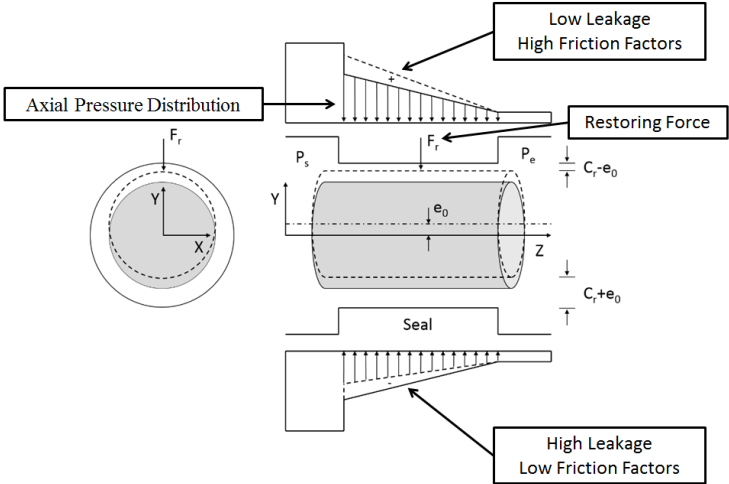
Figure 4. Depiction of the Lomakin Effect

The Lomakin effect creates a centering force that depends on ΔP that is (theoretically) independent of running speed (ω). In a pump, ΔP is proportional to ω^2, but the Lomakin centering force mainly arises directly due to ΔP.

6

In 1980, Benckert and Wachter [15] produced test results for the direct and cross-coupled coefficients of several gas annular seals with and without swirl brakes. They were the first to show that inlet swirl in gas annular seals create destabilizing forces. They showed that swirl brakes reduce the circumferential velocity of the fluid film entering annular seals and reduce the seals destabilizing cross-coupled stiffness coefficients.

In 1985, Massey [2] first demonstrated swirl brakes as a viable method for enhancing stability in pumps. The paper dealt with two high-speed, 11-stage, straight-through-design, centrifugal pumps. They were pumping a light hydrocarbon and failed to produce adequate head within 100 hours of operation. A subsynchronous vibration was occurring at 70% of the running speed, which caused rubbing and doubled the running clearances in the 100-hour period. Many modifications were made to the pump including replacing grooved seals with smooth seals. Only after a swirl brake was added to the modified smooth balance-piston seal was the problem remedied.

In 1988, Valantas and Bolleter [16] encountered severe subsynchronous vibration problems with a 5-stage, straight-through, high-speed, water centrifugal pumps. The pumps were put into service under similar operating conditions and began to have multiple failures which led to extended downtimes. Swirl brakes were applied, and they fixed the vibration response problems. As shown in Fig. 5, calculations predicted that the percentage damping increased after swirl brakes were added to the pump. The predicted percentage damping increase is critical as it eliminated the unstable pump motion.
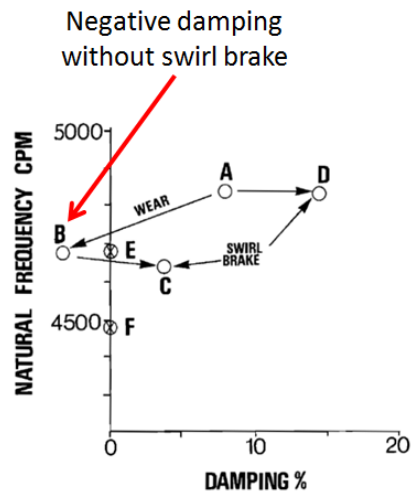
Figure 5. Valantas and Bolleter's [16] damping chart A – No Swirl Brakes original geometry, B - No Swirl Brakes worn clearance, C – Swirl brakes added and worn clearance, D – Swirl Brakes only original geometry

In 1990, a pump test rig was created by Frei et al. [17] to analyze vibration and operating problems in pumps to be used in subcritical steam generation plants. The test pump was a 3-stage, straight-through barrel type pump designed to run at its best efficiency point (BEP). Tests were run from 4800 to 7900 rpm with the inlet pressure at the seal being 12 bar. The results included the pump vibration spectra. Frei et al. [17] stated, "A swirl brake at the balance piston entrance drastically reduced the amplitude of unbalance excited vibrations. Installing throttling clearances with good stiffness and damping properties, together with introducing swirl brakes at selected locations, is one of the key design steps to obtain good rotordynamic behavior." Figure 6 shows that the swirl brake drastically decreased the synchronous response of the pump.

8
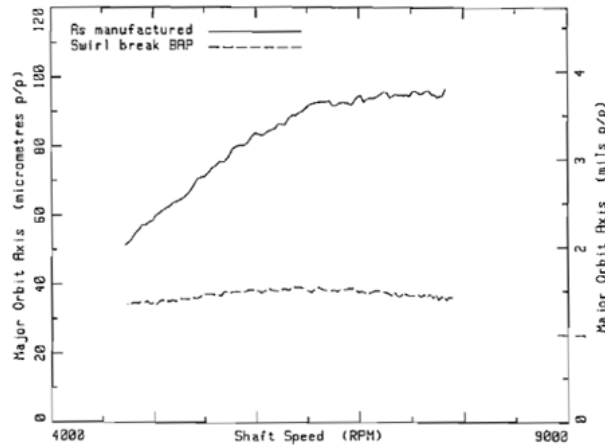
Figure 6. Reduction of Shaft Vibrations due to Swirl Brake at the Balance Piston [17]

The impact of applying swirl brakes to ESPs was studied analytically by Childs et al. [3] in 2014. A rotordynamic model was used to predict the dynamic characteristics of an ESP with and without swirl brakes at single (new), double, and triple radial clearance. Childs et al. [3] stated that adding swirl brakes to ESP annular seals produce positive effects for seals with turbulent flow (low viscosity fluids). Adding swirl brakes would increase the pump's Onset Speed of Instabilities (OSIs) and decrease the pump's vibration amplitude at critical speeds. Simply stated, ESPs using low viscosity fluids can have instabilities prevented by adding swirl brakes for a range of clearances.

9

2. STATEMENT OF WORK

The goal of this investigation is to measure the rotordynamic characteristics of a smooth annular seal operating with swirl brakes across three pre-swirl ratios (PSR), multiple ω's, different ΔP's, and varying ε_0 conditions. The proposed test matrix displayed in Table 1 is based on potential operating ranges of an ESP.

Table 1. Test Matrix: Target conditions for test points

Target Description	Target Values
Speeds (krpm)	$\omega = 2,\ 4,\ 6,\ 8$
Pressure Drops (bar)	$\Delta P = 2.07,\ 4.14,\ 6.21,\ 8.27$
Eccentricity Ratios	$\varepsilon_0 = 0.00,\ 0.27,\ 0.53,\ 0.80$

A data point occurs when dynamic data are acquired for specific values of ω, ΔP and ε_0. (Example: 2 krpm, 2.07 bar, $\varepsilon_0 = 0.00$) For each pre-swirl insert, static and dynamic data will be recorded for 64 data points, totaling 192 points for the swirl brake test geometry. Three different pre-swirl inserts are used: Radial Injection ("Zero" Pre-Swirl), Medium Pre-Swirl, and High Pre-Swirl.

A comparison of the dynamic and static characteristics of the seal with swirl brakes (SB) and without swirl brakes (NSB) will be made. The NSB test data was taken by an earlier M.S. student and have yet to be published.

ExxonMobil ISO VG 2 Spindle Oil was used as the process fluid. Typical inlet temperature and viscosity for the test fluid are shown in Table 2.

Table 2. Operating conditions during testing

Description	Measured Values
Process Fluid	Exxon ISO VG2 'Spindle Oil'
Inlet Temperature	$T_i = 46.1 \,°C$
Inlet Viscosity @ Temperature	$\mu = 1.77cP$

Limited literature is available for consideration of swirl brake design for pumps. The only papers that give suggestions for swirl brake design are for annular gas seals. In 1998, Nielsen et al. [18] conducted swirl brake computational fluid dynamics (CFD) calculations for gas annular seals in compressors. In 2014, Baldassarre et al. [1] provided similar results for gas seals in turbines with a CFD analysis and experimental results to back the CFD findings. Both papers state an ideal geometry, including separation between brakes and number of brakes for optimized inlet swirl reduction. Note that swirl-brake designs in turbines and compressors do not need to be as structurally robust as for centrifugal pumps. The swirl brakes given in [1,18] are not considered to be useful for pump applications. The swirl brake geometries used here are based on the successful swirl brake designs for the Massey [2] and the Vallantas and Bolleter [16] pumps. The thesis test hardware in the NSB and SB configurations are presented in Fig. 7.
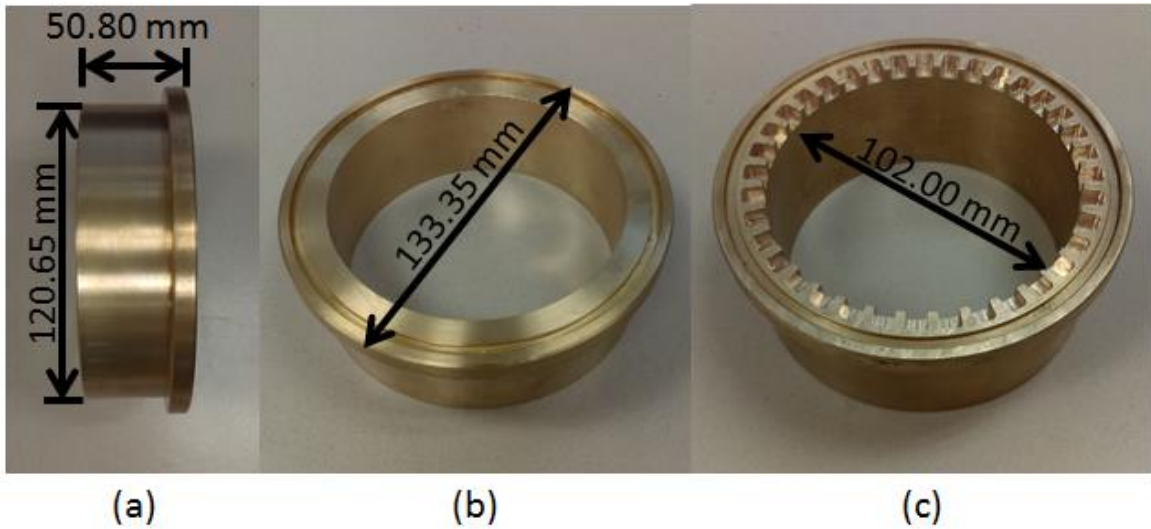
Figure 7. (a) Axial view of NSB seal (b) Isometric view of NSB seal (c) Isometric view of SB seal

The base test-seal geometry is based on dimensions from an ESP balance-piston seal. The NSB configuration had a length-to-diameter ratio (L/D) of 0.50, where $D = 102.00\ mm$, and $L = 50.80\ mm$. When the swirl brake was added to the annular seal, the direct length of the seal decreased, reducing L/D for the SB seal to 0.45. The C_r/R of both the SB and NSB seals is 0.004, which falls within expected ranges for an ESP annular seal. Relevant seal dimensions of both seals are displayed in Table 3.

Table 3. Geometric Properties of SB and NSB configurations

Seal Geometry	Nominal Clearance C_r [μm]	C_r/R [-]	L/D [-]	Axial Seal Length [mm]	Rotor Diameter [mm]
Smooth Seal SB	203.2	0.004	0.45	45.7	101.6
Smooth Seal NSB	203.2	0.004	0.50	50.8	101.6

3. TEST STAND DESCRIPTION

The test stand was designed and fabricated by Kaul [19] in 1999 to test annular bushing oil seals for centrifugal compressors. Kaul derived the design from a concept created by Glienicke [20] in 1966. Glienicke used a "shake-the-stator" design to test hydrodynamic bearings. Since 1999, multiple modifications have been made. The configuration was highly dependent upon the test element and static requirements for testing.

The current test stand is shown in Fig. 8 and can be categorized into five separate sections: support structure, the stator housing (where test elements reside), process fluid supply system, the excitation system, and instrumentation. Descriptions of the process fluid supply system, excitation element, and instrumentation can be found in Appendix B.
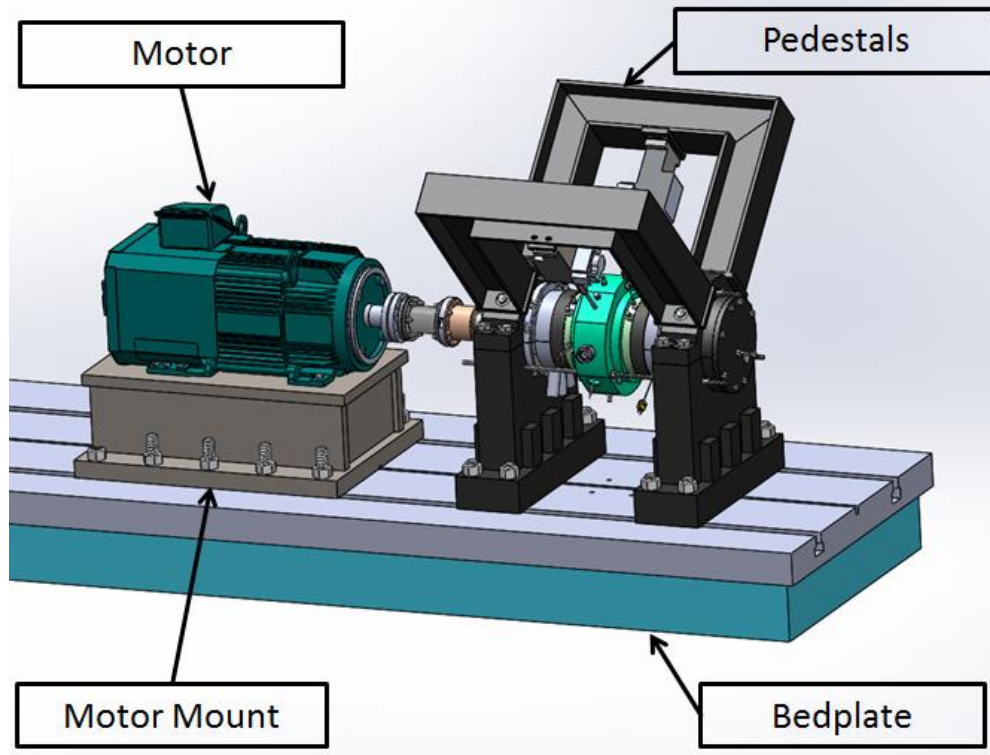
Figure 8. Full Isometric view of test stand as a CAD model

In Fig. 9, the pedestal supports hold the test rotor on ball bearings. The bedplate, rotor and lower pedestals were never removed or modified from the test stand to ensure proper alignment of the rotor to the motor for each assembly. The smooth rotor is made from stainless steel and has a length of 422mm. The dimensions of the rotor were verified, and the rotor was precision balanced before testing. The motor speed is controlled by a variable frequency drive. Output of the motor was 29.8 kW (40hp), and it had a maximum speed of 8 krpm.
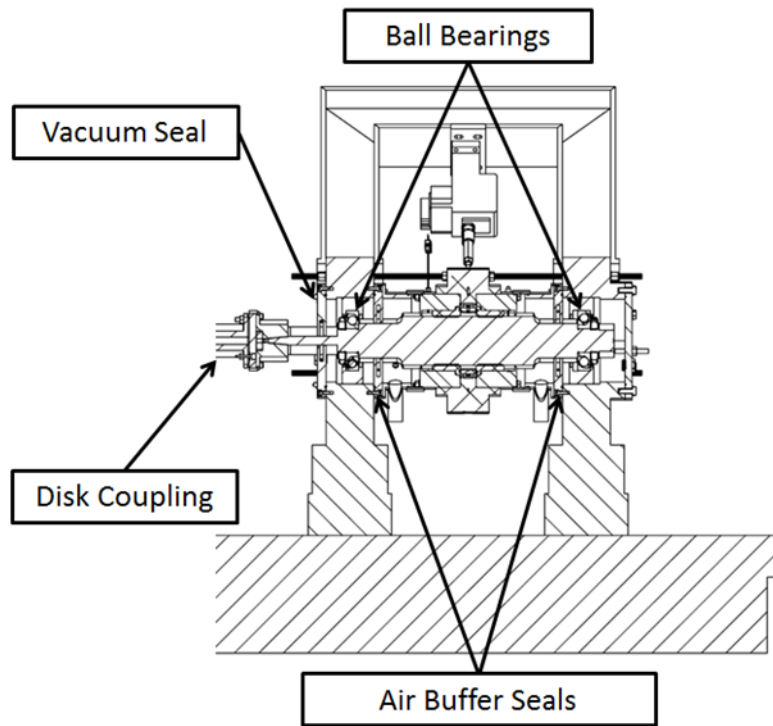
Figure 9. Cross sectional view of test stand.

The stator assembly in Fig. 10 consists of the stator housing, the test element (annular seals), seal holders, and a pre-swirl insert. Pitch stabilizers connect to the casing of the stator to prevent axial motion and minimize pitch and yaw misalignment
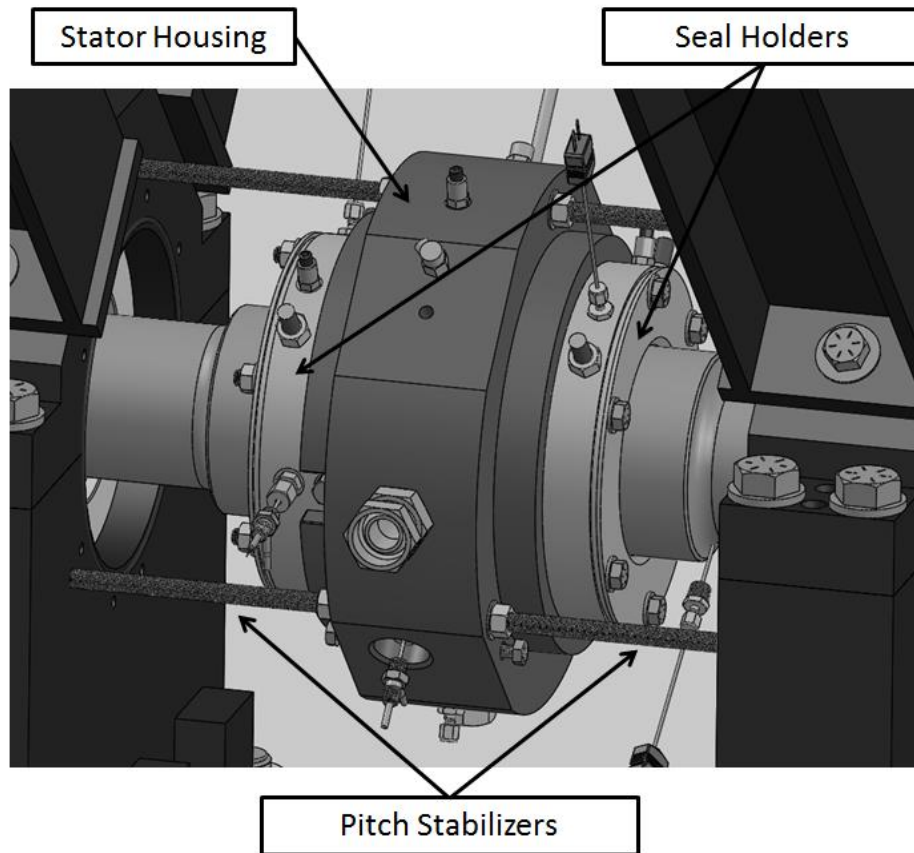
Figure 10. Isometric view of stator housing. Note: Collection chambers, drive end air buffer seals and Y Zonic were removed from the figure for viewing purposes

Pre-swirl inserts in Fig. 11 are used to vary the amount of pre-swirl into the main test section. A different stator was used for each pre-swirl because each pre-swirl insert was interference fitted into its stator housing. Radial injection imposes 'zero' or minimal pre-swirl conditions to the test section. Higher pre-swirl values were imposed through injection with a circumferential component. To impose higher pre-swirl values, the nozzle diameters were reduced from 4.978 mm in the medium pre-swirl ring to 4.039 mm in the high pre-swirl ring. The angle of the nozzle for both the medium and high pre-swirl inserts is 55.7°.
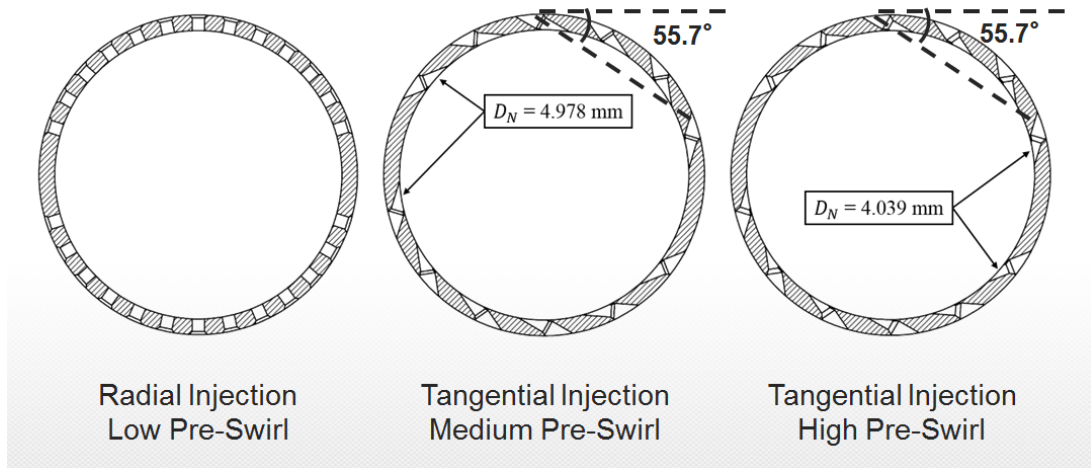
Figure 11. Pre-Swirl Inserts used in testing

The circumferential fluid velocity at the inlet and outlet of the test seals are measured with pitot tubes seen in Fig 12. The pitot tubes are tangent to the rotor. The inlet pressure difference measured by the pitot tubes are used to determine PSR and outlet swirl ratio (OSR).
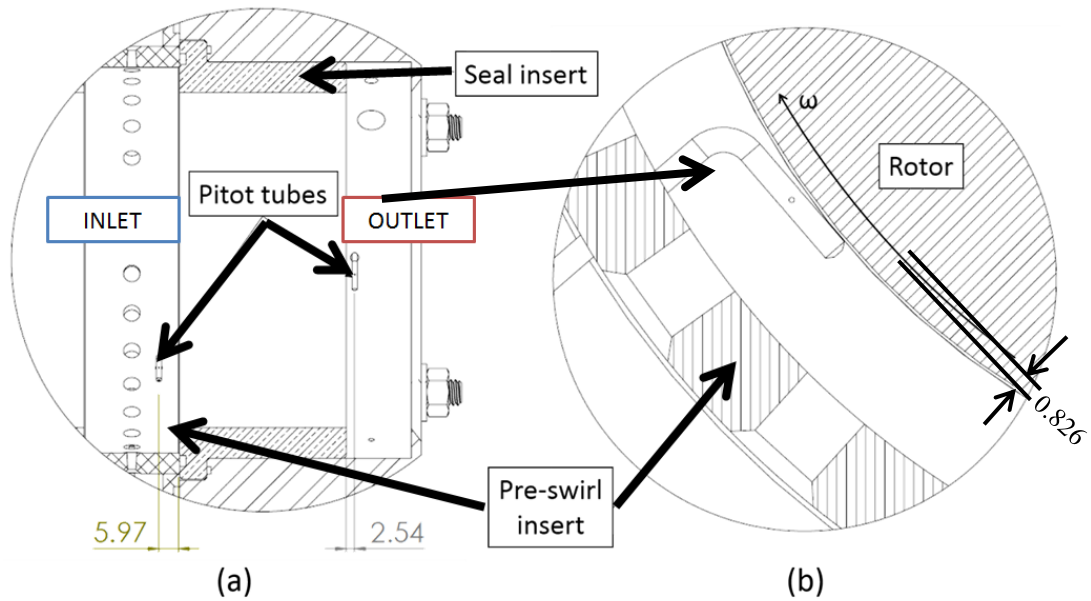
Figure 12. (a) Side cross section depicting pitot tube placement at inlet and outlet (b) axial cross section of stator housing depicting pitot tube placement with relation to rotor. Note dimensions presented are in mm.

A liquid annular seal test element can be seen in Fig. 13. A total of 36 slots were machined into the NSB seals with the centerline of each slot installed 10 degrees circumferentially from one another. The height, chord, and length of each slot are all 5.08mm with a fillet of 1.58mm.

<center>(*a*)　　　　　　　　　　　　　　　　　(*b*)</center>
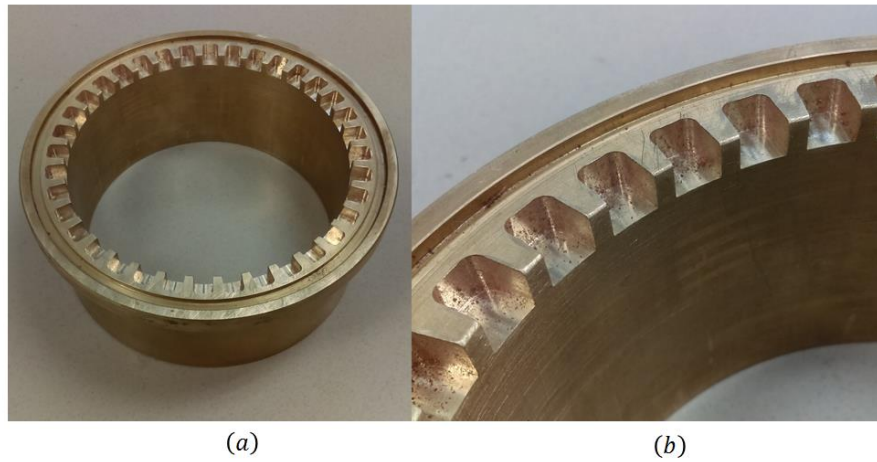
Figure 13. (a) Isometric view of the test element (b) Close up view of the swirl brakes

The SB seals were press fitted into the end caps, and the swirl brake face is made
to be flush with the top surface seen in Fig. 14. There is a labyrinth tooth at the exit of
the endcaps to prevent air pockets within the seal exit chamber. The seals were faced
oppositely of one another, aligned onto the stator housing via a mandrel, and precisely
secured.
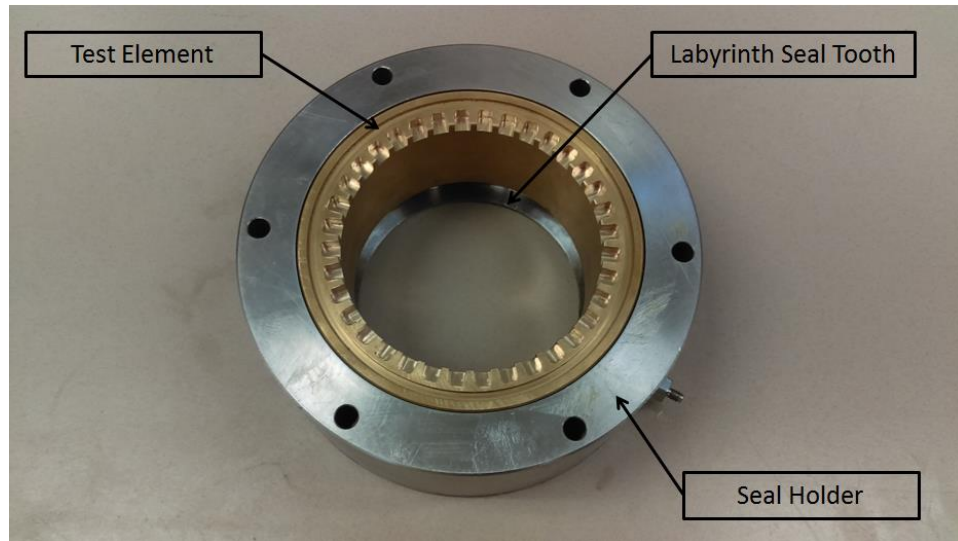
Figure 14. Top view test element press fit into the seal holder

Fig. 15 displays the fluid flow through the stator section. The rotor axis runs horizontally in this figure. Flow into the test rig was regulated by a manually controlled electro-pneumatic control valve. The process fluid enters through the inlets that face one another and are orthogonal to the test elements. The fluid accelerated through the pre-swirl inserts and entered the main test chamber. The test fluid then moved axially along the shaft and then exited the seals.
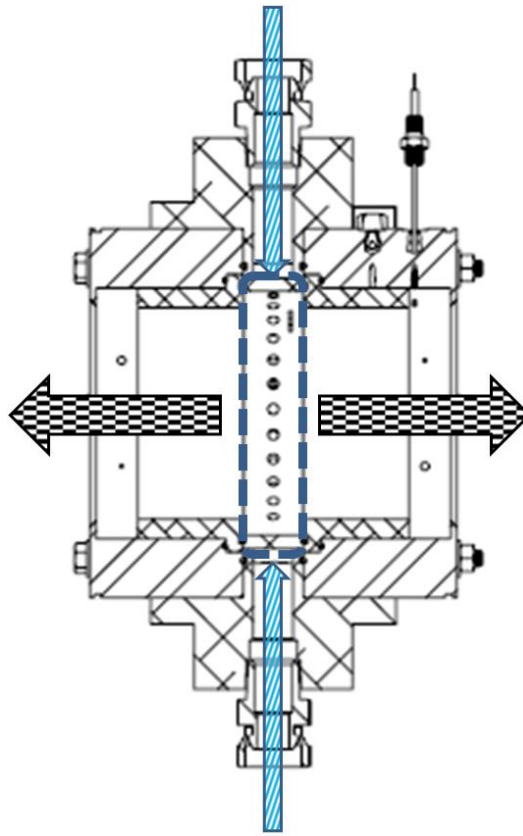
Legend	
Inlet	
Pre-Swirl Ring	
Outlet	

Figure 15. Stator process fluid flow path

4. STATIC DATA AND ANALYSIS

4.1 Test Procedure

Before testing, the operator adjusted $\dot{Q}$, ΔP, and ω. The test stand was allowed to reach a steady state inlet and exit temperature. At this point the instrumentation was used to record readings on the computer acquisition program (DAQ). Static measurements are taken before dynamic measurements. Static measurements fall into the following categories: (a) Hot clearance measurements (b) Flow rate - ΔP measurements, and (c) static load-displacement measurement. The steady state data recorded are the inlet and outlet pressures (giving ΔP), inlet and outlet temperatures, X and Y positions of the rotor from proximity probes, F_s, $\dot{Q}$, and ω. The static data presented in this section are to highlight important trends. The full set of recorded static data is available in Appendix A for the SB seals. Data is presented with uncertainty-analysis results; this analysis is discussed in Appendix C.

4.2 Clearance Measurements

Before testing, preparatory measurements had to be made to determine the static and dynamic characteristics of the system. First, a 'cold-clearance' was taken. The stator was precessed around the rotor while in constant (light) contact, producing a clearance circle. This cold-clearance serves as a reference for an 'approximate center' of the seal for taking baselines and hot clearances. Note, this is not necessarily the precise center or clearance for the test rig at steady state.

After the cold-clearance circle measurement, a 'hot-clearance' test was

conducted. The process fluid was run through the system and brought up to steady state

temperature (46.1°C). Once steady state conditions were achieved, the pumps moving

the process fluid through the test housing were immediately shut off. Before the stator

housing could cool down, another clearance circle measurement similar to that of the

cold clearance was conducted. An example measurement is shown in Fig. 16. The hot

clearance gives a better indicator of the true center and clearance circle used during the

testing procedure.
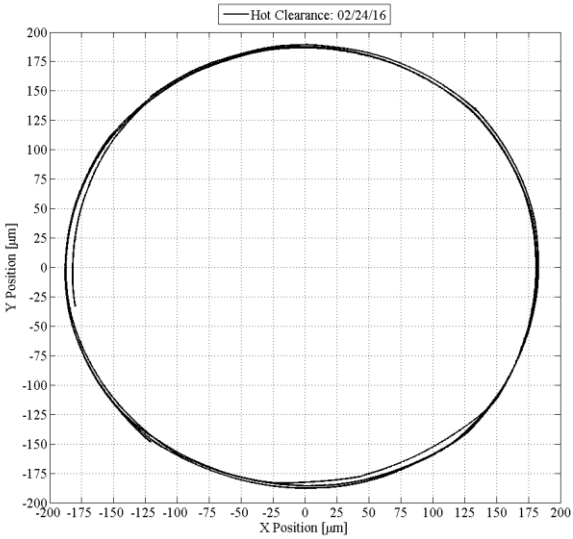
Figure 16. Example of a clearance overlay from high pre-swirl test

The original geometry of the NSB and SB seals had a C_r value of 203.2 μm

before the process fluid was in the test section. Table 4 displays the clearance data for all

three pre-swirl insert tests. The hot clearance C_r values in Table 4 are lower than the

original design specification. This outcome was due to thermal growth from heated

process fluid flowing through the system.

Table 4. Measured C_r hot clearances for data for each assembly

Assembly Configuration	Assembly 1 High Pre-Swirl	Assembly 2 Medium Pre-Swirl	Assembly 3 High pre-swirl
Cold Clearance; C_r [μm]	203.2	203.1	203.2
Hot Clearance; C_r [μm]	189.9	189.2	189.9

4.3 Leakage Measurements

Recall that two seal elements were placed into the stator housing. The measured

$\dot{Q}$ values were for both seals and were divided by two. Figure 17 examines $\dot{Q}$ trends for

SB seals across all three pre-swirl cases. Figure 17a shows (as expected) that $\dot{Q}$ increases

significantly as ΔP increases. In Fig. 17b, $\dot{Q}$ decreases slightly with increasing ω. ΔP has

a greater impact on $\dot{Q}$ than ω. From Fig. 17a and 17b, as the pre-swirl injection rate

increases, $\dot{Q}$ decreases. The high pre-swirl insert has the lowest $\dot{Q}$ values.
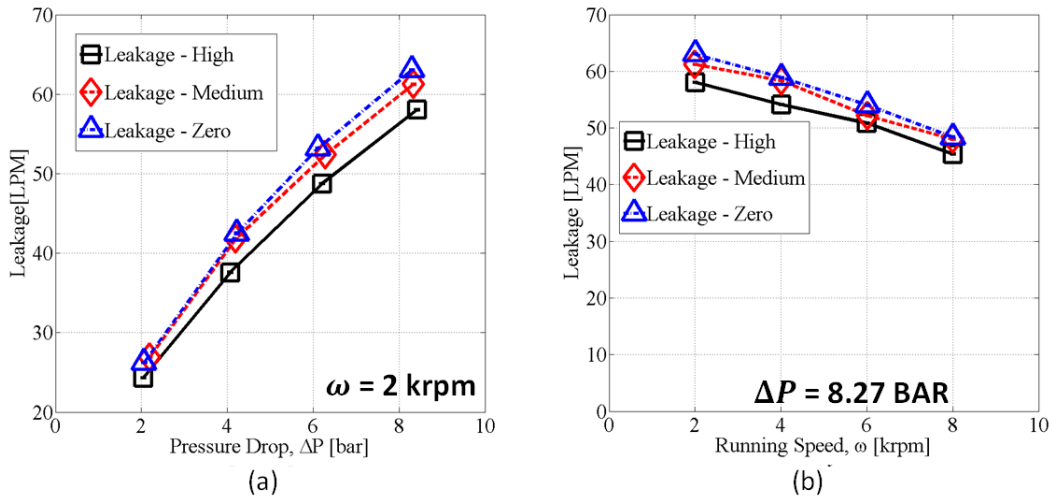
Figure 17. $\dot{Q}$ **in the centered position for SB seals across all pre-swirl inserts against (a)** ΔP **with** ω **= 2 krpm and (b)** ω **with** ΔP **= 8.27 bar**

Figure 18 displays $\dot{Q}$ versus ΔP comparisons for SB and NSB seals. Figure 18a shows that at $\omega = 2\ krpm$ $\dot{Q}$ is essentially the same for SB and NSB seals. At higher ω, Fig. 18b shows at $\omega = 8\ krpm$ the $\dot{Q}$ for SB seals is higher than NSB seals. This result is somewhat expected given the greater length of the NSB seals. Note that $\dot{Q}$ values are not greatly affected by changes with ε_0.
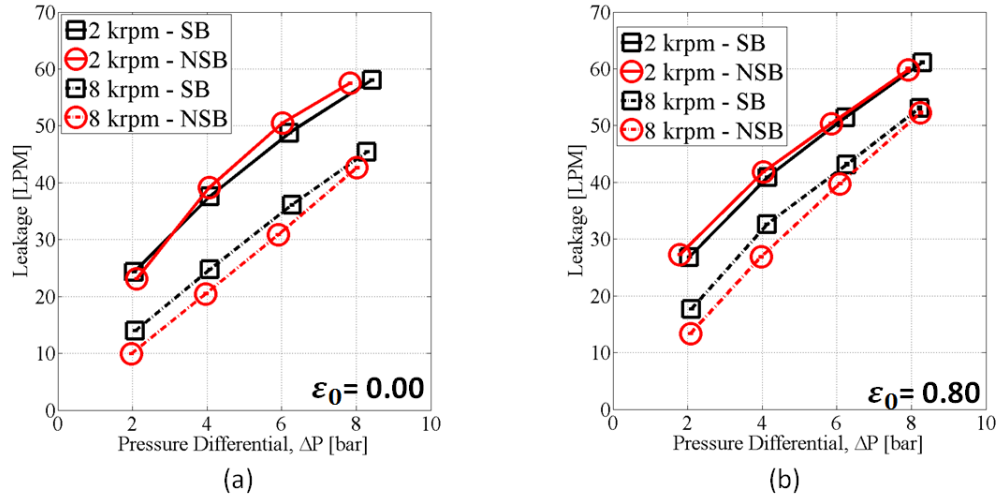
Figure 18. SB vs. NSB comparison High Pre-Swirl Insert $\dot{Q}$ against ΔP for (a) ε_0 = 0.00 (b) ε_0 = 0.80

4.4 Calculated Reynolds Numbers

Reynolds numbers for axial and circumferential flow, Re_Z and Re_θ are

$$Re_Z = \rho 2C_r W/\mu \qquad (10)$$

$$Re_\theta = \rho R\omega C_r/\mu \qquad (11)$$

where W is the average axial flow velocity defined by

$$W = \dot{Q}/A \qquad (12)$$

and

$$A = 2\pi R C_r \qquad (13)$$

Note that the hydraulic radius ($2C_r$) is used in the definition of Eq. (11). The vector

Reynolds number is then defined by

$$Re = \sqrt{Re_z^2 + Re_\theta^2} \qquad (14)$$

26

Zirkelback and San Andrés [21] state that for annular pressure seals that the Reynolds numbers (Re) range for transitional flow is $1000 < Re < 3000$; with Re values below 1000 being laminar and values above 3000 being turbulent.

Figure 19 displays Re_Z for the SB seals across all pre-swirl inserts. In Fig. 19a, Re_Z increases as ΔP increases. From Fig. 19b Re_Z decreases as ω increases. The range of Re_Z values range from approximately 600 to 2700.
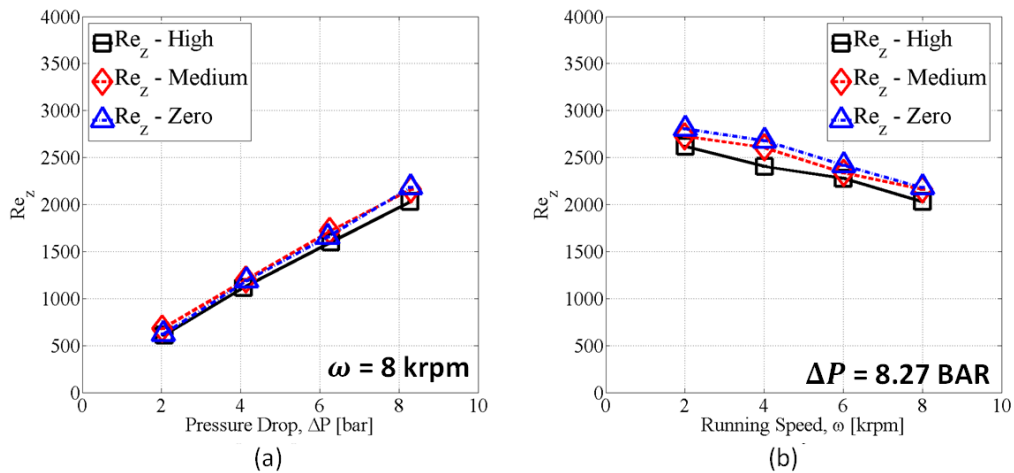
Figure 19. Re_Z for the SB seal across all pre-swirl inserts in the centered position at (a) ΔP at ω = 8 krpm and (b) ω at ΔP = 8.27 bar

Figure 20 shows a plot of Re_θ for the SB seals across all pre-swirl inserts. In Fig. 20a Re_θ remains constant as ΔP increases. From Fig. 20b Re_θ increases as ω increases. The range of Re_θ range from approximately 700 to 3600.
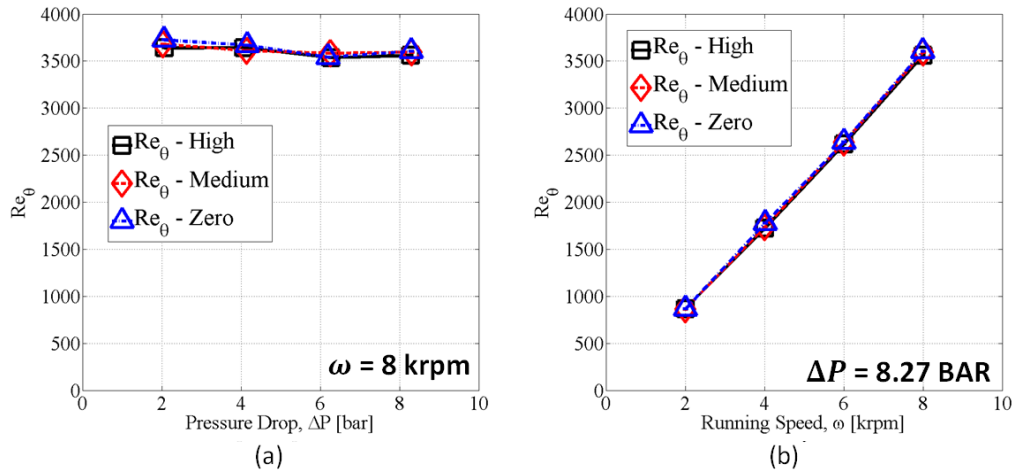
Figure 20. Re_θ **for the SB seal across all pre-swirl inserts in the centered position at (a)** ΔP **at** ω **= 8 krpm and (b)** ω **at** ΔP **= 8.27 bar**

Fig. 21 is a plot of Re for the SB seals across all pre-swirl inserts. Figure 21a displays Re increasing slightly as ΔP increases. Figure 21b shows Re increasing as ω increases. The range of Re were from approximately 1400 to 4200. According to the Zirkelback and San Andrés [21] definition, these values lie within transitional and turbulent flow.
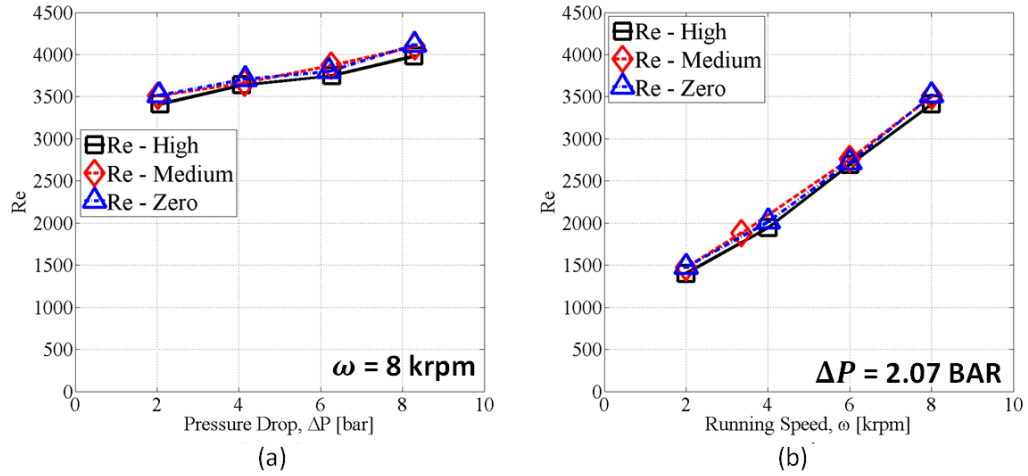
Figure 21. *Re* for the SB seal across all pre-swirl inserts in the centered position at (a) *ΔP* at *ω* = 8 krpm and (b) *ω* at *ΔP* = 2.07 bar

4.5 Pre-Swirl and Post-Swirl Measurements

The pitot tubes were used to estimate the circumferential velocity (v) at specific locations. The pitot tubes were placed upstream and downstream of the seals to determine the corresponding PSR and OSR values. The measured pitot tube differential-pressure measurement (ΔP_u) was recorded. Note process fluid density (ρ) and viscosity (μ) are determined from steady-state temperature. The v of the process fluid is

$$v = \sqrt{\frac{2\Delta P_u}{\rho}} \qquad (7)$$

The swirl ratios are:

$$PSR = \frac{v(upstream)}{\omega R} \qquad (8)$$

$$OSR = \frac{v(downstream)}{\omega R} \qquad (9)$$

Note from Fig. 12 that the inlet circumferential velocity (v_i) is only measured at one location upstream of the SB seals. Figure 22 displays v_i for the SB seals across all

29

pre-swirl inserts. From Fig. 22a as pre-swirl inserts change from zero to medium to high v_i steadily increases. From Fig. 22b note that v_i drops in moving from the zero insert to medium insert and then increases in moving from the medium to high insert. From Fig. 22, changing ε_0 does not have much effect on v_i.
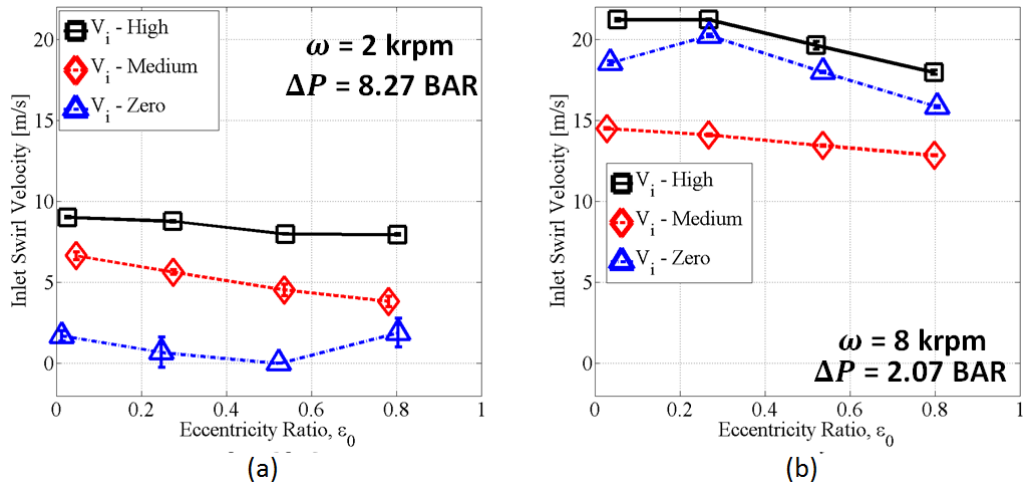
Figure 22. Inlet Circumferential Velocity for the SB seals across all pre-swirl inserts against ε_0 at (a) $\omega = 2$ krpm and $\Delta P = 8.27$ bar (b) $\omega = 8$ krpm and $\Delta P = 2.07$ bar

Figure 23a shows PSR increasing for increasing ΔP for the medium and high pre-swirl inserts. The radial injection (zero) behaves differently in that PSR decreases until reaching $\Delta P = 6.21$ bar, and then increases. Figure 23b shows v_i decreasing with increasing ω for the high and medium pre-swirl inserts. For radial injection PSR, v_i increases with increasing ΔP. In Fig. 23, the highest PSR values decrease from high to medium to radial injection. Imposed PSR produces less variability at high ω and at low ΔP.
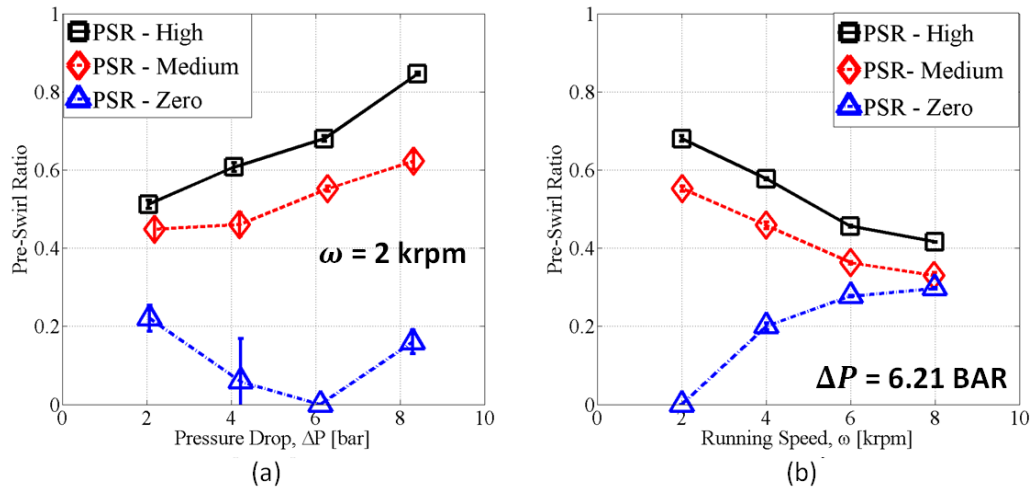
Figure 23. PSR plot for SB seals across all pre-swirl inserts in the centered position for (a) *ω* = 2 krpm and (b) Δ*P* = 6.21 bar

For all inserts, the range of PSRs across the speed range is presented in Table 5. As expected, the greatest range of PSR values occur at lower ω's across all pre-swirl inserts. The smallest range in PSR occur at higher ω's. Highest values for PSR generally decrease as ω increases.

Table 5. Range of PSR versus speed for all three pre-swirl inserts

Running Speed, ω [rpm]	Radial Injection		Medium Pre-Swirl Insert		High Pre-Swirl Insert	
	Highest PSR Value	Lowest PSR Value	Highest PSR Value	Lowest PSR Value	Highest PSR Value	Lowest PSR Value
2	0.22	0.00	0.62	0.27	0.84	0.41
4	0.31	0.12	0.56	0.27	0.58	0.39
6	0.15	0.00	0.39	0.27	0.43	0.38
8	0.10	0.00	0.34	0.28	0.49	0.28

Table 6 compares PSR values between SB and NSB seals. Table 6 shows that the circumferential velocity of the fluid entering the seal is decelerated via the swirl brake. Greatest reduction in PSR occur at lower ω's and generally toward the centered position. Note that the v_i measurement is made upstream of the seal (SB or NSB) and (from Fig. 18) there is very little difference in $\dot{Q}$ between the SB and NSB seals. None the less, at lower ω values, the NSB seals have substantially lower PSR values then corresponding values for the SB seals.

Table 6. High pre-swirl insert PSR comparison for a speed series at $\varepsilon_0 = 0.00$ and 0.80 for $\Delta P = 8$ bar

Running Speed, ω [rpm]	No Swirl Brake Seals		Swirl Brake Seals		Percent Difference	
	PSR $\varepsilon_0=0.00$	PSR $\varepsilon_0=0.80$	PSR $\varepsilon_0=0.00$	PSR $\varepsilon_0=0.80$	PSR $\varepsilon_0=0.00$	PSR $\varepsilon_0=0.80$
2	1.41	1.28	0.84	0.74	-50.66%	-53.46%
4	0.66	0.64	0.44	0.46	-40.00%	-32.72%
6	0.47	0.47	0.40	0.42	-16.09%	-11.23%
8	0.38	0.34	0.34	0.33	-11.11%	-2.98%

Note from Fig. 12 that the outlet circumferential velocity (v_o) is only measured at one location downstream of the SB seals. The values may be helpful in performing computational fluid dynamics (CFD) for the flow conditions. Figure 24a shows v_o increasing with an increase in PSR. This outcome is mainly driven by high ΔP and low ω. Figure 24b shows the impact of increasing ω and dropping ΔP. Note significantly

higher v_o values from Fig. 24a to Fig. 24b. From Fig. 24, ε_0 does not have much effect upon v_o.
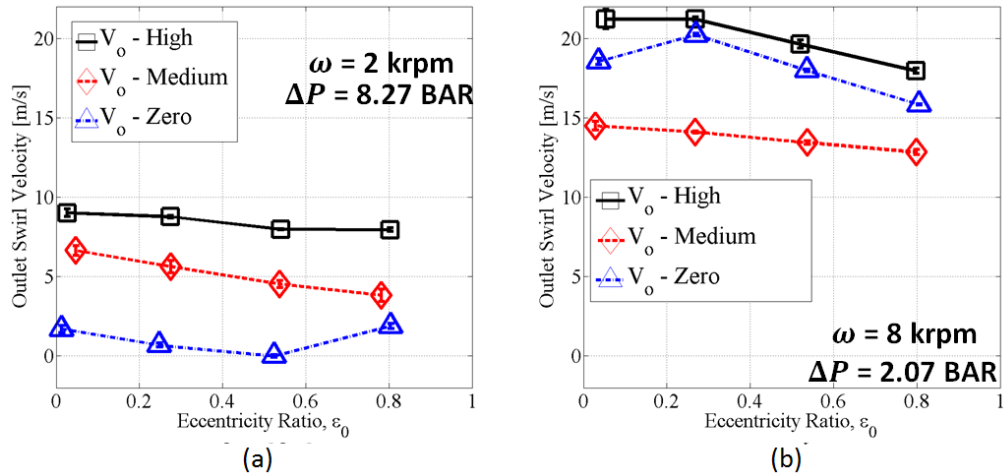
Figure 24. Outlet Circumferential Velocity for the SB seals across all pre-swirl inserts at (a) ω = 2 krpm and ΔP = 8.27 bar (b) ω = 8 krpm and ΔP = 2.07

Fig. 25 displays plots of OSR for the SB seals across all the pre-swirl cases. In Fig. 25a the OSR increases slightly as ΔP increases and is approximately 0.25. Figure 25b shows that, as ω increases, OSR stays around 0.25. Clearly, in Fig. 25 OSR is independent of the imposed inlet pre-swirl condition. This means the inlet condition (high, medium, radial injection) has little effect on OSR. For a long smooth seal, the expected OSR at the seal exit is 0.5, but the values in Fig. 25 are 2.54 mm downstream from the seal exit.
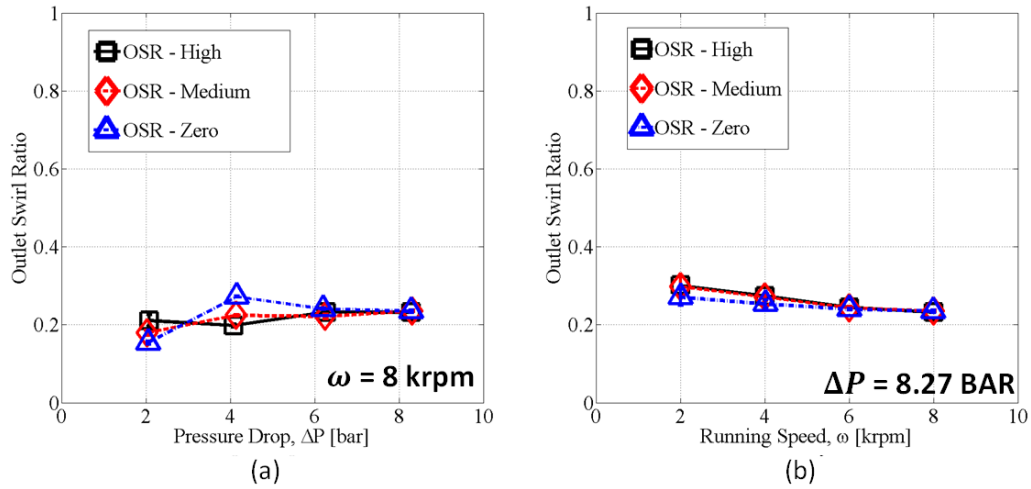
Figure 25. OSR of the SB seal in the centered position against (a) ΔP at ω = 8 krpm and (b) ω at ΔP = 8.27 bar

4.6 Static-Load and Eccentricity Ratio Measurements

To determine the eccentricity of the seal rotor's position with respect to its stator, the geometric center (O_s) of the rotor-stator clearance circle had to be determined. From the clearance-circle-measurement, O_s was determined from X and Y elements of the center's geometric center. Once the center of the stator had been established, the center of the journal ($\boldsymbol{O_j}$) was found in reference to O_s. $\boldsymbol{O_j}$ was found through e_0's individual X and Y elements (e_{OX} and e_{OY}) measured by proximity probes. The relationships between, O_s, $\boldsymbol{O_j}$, attitude angle (ϕ), e_0, F_s are displayed in Fig. 26.
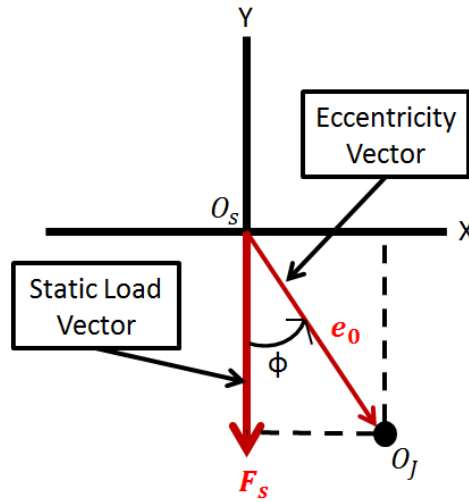
Figure 26. Test Stand Coordinate System displaying Static Load, Eccentricity, and Attitude Angle Relationship

Note that the F_s was always applied in the $-Y$ direction with the Zonic unit in load control producing a specified static e_0. The eccentricity-ratio components are

$$\varepsilon_{OX} = \frac{e_{OX}}{C_r} \tag{3}$$

$$\varepsilon_{OY} = \frac{e_{OY}}{C_r} \tag{4}$$

Taking the individual elements of e_{OX} and e_{OY}, e_0 is

$$e_0 = \sqrt{e_{OX}^2 + e_{OY}^2}, \tag{5}$$

while the attitude angle (ϕ) is

$$\phi = \tan^{-1} \frac{e_{OX}}{e_{OY}} \tag{6}$$

Fig. 27 shows seal load-eccentricity loci results for the SB seal with the hot clearance circle overlay. The loci drift slightly to the right due to fluid rotation, and that result is fairly consistent across the various ΔP values.
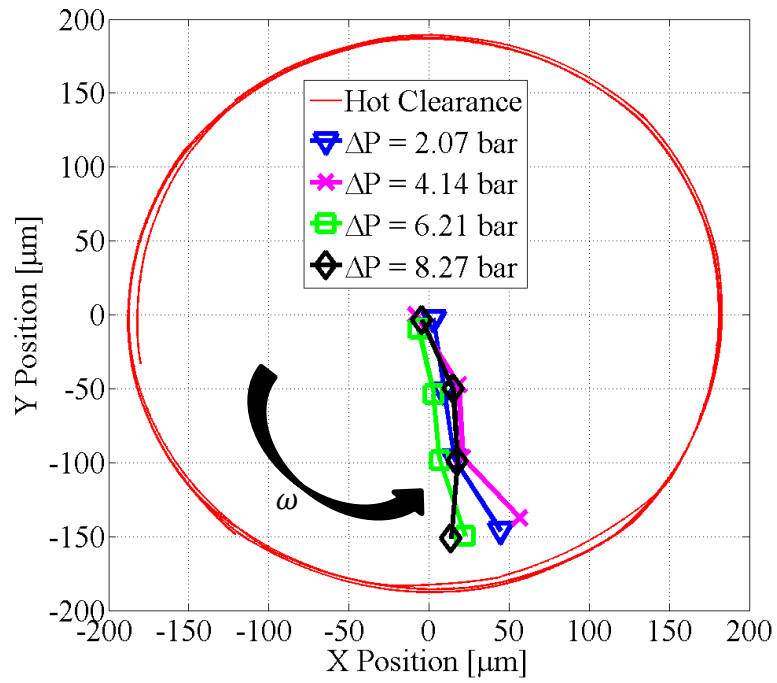
Figure 27. Clearance overlay of SB seals for the high pre-swirl insert at $\omega = 4\ krpm$

5. DYNAMIC DATA AND ANALYSIS

5.1 Dynamic Testing and Data Reduction

Before dynamic testing could begin, the operator adjusted ε_0 by applying a load in the $-Y$ direction. The depiction of the Zonic units in relation to the test rig can be viewed in Fig. 28.
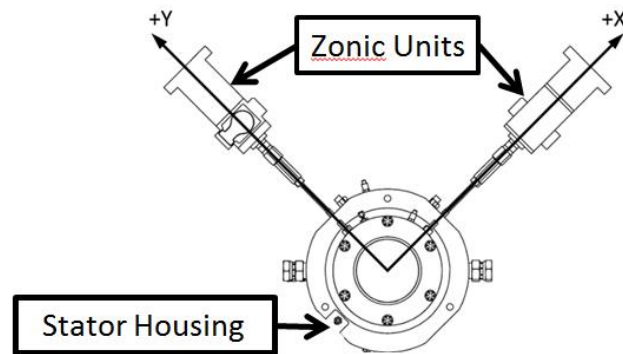
Figure 28. Axial view of the stator housing and the Zonic units

Dynamic testing procedures followed the excitation method cited by Rouvas-Childs [22]. The hydraulic shakers (Zonic units) excited the stator about a static equilibrium position with an amplitude of approximately 10% of C_r. The methodology utilized a pseudo-random waveform that adjusted phases to minimize the peak factor. Simply stated, maximum excitation was provided over an ensemble of frequencies while overall excitation was kept low. These excitation frequencies occurred on intervals of 10*1000/1024, or ~9.765 Hz. During the excitation period these intervals run nominally

from 10 to 350 Hz consisting of 320 shakes over 32.768 seconds. The DAQ software

recorded all data during this time period.

Childs and Hale [23] outlined a method for measuring rotordynamic coefficients,

starting with the stator EOM

$$M_s \begin{Bmatrix} \ddot{X}_s \\ \ddot{Y}_s \end{Bmatrix} = \begin{Bmatrix} f_X \\ f_Y \end{Bmatrix} + \begin{Bmatrix} f_{rX} \\ f_{rY} \end{Bmatrix} \tag{15}$$

where M_s is the stator mass, and the fluid film reaction-force components in the X and Y

directions are f_{rX} and f_{rY} respectively. Substituting the reaction-force definition of Eq.

(2) into Eq. (15) produces

$$\begin{Bmatrix} f_X \\ f_Y \end{Bmatrix} - M_s \begin{Bmatrix} \ddot{X}_s \\ \ddot{Y}_s \end{Bmatrix} = \begin{bmatrix} K_{XX} & K_{XY} \\ K_{YX} & K_{YY} \end{bmatrix} \begin{Bmatrix} \Delta X \\ \Delta Y \end{Bmatrix} + \begin{bmatrix} C_{XX} & C_{XY} \\ C_{YX} & C_{YY} \end{bmatrix} \begin{Bmatrix} \Delta \dot{X} \\ \Delta \dot{Y} \end{Bmatrix} + \begin{bmatrix} M_{XX} & M_{XY} \\ M_{YX} & M_{YY} \end{bmatrix} \begin{Bmatrix} \Delta \ddot{X} \\ \Delta \ddot{Y} \end{Bmatrix} \tag{16}$$

The data was then arranged into four sets in the time domain of equal duration.

The measured data is converted to the frequency domain using a discrete Fourier

Transform resulting in

$$\begin{Bmatrix} F_X - M_s A_X \\ F_Y - M_s A_Y \end{Bmatrix} = \begin{bmatrix} H_{XX} & H_{XY} \\ H_{YX} & H_{YY} \end{bmatrix} \begin{Bmatrix} D_X \\ D_Y \end{Bmatrix} \tag{17}$$

(F_X, F_Y) ,(A_X, A_Y) and (D_X, D_Y) are the complex components of the excitation force,

acceleration and relative displacement vectors respectively.

When excitation forces are independently applied in both the X and Y directions

the following equation occurs

$$\begin{bmatrix} F_{XX} - M_s A_{XX} & F_{XY} - M_s A_{XY} \\ F_{YX} - M_s A_{YX} & F_{YY} - M_s A_{YY} \end{bmatrix} = \begin{bmatrix} H_{XX} & H_{XY} \\ H_{YX} & H_{YY} \end{bmatrix} \begin{bmatrix} D_{XX} & D_{XY} \\ D_{YX} & D_{YY} \end{bmatrix} \tag{18}$$

There are four equations and four H_{IJ} unknowns. The dynamic stiffness coefficients can

be stated in terms of the rotordynamic coefficients as

$$H_{IJ} = \left(K_{ij} - \Omega^2 M_{ij}\right) + j\left(\Omega C_{ij}\right) \tag{19}$$

The excitation frequency is Ω, and $j = \sqrt{-1}$.

To solve for the fluid film dynamic stiffness coefficients, baseline values taken in preparation to testing were subtracted from the test dynamic stiffnesses. This 'dry baseline' was taken with no process fluid contained in the system. The procedure isolates the dynamic properties of the test stand per each assembly without the fluid flow that is seen during typical test points. The resultant values were divided by two because there were two seals in the system. Next, a least squares regression fit was applied to the real and imaginary parts of H_{IJ}; i.e.,

$$\text{Re}\left(H_{IJ}\right) = K_{ij} - \Omega^2 M_{ij} = K_{ij} - \Lambda M_{ij} \tag{20}$$

$$\text{Im}\left(H_{IJ}\right) = \Omega C_{ij} \tag{21}$$

The curve fit using Λ in Eq. (20) and Ω in Eq. (21) follows a linear trend displayed by

$$y(x_i) = a + bx_i \tag{22}$$

where a is the intercept and b is the slope. Then a and b are represented by

$$a = \frac{\sum y_i \sum x_i^2 - \sum x_i \sum x_i y_i}{n \sum x_i^2 - (\sum x_i)^2} \tag{23}$$

$$b = \frac{n \sum x_i y_i - \sum x_i \sum y_i}{n \sum x_i^2 - (\sum x_i)^2} \tag{24}$$

This curve fitting method was used for Ω, up to 1.5 times ω, approximately 200 Hz.

Figures 29a and 29b represent the components of direct and cross-coupled H_{IJ} coefficients, which give stiffness and virtual mass coefficients. The intercepts of Fig. 29a produce the direct stiffness, while Fig. 29b intercepts produce the cross coupled

stiffness. The curvature of Fig. 29a give the direct virtual mass while the curvature of

Fig. 29b produces the cross coupled virtual mass.
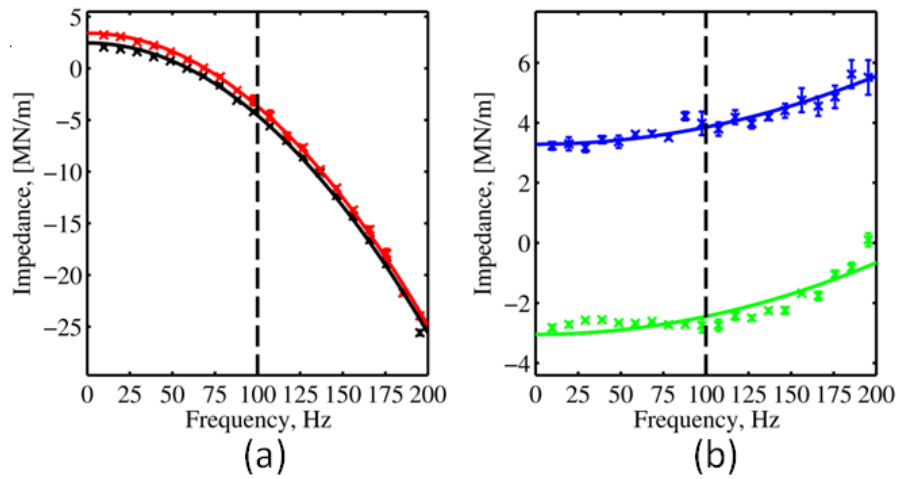
Figure 29. Impedance plots for High pre-swirl at $\omega = 6$ krpm, $\Delta P = 6.21$ bar, $\varepsilon_0 = 0.53$ for (a) Real Direct and (b) Cross-Coupled

Figure 30c and 30d represent imaginary components of the direct and cross-

coupled H_{IJ} coefficient. The slopes of Fig. 30c and Fig. 30d produce the direct damping

and cross coupled damping coefficients, respectively.
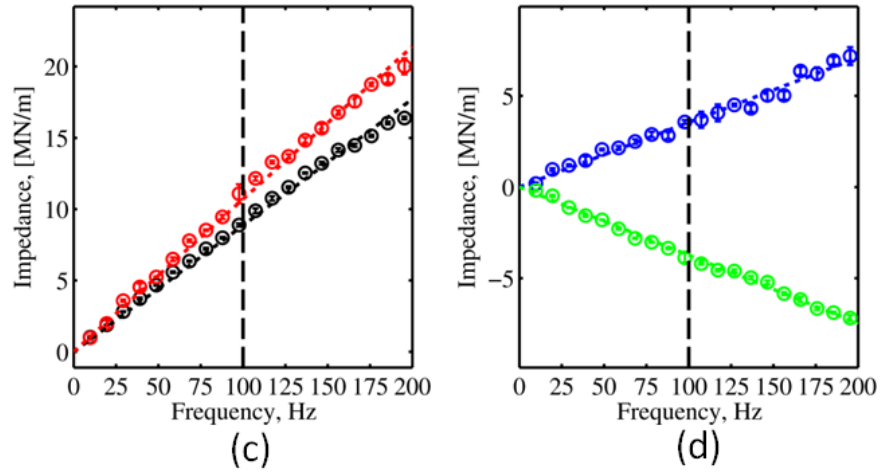
Figure 30. Impedance plots for High pre-swirl at ω = 6 krpm, ΔP = 6.21 bar, ε_0 = 0.53 for (c) Imaginary Direct and (d) Cross-Coupled

Some of the impedance data showed inconsistencies above Ω = 160 Hz. By comparison, the maximum running speed is ω = 8 krpm (133Hz). Hence, the curve fits work well for excitation frequencies through the running speeds.

Each section will address the SB seal testing coefficients and then draw a comparison to the NSB seals. Note for each rotordynamic coefficient the *Y* direction was chosen because F_s was applied in the –*Y* direction. All comparisons done between SB and NSB seals are with the high pre-swirl insert.

5.2 SB Direct-Stiffness-Coefficient Results

Figure 31a displays K_{YY} for all pre-swirl inserts plotted against ΔP at the centered position and ω = 8 krpm. As expected, K_{YY} increases with increasing ΔP. Clearly K_{YY} is independent of the imposed pre-swirl condition.

Figure 31b shows K_{YY} for all pre-swirl inserts versus ε_0 at $\Delta P = 8.27$ bar and $\omega = 8$ krpm. K_{YY} remains constant up to $\varepsilon_0 \leq 0.53$; then sharply increases at $\varepsilon_0 = 0.80$. The highest K_{YY} values occur with the medium pre-swirl. The next highest values are with the radial injection and then the high pre-swirl insert.
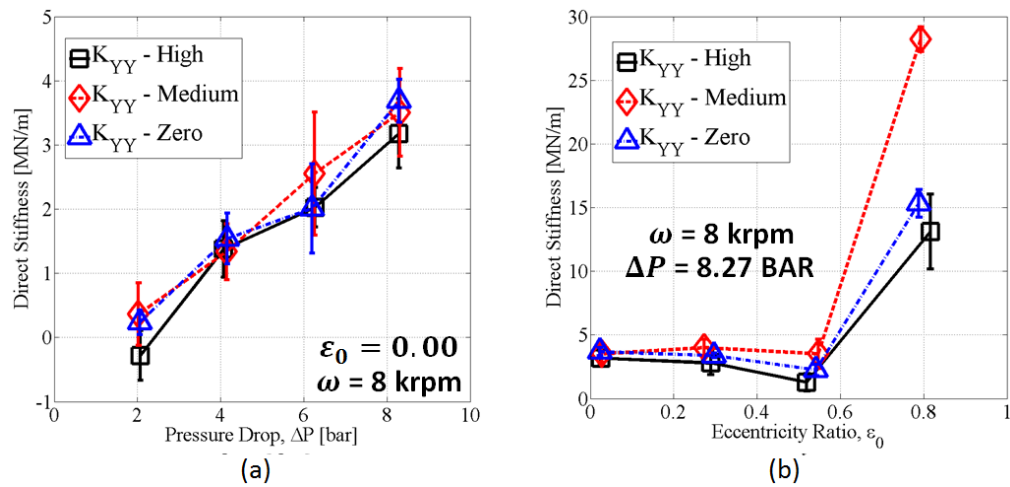
Figure 31. K_{YY} of SB seals for all pre-swirl inserts at $\omega = 8$ krpm plotted against (a) ΔP at $\varepsilon_0 = 0.00$ (b) ε_0 at $\Delta P = 8.27$ bar

Figure 32a shows K_{YY} for all pre-swirl inserts versus ω at $\Delta P = 8.27$ bar and at the centered position. K_{YY} behaves remarkably with increasing ω. K_{YY} would be expected to remain fairly constant with increasing ω. However, a sudden drop in K_{YY} occurs at ω = 4 krpm for all pre-swirl cases. The radial injection insert has the highest K_{YY} values followed by the medium pre-swirl and radial injection inserts.

Figure 32b displays Re versus ω for the conditions seen in Fig. 32a. At ω = 4 krpm Re ranges from 2900-3200. As expected, K_{YY} increases steadily with increasing

ΔP. The drop in K_{YY} in Fig. 32a could be attributed to a change in flow conditions at $\omega = 4$ krpm and at $Re \cong 3000$. This Re range is within the transitional regime Reynolds numbers cited by Zirkelback and San Andrés [21]. The flow could be laminar at $\omega = 2$ krpm, within the transition regime at $\omega = 4$ krpm, and turbulent at 8 krpm. This consideration will be discussed further in regard to Fig. 35.
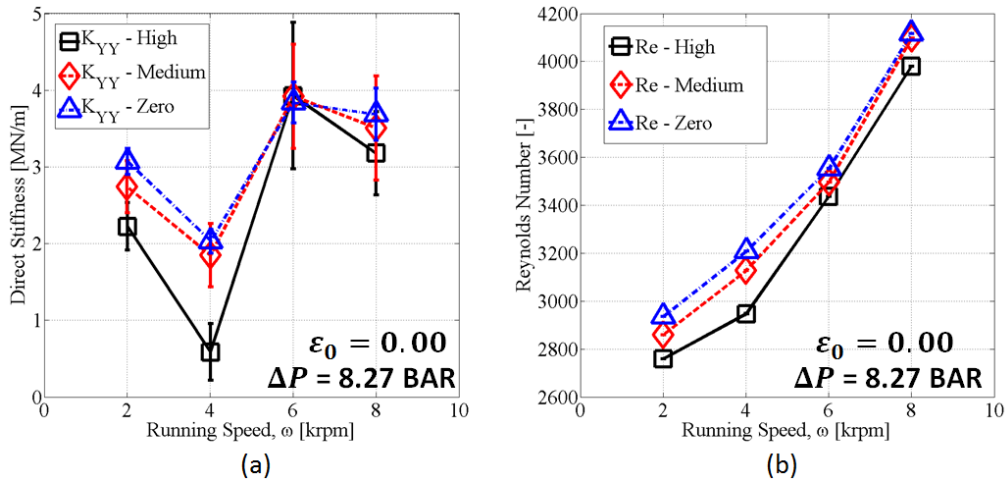
Figure 32. SB seals for all pre-swirl inserts plotted ω at ΔP = 8.27 bar and $\varepsilon_0 = 0.00$ against (a) K_{YY} and (b) Reynolds Number

5.3 Direct Stiffness Comparison SB vs. NSB

Figure 33a shows K_{JJ} for SB and NSB seals versus ΔP at $\omega = 8$ krpm and at the centered position with the high pre-swirl insert. For the NSB seal, at $\Delta P = 2.07$ and 4.14 bar K_{JJ} turns from negative to positive. At $\Delta P = 6.21$ and 8.27 bar the SB K_{JJ} values are nearly double the NSB seal values. In the case studies by Massey [2] and Vallantas and Bolleter [16], the elimination of pump instabilities by adding swirl brakes has been largely credited to a reduction in cross-coupled stiffness. The marked increases in K_{JJ}

shown in Fig. 33a would also significantly enhance stability by elevating the pump rotor's first natural frequency.

Figure 33b displays K_{JJ} for SB and NSB seals versus ε_0 at $\Delta P = 2.07$ bar and $\omega = 6$ krpm for the high pre-swirl insert. The NSB K_{JJ} are negative for $\varepsilon_0 \leq 0.53$. At $\varepsilon_0 = 0.80$ the data is more erratic for both the SB and NSB seals. For the SB and NSB seals, K_{XX} is higher compared to K_{YY} for most cases; except at $\varepsilon_0 = 0.80$. When approaching higher ε_0, K_{YY} is expected to be higher than K_{XX}. At $\varepsilon_0 = 0.80$ the NSB seals behave interestingly in that K_{XX} is higher than K_{YY}; which is not the case for the SB seals. The K_{JJ} are generally higher for the SB seals compared to the NSB seals.
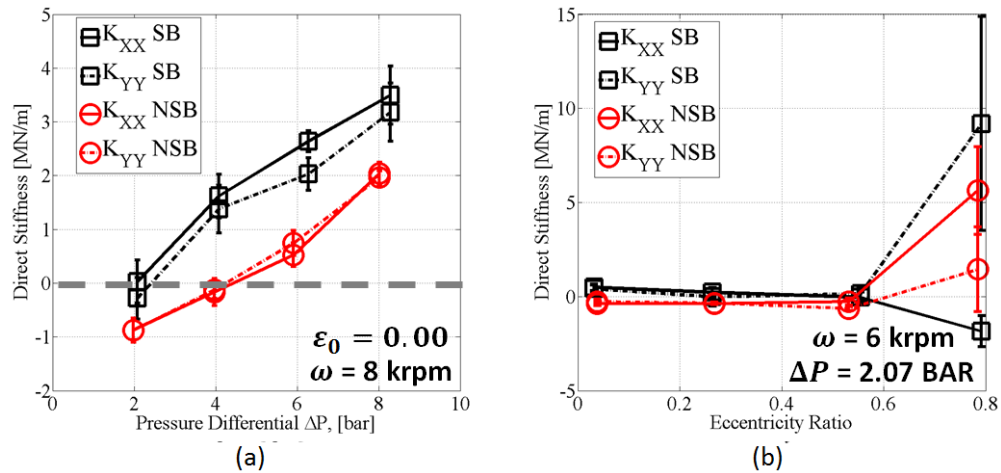
Figure 33. SB vs. NSB comparison for the high pre-swirl insert of K_{JJ} versus (a) ΔP at $\omega = 8$ krpm and $\varepsilon_0 = 0.00$ (b) versus ε_0 at $\Delta P = 2.07$ bar and $\omega = 6$ krpm

Figure 34 shows K_{JJ} for the SB and NSB seals plotted against ω at $\Delta P = 8.27$ bar

and at the centered position for high pre-swirl. Both seals have the same remarkable

behavior with K_{JJ} dropping abruptly as ω increases from 2 krpm to 4 krpm. K_{JJ} values

then jump to higher magnitudes at $\omega = 6$ krpm before dropping again at 8 krpm. This

behavior resembles what was seen in Fig. 32a. Clearly SB seals generally increase K_{JJ}

compared to NSB seals, despite the erratic behavior of K_{JJ}.

(a)
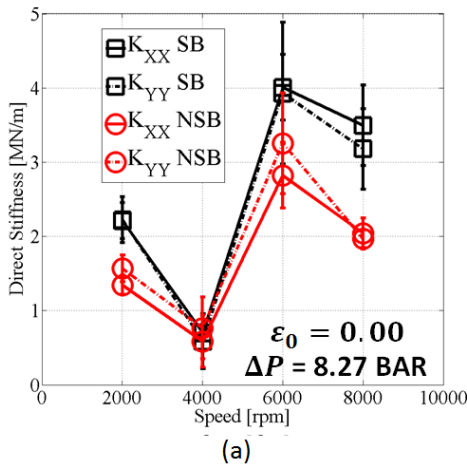
Figure 34. SB vs. NSB comparison for the high pre-swirl insert of K_{JJ} against ω at $\Delta P = 8.27$ bar and $\varepsilon_0 = 0.00$

Attempting to explain the results in Fig. 32a and 34, Fig. 35 shows the

Zirkelback and San Andrés [21] plot for friction factor versus Reynolds number. They

state, "Transition from laminar to turbulent flow is generally accepted to occur at flow

Reynolds numbers between 1000 to 3000." Note the increase in friction factor with

increasing Reynolds number for Re in the range of 1000-3000. The Lomakin effect

explains the positive direct stiffness developed when the friction factor drops with

45

increasing *Re*. When the friction factor increases with increasing *Re*, the Lomakin effect

reverses, and reduced or negative stiffness values can be predicted.
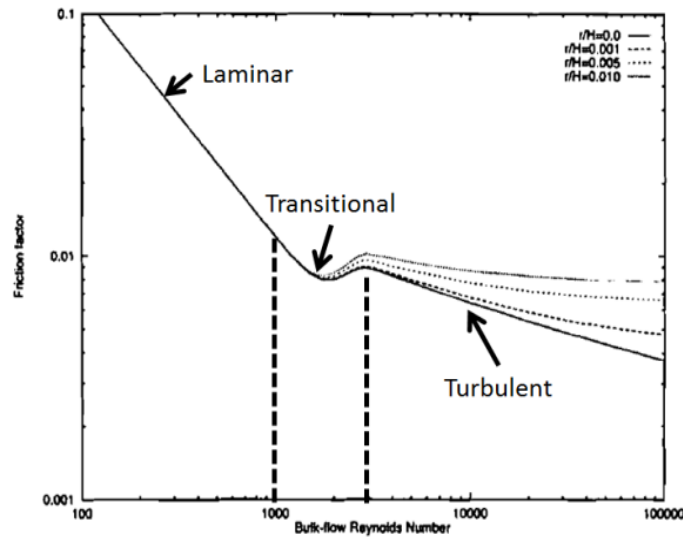
Figure 35. Friction Factor versus Reynolds number plot, adapted from Zirkelback and San Andrés [21]

Figure 36 shows *Re* versus ω for the conditions seen in Fig. 34. At ω = 4 krpm

the Reynolds number is approximately 3000. The change in K_{JJ} at 4 krpm in Fig. 34

could be attributed to operating in the transitional regime; it could also explain the

results in Fig. 32a.
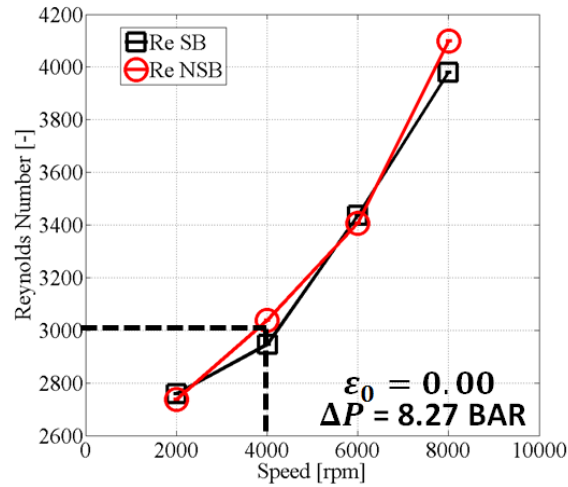
Figure 36. SB vs. NSB comparison for the high pre-swirl insert of Re against ω at $\Delta P = 8.27$ bar and $\varepsilon_0 = 0.00$

Figure 37a shows K_{JJ} for the SB and NSB seals versus ΔP at the centered position and $\omega = 2$ krpm for high pre-swirl. Another remarkable case happens for the NSB only. The K_{JJ} of the NSB seals increases from $\Delta P = 2$ bar to 4 bar. It then rapidly decreases at $\Delta P = 6$ bar and increases again at 8 bar. Differing from Fig. 34, only SB seals' K_{JJ} value jump erratically increasing ω.

Figure 37b shows Re for the SB and NSB seals versus ΔP for the conditions seen in Fig. 37a. The $\Delta P = 2$ bar and 4 bar values in Fig. 37a could both be in the laminar regime. The $\Delta P = 6$ bar test condition could be in the transitional regime ($Re = 2400$), and the $\Delta P = 8$ bar condition could be in the turbulent regime.

The K_{JJ} results for the SB seals are surprising to the extent they do not increase substantially with increasing ΔP as shown previously in Fig. 33a. These SB results were checked carefully by the author.

47
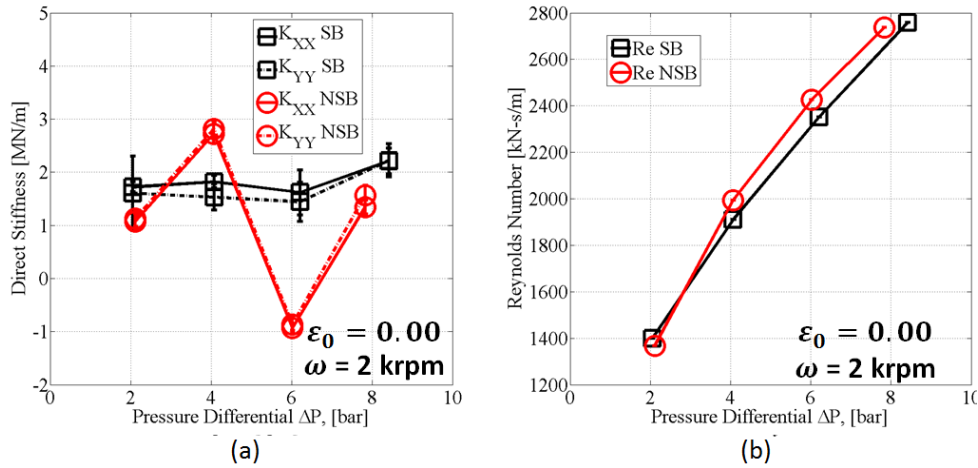
Figure 37. SB vs. NSB comparison of the high pre-swirl insert for (a) K_{JJ} against ΔP at ω = 2 krpm and $\varepsilon_0 = 0.00$ (b) Reynolds number against ΔP at ω = 2 krpm and $\varepsilon_0 = 0.00$

5.4 SB Cross Coupled Stiffness Coefficient Results

Figure 38a shows K_{XY} for all pre-swirl inserts versus ΔP at the centered position and $\omega = 8$ krpm. K_{XY} decreases slightly with increasing ΔP. K_{XY} is not consistently dependent on the imposed PSR inlet condition, demonstrating the favorable impact of the swirl brake.

Figure 38b shows K_{XY} for all pre-swirl inserts versus ω for $\Delta P = 8.27$ bar and $\varepsilon_0 = 0.00$. K_{XY} increases substantially with increasing ω. K_{XY} is somewhat consistently dependent upon the imposed PSR inlet condition; specifically, the high and medium inserts K_{XY} values are higher compared to that of the radial injection. In comparison to Fig. 38a, ω has noticeably more influence on K_{XY} than ΔP.

48
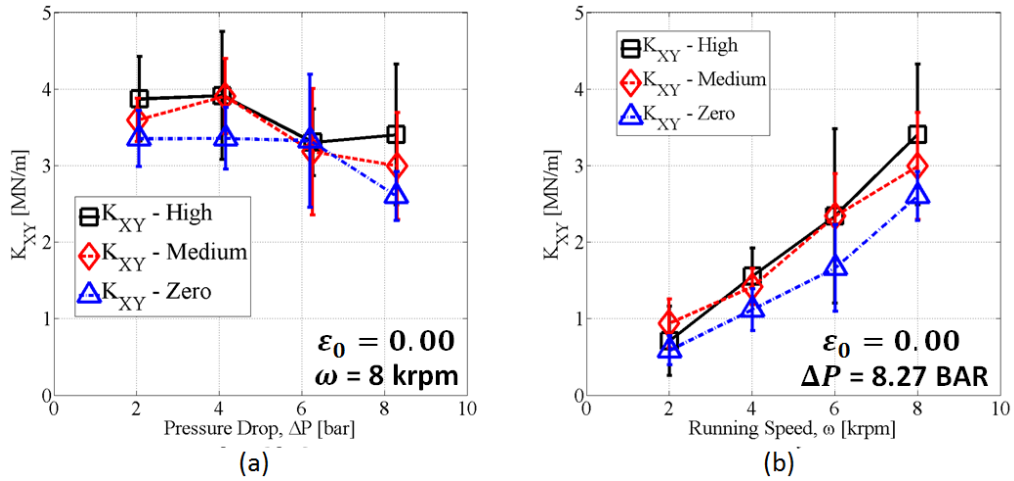
Figure 38. Plot for K_{XY} of SB seals for all pre-swirl inserts plotted against (a) ΔP at ω = 8 krpm and $\varepsilon_0 = 0.00$ (b) ω at ΔP = 8.27 bar and $\varepsilon_0 = 0.00$

Figure 39 shows K_{XY} for all pre-swirl inserts versus ε_0 for ω = 8 krpm and ΔP = 8.27 bar: K_{XY} increases substantially with increasing ε_0. Clearly, the imposed inlet pre-swirl condition has little effect on K_{XY}. The dependency of K_{YX} on ΔP, ω, and ε_0 is covered in the next section.
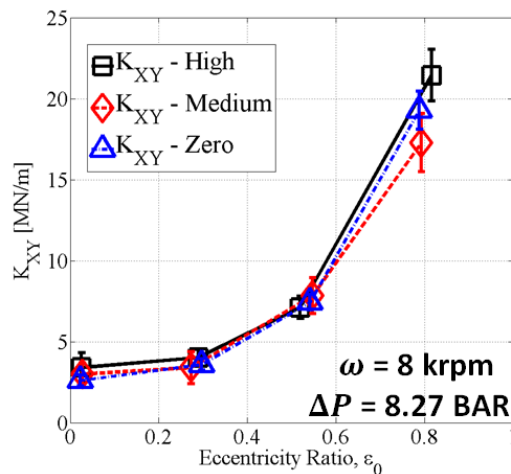
Figure 39. Plot for K_{XY} of SB seals for all pre-swirl inserts against ε_0 at ω = 8 krpm and ΔP = 8.27 bar

5.5 Cross Coupled Stiffness Comparison SB vs. NSB

Figure 40a displays K_{IJ} for the SB and NSB seals versus ω for $\varepsilon_0 = 0.00$ and $\Delta P = 2.07$ bar for the high pre-swirl insert. $K_{YX} \cong -K_{XY}$, and both magnitudes increase in a nominally linear fashion with increasing ω. There is only a modest reduction in $\left| K_{IJ} \right|$ from NSB to SB.

Figure 40b displays K_{IJ} for the SB and NSB seals versus ω for $\varepsilon_0 = 0.00$ and $\Delta P = 8.27$ bar for the high pre-swirl insert. $K_{YX} \cong -K_{XY}$, and both magnitudes increase in a nominally linear fashion with increasing ω. Note the marked reduction in $\left| K_{IJ} \right|$ in moving from NSB to SB seals.

The difference between Fig. 40a and Fig 40b is an increase in ΔP from 2.07 bar to 8.27 bar. Compare Fig. 40a and Fig. 40b; at lower ΔP such as the 2.07 bar in Fig. 40a, the reduction in $\left| K_{IJ} \right|$ is not as substantial as in Fig 40b at a higher ΔP. A higher ΔP produces a higher inlet pre-swirl velocity through the pre-swirl rings of Fig. 11 with a greater possibility of reduction from the swirl brake. Visible in Fig. 40 is the destabilizing K_{IJ} terms are reduced with the application of swirl brakes, most effectively at high ΔP and low ω. This trend is similar to the trend in the reduction of PSR in Table 6.
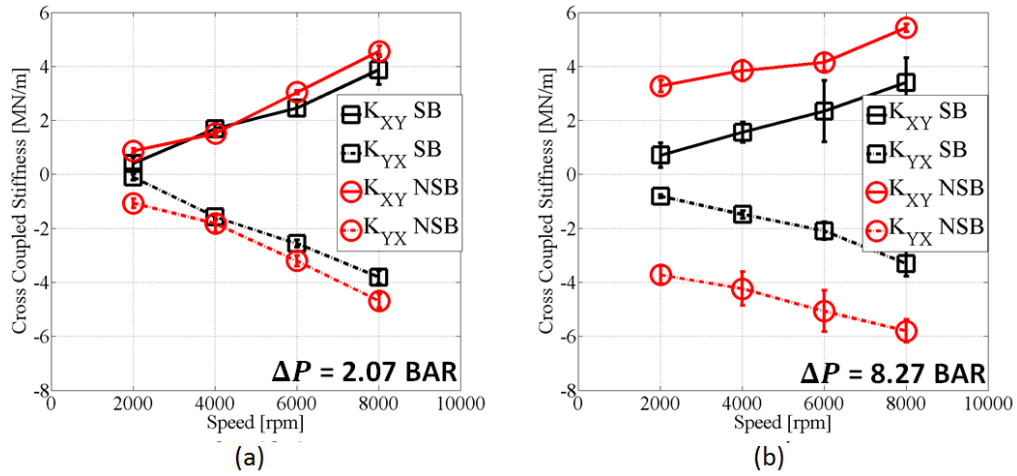
Figure 40. K_{IJ} comparison of SB versus NSB seals for the high pre-swirl insert versus ω for $\varepsilon_0 = 0.00$ at (a) $\Delta P = 2$ bar and (b) $\Delta P = 8$ bar

Figure 41 shows K_{IJ} for the SB and NSB seals versus ε_0 at ω = 8 krpm and $\Delta P = 8.27$ bar for the high pre-swirl insert. For $\varepsilon_0 \leq 0.53$, the $|K_{IJ}|$ remains fairly constant; while $|K_{IJ}|$ increases at $\varepsilon_0 = 0.80$. $|K_{IJ}|$ for SB seals is smaller than compared to NSB seals. Note that K_{XY} and K_{YX} have opposite signs (destabilizing) for both SB and NSB seals. Surprisingly, K_{XY} (SB) is larger then K_{XY} (NSB) at $\varepsilon_0 = 0.80$.

51
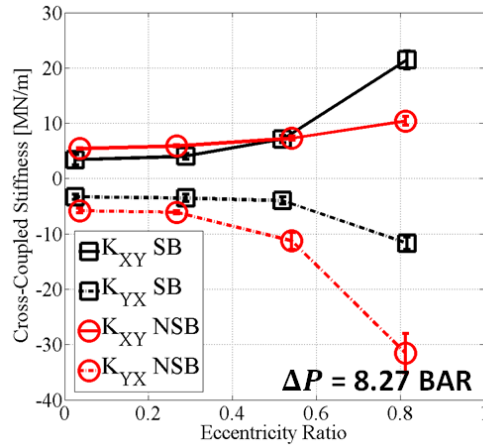
Figure 41. K_{IJ} comparison of SB versus NSB seals for the high pre-swirl insert against ε_0 at $\omega = 8$ krpm and $\Delta P = 8.27$ bar

5.6 SB Direct Damping Coefficient Results

Figure 42a shows C_{YY} for the three pre-swirl inserts versus ΔP for $\omega = 8$ krpm and at the centered position. C_{YY} increases with increasing ΔP. C_{YY} is slightly higher for the high pre-swirl insert compared to that of the medium and radial injection insert.

Figure 42b shows C_{YY} for the three pre-swirl inserts versus ω at $\Delta P = 8.27$ bar and at the centered position. C_{YY} decreases slightly as ω increases. C_{YY} values are largely independent of the imposed pre-swirl condition. Comparing Fig. 42a and 42b, changing ΔP at $\omega = 8$ krpm has a larger effect on C_{YY} than changing ω at $\Delta P = 8.27$ bar.
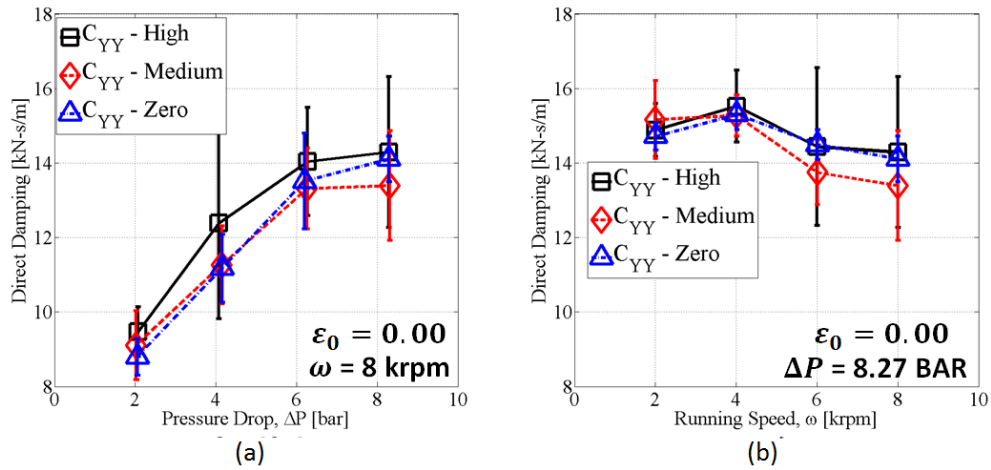
Figure 42. C_{YY} **for SB seals across all pre-swirl inserts for** $\varepsilon_0 = 0.00$ **against (a)** ΔP **at** $\omega = 8$ **krpm (b)** ω **at** ΔP **= 8.27 bar**

Figure 43 shows C_{YY} versus ε_0 at $\omega = 8$ krpm and $\Delta P = 8.27$ bar. C_{YY} increases substantially with increasing ε_0. Clearly, the imposed inlet pre-swirl condition has little effect on C_{YY}.
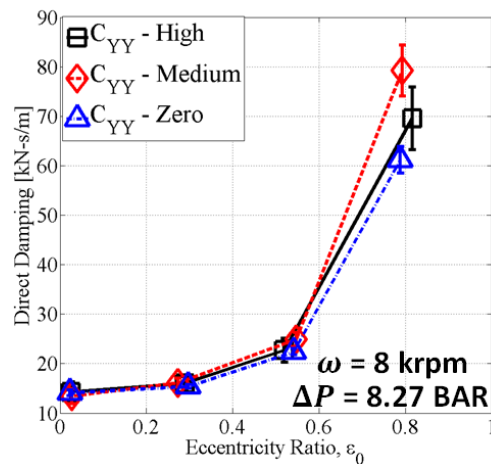
Figure 43. C_{YY} **for SB seals across all pre-swirl inserts against** ε_0 **at** $\omega = 8$ **krpm and** $\Delta P = 8.27$ **bar**

5.7 Direct Damping Comparison SB vs. NSB

Figure 44a shows C_{JJ} for SB and NSB seals versus ΔP at the centered position and $\omega = 8$ krpm for the high pre-swirl insert. $|C_{JJ}|$ increases as ΔP increases. There is a slight increase in $|C_{JJ}|$ from SB to NSB seals.

Figure 44b shows C_{JJ} for SB and NSB seals versus ω at the centered position and $\Delta P = 8.27$ bar for the high pre-swirl insert. There is a minimal decrease in C_{JJ} as ω increases from 2 krpm to 8 krpm. In both Fig. 44a and 44b, C_{XX} is greater than the C_{YY} for both the SB and NSB seals. Clearly in Fig. 44, increasing ΔP at $\omega = 8$ krpm has a greater impact upon $|C_{JJ}|$ than increasing ω at $\Delta P = 8.27$ bar. The $|C_{JJ}|$ is slightly higher for SB than NSB seals.
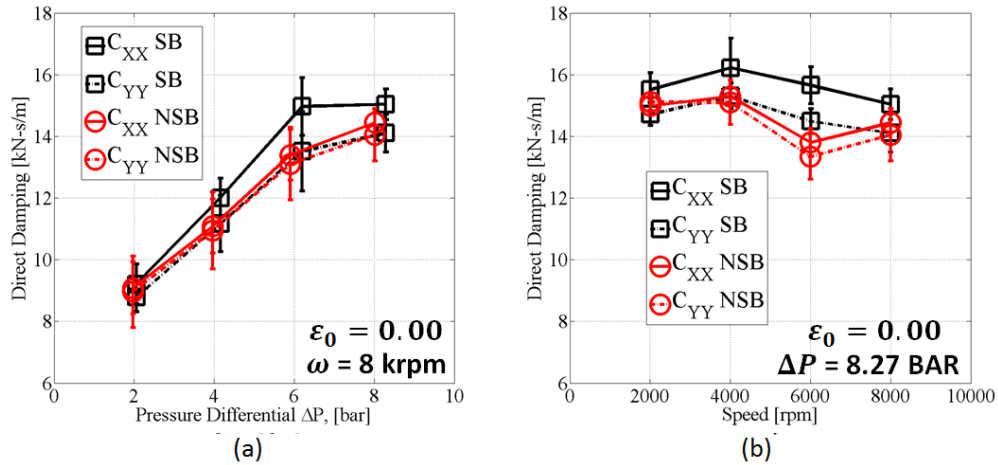
Figure 44. SB vs. NSB comparison for the high pre-swirl insert of C_{YY} at $\varepsilon_0 = 0.00$ against (a) ΔP at $\omega = 8$ krpm and (b) ω at $\Delta P = 8.27$ bar

Figure 45 shows C_{JJ} versus ε_0 at $\omega = 8$ krpm and $\Delta P = 8.27$ bar for the SB and NSB seals with the high pre-swirl insert. For $\varepsilon_0 \leq 0.53$, C_{JJ} increase slightly with

increasing ε_0; while in moving from $\varepsilon_0 = 0.53$ to $\varepsilon_0 = 0.80$ C_{JJ} increased markedly.

When approaching higher ε_0, C_{YY} is expected to be higher than C_{XX}. At $\varepsilon_0 = 0.80$ the

NSB seals behave interestingly in that C_{XX} is higher than C_{YY}; which is not the case for

the SB seals. From Fig. 44 and 45, C_{JJ} is not greatly affected with the application of

swirl brakes.
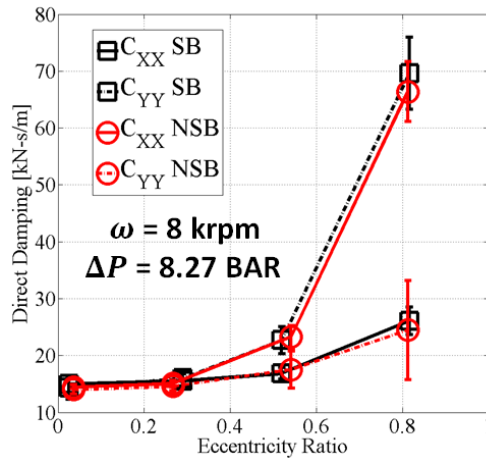
Figure 45. SB vs. NSB comparison for the high pre-swirl insert of C_{YY} against ε_0 at ω = 8 krpm and ΔP = 8.27 bar

5.8 SB Cross-Coupled Damping Coefficient Results

Figure 46a shows C_{XY} for all pre-swirl inserts versus ΔP at $\omega = 2$ krpm and at the

centered position. C_{XY} remains fairly constant as ΔP increases. C_{XY} increases in moving

from radial injection to medium and then to high pre-swirl.

Figure 46b shows C_{XY} for all pre-swirl inserts versus ω at $\Delta P = 8.27$ bar and at

the centered position. C_{XY} increases substantially as ω increases. C_{XY} increases from

55

radial injection to medium and then to high pre-swirl. Comparing Fig. 46a and 46b increasing ω at $\Delta P = 8.27$ bar has markedly more influence than increasing ΔP at $\omega = 2$ krpm, similar to the results for K_{XY} in Fig 38.
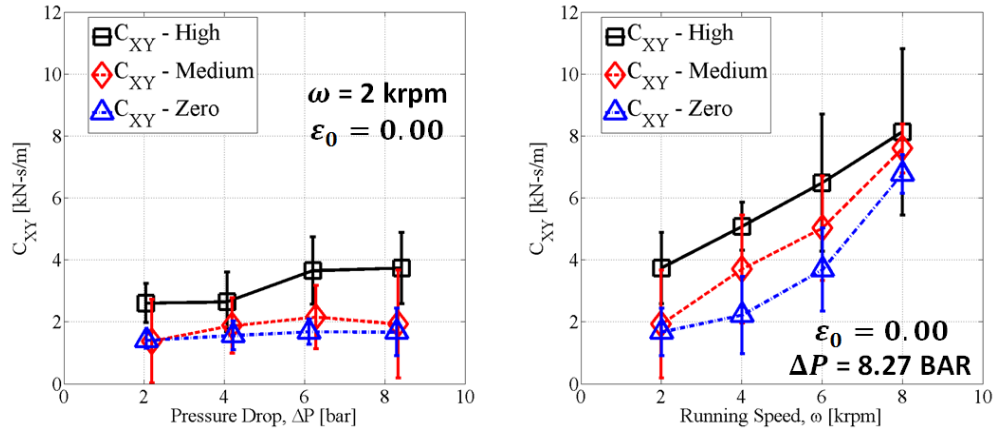
Figure 46. C_{XY} **of SB seals for all pre-swirl inserts in the centered position plotted against (a)** ΔP **at** $\omega = 2$ **krpm and (b)** ω **at** $\Delta P = 8.27$ **bar**

Figure 47 shows C_{XY} for all pre-swirl inserts versus ε_0 at $\omega = 2$ krpm and $\Delta P = 8.27$ bar. C_{XY} remains fairly constant for $\varepsilon_0 \leq 0.53$. At $\varepsilon_0 = 0.80$, C_{XY} decreases rapidly for all pre-swirl inserts. Clearly, the imposed inlet pre-swirl condition has no consistent effect on C_{XY}.
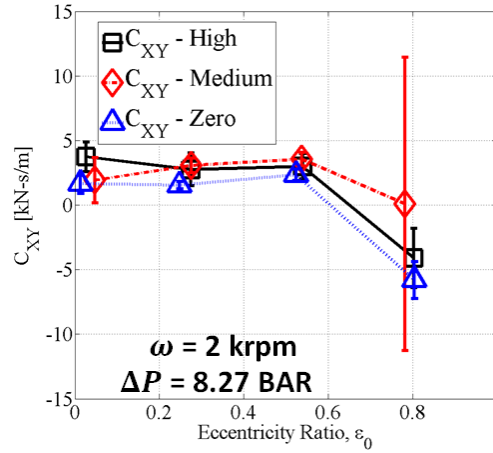
Figure 47. C_{XY} of SB seals for all pre-swirl inserts against ε_0 at $\omega = 2$ krpm and $\Delta P = 8.27$ bar

5.9 Cross Coupled Damping Comparison SB vs. NSB

Figure 48a shows C_{IJ} for SB and NSB seals versus ΔP at $\omega = 2$ krpm and at the centered position for the high pre-swirl insert. $\left|C_{IJ}\right|$ remains constant for increasing ΔP for the SB seals, but increases modestly for the NSB seals. C_{XY} and C_{YX} have approximately equal magnitudes and opposite signs for both the SB and NSB seals. The reduction in $\left|C_{IJ}\right|$ from the NSB to the SB configuration is relatively constant and independent of ΔP.

Figure 48b shows C_{IJ} versus ω at $\Delta P = 8.27$ bar and at the centered position for the high pre-swirl insert. $\left|C_{IJ}\right|$ linearly increases for both SB and NSB seals as ω increases; with $C_{XY} \cong -C_{YX}$. Figures 48a and 48b show a consistent reduction in $\left|C_{IJ}\right|$ from NSB to SB seals.

57
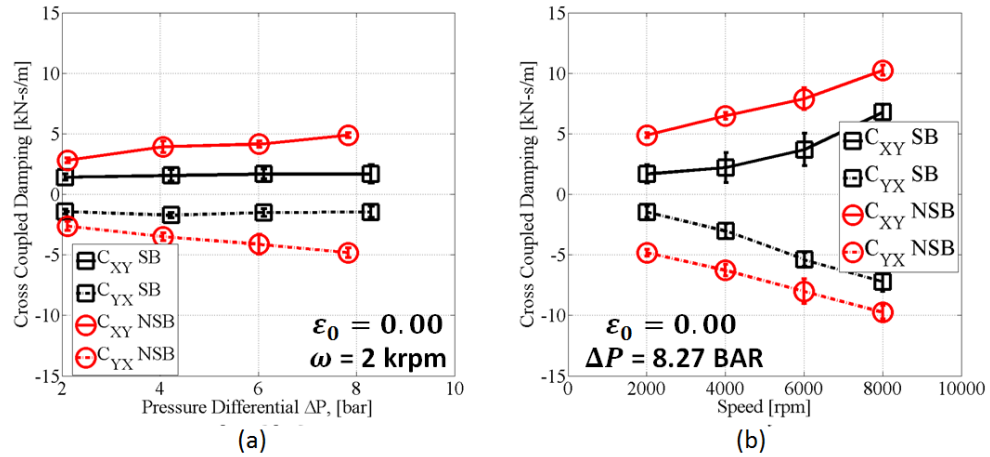
Figure 48. Comparison of SB to NSB seals for the high pre-swirl inserts of C_{IJ} at $\varepsilon_0 = 0.00$ plotted against (a) ΔP at $\omega = 2$ krpm (b) ω at $\Delta P = 8.27$ bar

Figure 49 shows C_{IJ} for the SB and NSB seals versus ε_0 at $\omega = 2$ krpm and $\Delta P = 8.27$ bar for the high pre-swirl insert. For $\varepsilon_0 \leq 0.53$, $|C_{IJ}|$ remains fairly constant for both the SB and NSB seals. While at $\varepsilon_0 = 0.80$: $|C_{IJ}|$ increases substantially. With opposite signs the C_{XY}, C_{YX} act as gyroscopic terms and do not dissipate energy. When C_{XY}, C_{YX} have the same sign, as at $\varepsilon_0 = 0.80$, they dissipate energy. $|C_{IJ}|$ is smaller for SB seals than for NSB seals.

58
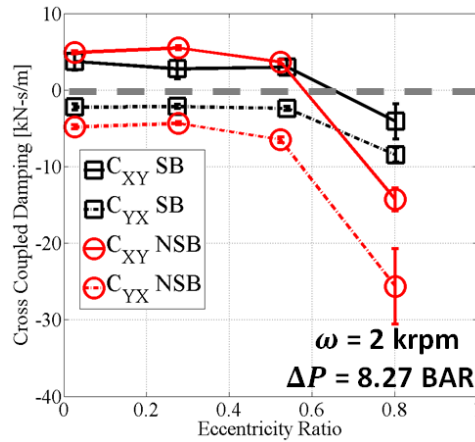
Figure 49. Comparison of SB to NSB seals for the high pre-swirl insert of C_{IJ} plotted against ε_0 at ω = 2 krpm and ΔP = 8.27 bar

5.10 **SB Direct Virtual Mass Coefficient Results**

Figure 50a shows M_{YY} versus ΔP at ω = 2 krpm and at the centered position for all pre-swirl inserts. M_{YY} gradually increases as ΔP increases. M_{YY} of the medium pre-swirl inserts is lower compared to that of the high and radial injection inserts.

Figure 50b shows M_{YY} versus ω at ΔP = 8.27 bar and at the centered position for all pre-swirl inserts. M_{YY} slowly decreases as ω increases. M_{YY} of the medium pre-swirl inserts is generally lower compared to that of the high and radial injection inserts.

59
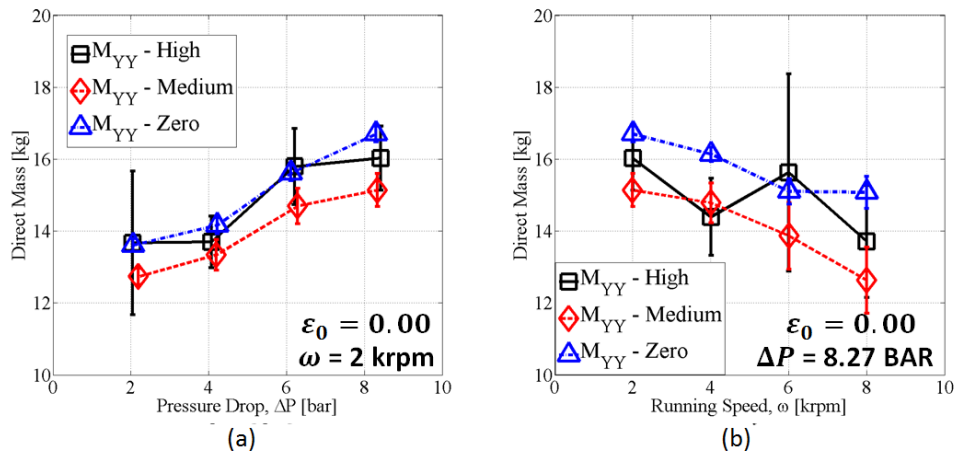
Figure 50. M_{YY} for SB seals all pre-swirl inserts at $\varepsilon_0 = 0.00$ against (a) ΔP at $\omega = 2$ krpm (b) ω at $\Delta P = 8.27$ bar

Figure 51 shows M_{YY} versus ε_0 at $\omega = 8$ krpm and $\Delta P = 8.27$ bar for all pre-swirl inserts. M_{YY} increases substantially with increasing ε_0. Clearly the imposed inlet pre-swirl condition has no consistent effect.
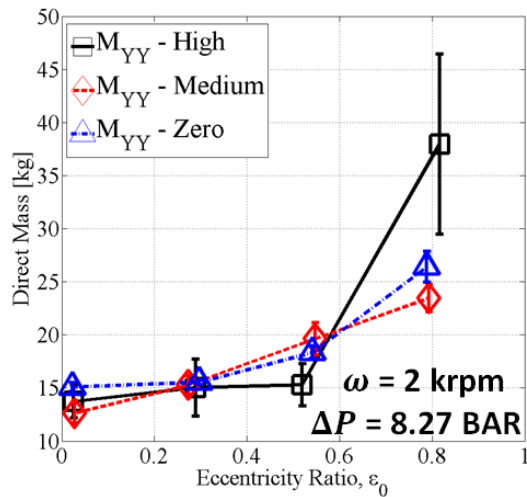
Figure 51. M_{YY} for SB seals all pre-swirl inserts ε_0 at $\omega = 8$ krpm and $\Delta P = 8.27$ bar

5.11 Direct Virtual Mass Comparison SB vs. NSB

Figure 52a shows M_{JJ} for the SB and NSB seals versus ω at $\Delta P = 2.07$ bar and at the centered position for the high pre-swirl insert. M_{JJ} decreases slightly as ω increases. $M_{XX} \cong M_{YY}$ for both SB and NSB seals; and they behave very similarly. The SB seals have lower M_{JJ} compared to that of the NSB seals.

Figure 52b shows M_{JJ} for the SB and NSB seals versus ΔP at the centered position and $\omega = 8$ krpm for the high pre-swirl insert. M_{JJ} increases as ΔP increases. $M_{XX} \cong M_{YY}$ for both SB and NSB seals; and they behave very similarly. For most cases, the SB seals tend to have a lower M_{JJ} value than that of the NSB seals.
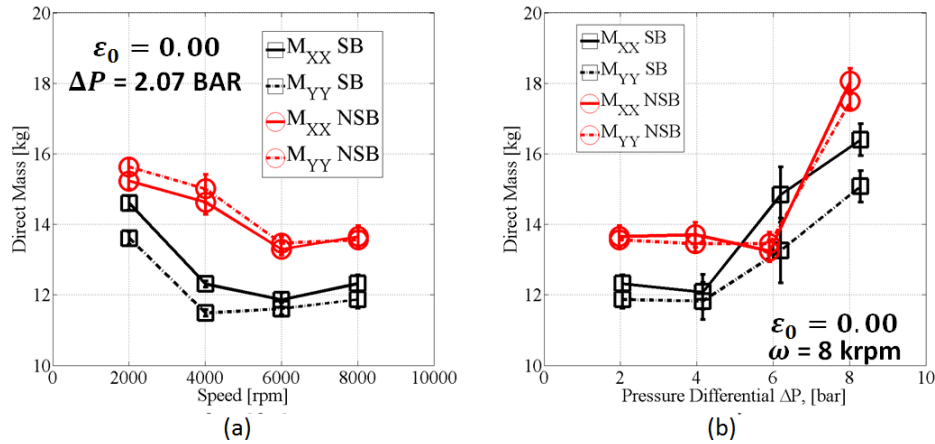
Figure 52. SB vs. NSB comparison for the high pre-swirl insert of M_{JJ} against (a) ω at $\Delta P = 2.07$ bar and ε_0 =0.00 (b) ΔP at ε_0 =0.00 and $\omega = 8$ krpm

Figure 53 shows M_{JJ} for the SB and NSB seals versus ε_0 at $\omega = 8$ krpm and $\Delta P = 8.27$ bar for the high pre-swirl insert. M_{JJ} increases as ε_0 increases. Except for the

$\varepsilon_0 = 0.80$ case, M_{JJ} for SB seals is slightly less for NSB seals. When approaching

higher ε_0, M_{YY} is expected to be higher than M_{XX}. At $\varepsilon_0 = 0.80$ the NSB seals behave

interestingly in that M_{XX} is higher than M_{YY}; which is not the case for the SB seals. M_{JJ}

for the SB seals is smaller compared to that of the NSB seals.
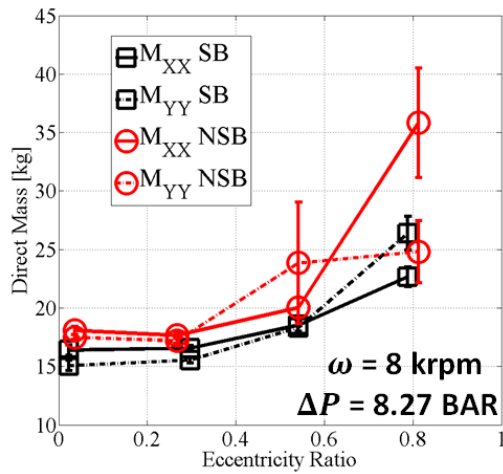
Figure 53. SB vs. NSB comparison of M_{JJ} plotted against ε_0 at ω = 8 krpm and ΔP = 8.27 bar

5.12 Cross-Coupled Virtual Mass Comparison SB vs. NSB

Note the impact that M_{IJ} has upon predicted stability. If $M_{XY} > 0$ and $M_{YX} < 0$

then the M_{IJ} terms stabilize forward whirl. If $M_{XY} < 0$ and $M_{YX} > 0$, the M_{IJ} terms

destabilize forward whirl. If M_{XY} and M_{YX} have the same sign they do not impact

stability. M_{XY}, M_{YX} will be integrated into an overall stability comparison in Section 6.

Figure 54a shows M_{IJ} for the SB and NSB seals versus ΔP at $\omega = 8$ krpm and at the centered position for the high pre-swirl insert. M_{IJ} remains fairly constant as ΔP increases. $\left| M_{IJ} \right|$ generally decreases in moving from NSB to SB seals.

Figure 54b shows M_{IJ} for the SB and NSB seals versus ω at $\Delta P = 2.07$ bar and at the centered position for the high pre-swirl insert. $\left| M_{IJ} \right|$ generally increases as ω increase. In some cases as at $\omega = 4$ krpm and 6 krpm, the signs of M_{XY} and M_{YX} are the same for the SB seal. $\left| M_{IJ} \right|$ is generally reduced from NSB to SB seals.
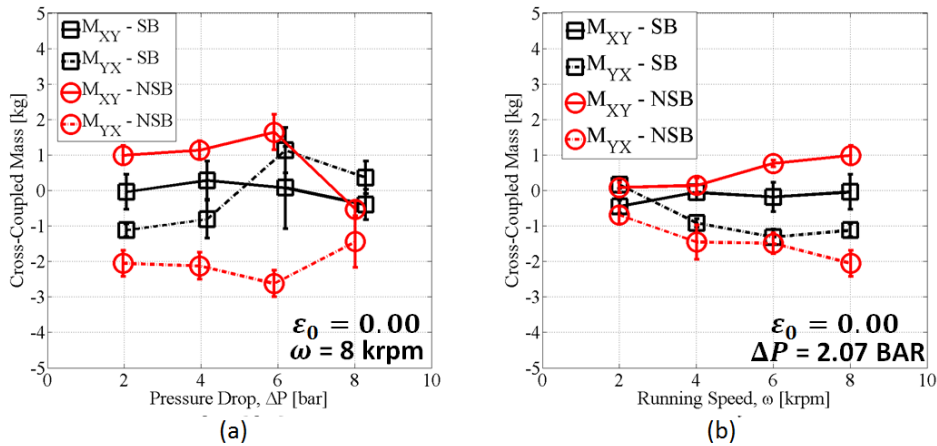
Figure 54. Comparison of SB vs NSB for the high pre-swirl insert of M_{IJ} at $\varepsilon_0 = 0.00$ plotted against (a) ΔP at $\omega = 8$ krpm and (b) ω at $\Delta P = 2.07$ bar

Figure 55 shows M_{IJ} for the SB and NSB seals versus ε_0 at $\omega = 8$ krpm and $\Delta P = 8.27$ bar for the high pre-swirl insert. For the SB seals, for $\varepsilon_0 \leq 0.53$, $\left| M_{IJ} \right|$ remains constant. For the NSB seal, $\left| M_{YX} \right|$ drops sharply for $\varepsilon_0 \geq 0.27$. At $\varepsilon_0 = 0.80$, $\left| M_{IJ} \right|$ increase for both SB and NSB seals. For all test points the sign of M_{IJ} for the SB seals is

negative, while the sign of M_{IJ} for the NSB seals is different for $\varepsilon_0 \leq 0.53$. Generally speaking, moving from NSB to SB seals eliminates the impact of M_{XY} and M_{YX} on stability.
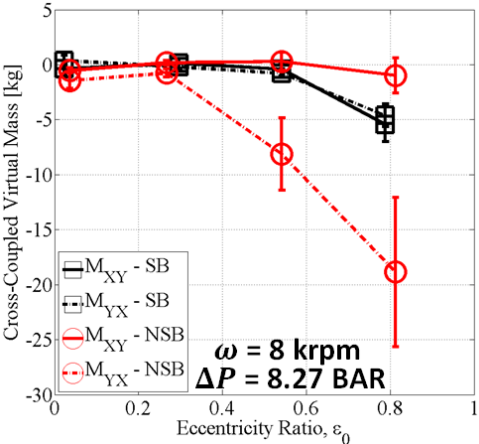
Figure 55. Comparison of SB vs NSB for the high pre-swirl insert for M_{IJ} plotted against ε_0 at $\omega = 8$ krpm and $\Delta P = 8.27$ bar

6. STABILITY COMPARISON

Rotordynamic stability is important when examining the influence of swirl brakes and their effectiveness. Two parameters used to characterize the rotordynamic stabilizing characteristics of an annular seal from the tests are whirl frequency ratio (WFR) and effective damping (C_{eff}).

6.1 Whirl Frequency Ratio

WFR is a good benchmark of determining the stability of a given seal at different operating conditions, particularly the impact of changes in ε_0. Defined by Lund [23], for a flexible rotor supported by hydrodynamic bearings, the onset speed of instability is

$$OSI = \frac{\omega_n}{WFR} \tag{23}$$

Lund's derivation for WFR is based on a Reynolds Equation model and does not include M_{XY} and M_{YX}. San Andrés [24] model will be used here for WFR because the M_{XY} and M_{YX} terms are not negligible, and in some cases have different signs.

Figure 56a shows WFR versus ΔP for the NSB seals at $\omega = 8$ krpm and $\varepsilon_0 = 0.00$ for all pre-swirl cases. WFR decreases as ΔP increases. WFR for the high pre-swirl insert is marginally larger than the medium and radial injection inserts. The $|WFR| \approx 0.5$ means that the NSB seals have characteristics that are similar to a plain journal bearing and follow the expected trends for long liquid annular seals.

Figure 56b shows WFR versus ω for the NSB seals at $\Delta P = 8.27$ bar and $\varepsilon_0 = 0.00$. WFR consistently drops in moving from high to medium to radial injection. At

lower ω, the high and medium pre-swirls are significantly higher than for radial injection. Results for all pre-swirl inserts tend to converge as ω approaches 8 krpm.

Figure 56c shows WFR versus ε_0 for the NSB seal at $\omega = 8$ krpm and $\Delta P = 8.27$ bar for all pre-swirl inserts. WFR increases slightly as ε_0 increases. Clearly WFR ≈ 0.5.
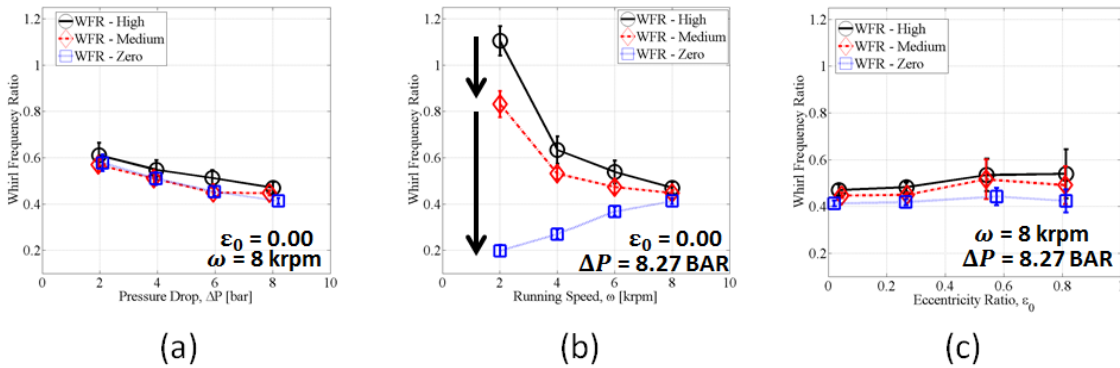
Figure 56. Plot for WFR for NSB seals across all pre-swirl inserts plotted against (a) ΔP at $\omega = 8$ krpm and $\varepsilon_0 = 0.00$ (b) ω at $\Delta P = 8.27$ bar and $\varepsilon_0 = 0.00$ (c) ε_0 at $\omega = 8$ krpm and $\Delta P = 8.27$ bar

Figure 57a shows WFR versus ΔP for the SB seal at $\omega = 8$ krpm and $\varepsilon_0 = 0.00$ for all pre-swirl inserts. WFR decreases as ΔP increases. This means the stability increases as ΔP increases. When comparing SB to NSB (Fig. 56a), WFR drops with increasing ΔP for both seals. The marked difference is that for SB seals the WFR is smaller (less destabilizing) than that of the NSB seals.

Figure 57b shows WFR versus ω for the SB seal at $\Delta P = 8.27$ bar and $\varepsilon_0 = 0.00$ for all pre-swirl inserts. WFR remains fairly constant as ω increases, meaning stability is not greatly dependent on ω. The radial injection insert is markedly lower than the high

and medium pre-swirls. Fig. 57b WFR values for NSB seals are markedly lower (less destabilizing) than for SB seals in 56b.

Figure 57c shows WFR versus ε_0 for the SB seal at $\omega = 8$ krpm and $\Delta P = 8.27$ bar for all pre-swirl inserts. WFR increases as ε_0 increases. This means as ε_0 increases the destabilizing effect increases. Comparing the WFR results of Fig. 57c for the NSB seals of Fig. 56c for NSB seals, WFR is consistently smaller (less destabilizing) for SB seals than NSB seals. However WFR increases more rapidly with increasing ε_0 for SB seals than NSB seals. Generally the WFR values increase in magnitude on moving from radial injection to medium injection and then to high pre-swirl injection.

All of Fig. 57 displays WFR< 0.5 for all cases. Reductions in WFR follow the prior changes in PSR with pre-swirl seen in Table 6. The WFR is reduced the greatest with swirl-brakes in the centered position, at low ω, and at higher ΔP.
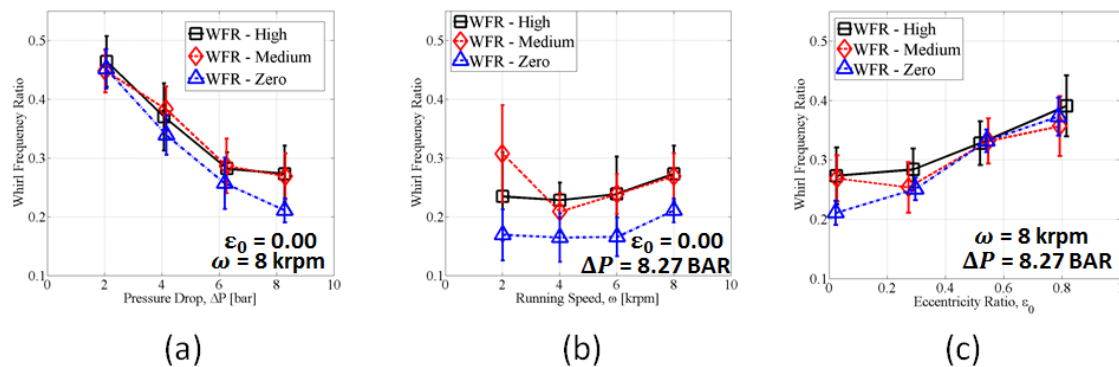
Figure 57. Plot for *WFR* for SB seals across all pre-swirl inserts plotted against (a) ΔP at $\omega = 8$ krpm and $\varepsilon_0 = 0.00$ (b) ω at $\Delta P = 8.27$ bar and $\varepsilon_0 = 0.00$ (c) ε_0 at $\omega = 8$ krpm and $\Delta P = 8.27$ bar

6.2 Effective Damping

From Eq. (1), C_{eff} is

$$C_{eff} = C - \frac{k}{\omega} + \frac{m}{\omega^2} \tag{25}$$

C_{eff} can be used to compare the stabilizing characteristics of two seals in the centered position.

Figure 58a compares C_{eff} versus ω for SB and NSB seals at $\Delta P = 8$ bar and $\varepsilon_0 = 0.00$ for the high pre-swirl insert. For increasing ω, the C_{eff} for the SB seals remain fairly constant versus the NSB seal that decreases. The negative C_{eff} at 2 krpm for the NSB seal shows the destabilizing characteristics of the NSB seal at those conditions.

Figure 58b compares C_{eff} versus ΔP between SB and NSB seals for $\omega = 4$ krpm and $\varepsilon_0 = 0.00$ for the high pre-swirl insert. C_{eff} increases as ΔP increases for SB and NSB seals. The SB seals C_{eff} value is approximately double comparable values for the to NSB. Clearly swirl brakes increase C_{eff} and improve the seals stabilizing capacity.
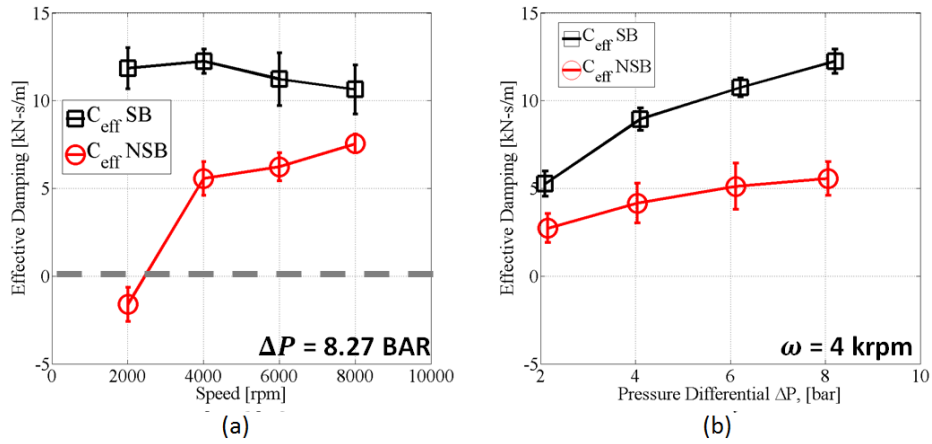
Figure 58. A comparison of C_{eff} of the high pre-swirl insert for SB and NSB seals plotted for ε_0 = 0.00 against (a) ω at ΔP = 8.27 bar and (b) ΔP at ω = 2 krpm

7. SUMMARY AND CONCLUSIONS

Smooth annular seals were modified from a no swirl-brake (NSB) configuration to a swirl brake (SB) configuration by modifying the stator; 36 slots were machined circumferentially at the seal inlet with a chord, depth, and height of 5.08 mm. The seal radial clearance C_r was 203.2 μm, and the seal had a length to diameter ratio (L/D) of 0.45. The seal was tested at three different imposed pre-swirl ratios (PSR), utilizing radial, medium, and high pre-swirl inserts. Tests were conducted across four running speeds (2, 4, 6, 8 krpm), four pressure drops (2, 4, 6, 8 bar), and four eccentricity ratios (0.00, 0.27, 0.53, 0.80). The process fluid was ISO VG 2 oil at an inlet temperature of 46.1 °C that seemed to produce laminar, transitional, and turbulent flow conditions. Test results were compared to results for a seal of similar geometry (L/D of 0.50) with no swirl brakes (NSB). Note that circumferential velocity was measured at one location upstream of the seal and two locations downstream of the seal.

The flow rate ($\dot{Q}$) increased as the imposed pre-swirl ratio (PSR) increased, meaning highest $\dot{Q}$ values were seen with the high pre-swirl case. $\dot{Q}$ increased with increasing pressure drop (ΔP) and decreased with increasing running speed (ω). The inlet circumferential velocity was determined upstream of the seal with pitot tubes and used to define PSR. Measured PSR for SB seals was surprisingly less than that of NSB seals. The greatest reduction in PSR values recorded were at high ΔP, low ω, and toward the centered position; a reduction of approximately 50%.

Dynamic characteristics were largely independent of the imposed pre-swirl condition for the SB seals. The direct stiffness coefficients (K_{YY} and K_{XX}) for SB seals were higher than NSB. This result is surprising as swirl-brakes are not generally thought to impact K_{YY},K_{XX}. As expected, the magnitude of the cross-coupled stiffness coefficients (K_{YX} and K_{XY}) were lower for SB seals than the NSB seal. Direct damping (C_{YY} and C_{XX}) increased only slightly for SB seals compared to NSB seals. The magnitude of the cross-coupled damping (C_{YX} and C_{XY}) values were lower for SB seals than NSB seals. Direct virtual mass (M_{YY} and M_{XX}) terms were lower for SB seals than NSB seals. The magnitude of the cross-coupled virtual mass terms (M_{YX} and M_{XY}) were generally lower for SB seals than NSB seals.

A notable phenomenon was observed with the direct stiffness. At certain test points the direct stiffness would abruptly increase and then decrease with steadily increasing ΔP and ω. The behavior could be arguably explained by moving through the laminar/transitional/turbulent boundaries.

Whirl frequency ratio (WFR) and effective damping (C_{eff}) were used for comparative stability analysis. The NSB seals' WFR was on average approximately 0.5, which is expected for long, smooth liquid annular seals. For SB seals, WFR was on average approximately 0.25. The WFR was lowest at ~0.20 for SB seals at high ΔP, low ω, and toward the centered position.

Effective damping, C_{eff}, can be used to compare the net damping of the two seal geometries in the centered position. C_{eff} was consistently and markedly higher for SB

seals compared to NSB seals, meaning swirl breaks increase the stabilizing characteristics of liquid annular seals. The increase in C_{eff} in moving from NSB to SB seals was also maximum at the same conditions as the lowest WFR values; namely high ΔP, low ω, and toward the centered position.

Decreases in PSR have a positive effect on SB seal rotordynamic performance. Clearly swirl brakes have a positive rotordynamic stability impact by decreasing seal inlet pre-swirl to the seal. The best improved results for WFR and C_{eff} were noted at lower ω's, higher ΔP's and at lower ε_0 values. At these conditions K_{XX} and K_{YY} for the SB seals is significantly higher than NSB seals.

Complete results of static and dynamic data for annular seals before and after swirl brake modification are now available for analysis. Future work could include: a CFD analysis of the results for better understanding of how the circumferential fluid flow interacts with the swirl brakes before entering the seal, finding a more efficient design for swirl brakes for liquid annular seal applications, and creating a predictive code to determine how swirl brake geometries will affect pump rotordynamics.

REFERENCES

[1] Baldassarre, L., Bernocchi, A., Fontana, M., Guliolmo, A., and Guido, M., 2014, "Optimization of Swirl Brake Design and Assessment of its Stabilizing Effect on Compressor Rotordynamic Performance," 43rd Turbomachinery & 30th Pump Users Symposium, Houston, TX

[2] Massey, I.C., 1984, "Subsynchronous Vibration Problems in High-Speed, Multistage Centrifugal Pumps," Proceedings of the Fourteenth Turbomachinery Symposium, pp. 11-16

[3] Gotlieb., M., Jacques, O., 2007, "Electrical Submersible Pump," U.S. Patent No. 8287235 B2

[4] Childs, D., Norrbin, C., Phillips, S., 2014, "A Lateral Rotordynamics Primer on Electrical Submersible Pumps (ESPs) for Deep Subsea Applications," 43rd Turbomachinery & 30th Pump Users Symposia, Houston, TX

[5] Black, H.F., 1969, "Effects of Hydraulic Forces in Annular Pressure Seals on the Vibrations of Centrifugal Pump Rotors," Journal of Mechanic Engineering Science, **11**, 206-213.

[6] Black, H.F., 1979, "Effect of Fluid-Filled Clearance Spaces on Centrifugal Pump and Submerged Motor Vibrations," Eighth Turbomachinery Symposium, College Station, Texas, Texas A&M University, pp. 29-34.

[7] Black, H.F., Allaire, P., and Barrett, L., 1981, "Inlet Flow Swirl in Short Turbulent Annular Seal Dynamics," Ninth International Conference of Fluid Sealing, Noordwijkerhout, Netherlands, pp. 141-152.

[8] Childs, D., 1983, "Dynamic Analysis of Turbulent Annular Seals Based on Hirs'

Lubrication Equation," Journal of Lubrication Technology, 105, pp. 429-436

[9] Hirs, G.G., 1973, "A Bulk-Flow Theory for Turbulence in Lubricant Films," Journal of Lubrication Technology, pp. 137-145.

[10] Childs, D., 1983, "Finite-Length Solutions for Rotordynamic Coefficients of Turbulent Annular Seals," ASME Journal of Lubrication, **105**, pp. 437-444.

[11] Nelson, C., and Nguyen, D., 1988, "Analysis of Eccentric Annular Incompressible Seals: Part 2 - Effects of Eccentricity on Rotordynamic Coefficients," Journal of Tribology, **110**, pp. 361-366.

[12] Pinkus, O., and Sternlicht, B., 1961, Theory of Hydrodynamic Lubrication, New York: McGraw- Hill.

[13] Childs, D., 2013, Turbomachinery Rotordynamics with Case Studies, Wellborn, Texas: Minter Spring Publishing

[14] Lomakin, A., 1958, "Calculation of Critical Number of Revolutions and the Conditions Necessary for Dynamic Stability of Rotors in High-Pressure Hydraulic Machines When Taking Into Account Forces Originating in Sealings," Journal for Power and Mechanical Engineering (In Russian), 14.

[15] Benckert, H., and Wachter, J., 1980, "Flow Induced Spring Constants of Labyrinth Seals for Applications in Rotor Dynamics," Proceedings of the 1st Workshop on Rotordynamic Instability Problems in High-Performance Turbomachinery, College Station, Texas, Texas A&M University, pp. 189-212

[16] Valantas, R., and Bolleter, U., 1988, "Solutions to Abrasive Wear-Related Rotordynamic Instability Problems on Prudhoe Bay Injections Pumps," Proceedings of the Fifth International Pump Users Symposium, pp. 3-10

[17] Frei, A., Guelich, J., Eichhorn, G., Eberl, J., and McCloskey, T., 1990, "Rotordynamic

and Dry Running Behavior of a Full Scale Test Boiler Feed Pump," Proceedings of the Seventh International Pump Users Symposium, pp. 81-92

[18] Nielsen, K.K., Van den Braembussche, R.A., 1998, "Optimization of Swirl Brakes by Means of a 3D Navier-Stokes Solver," International Gas Turbine & Aeroengine Congress and Exhibition, pp. V004T09A064-V004T09A064

[19] Kaul, A., 1999, *Design and Development of a Test Setup for the Experimental Determination of the Rotordynamic and Leakage Characteristics of Annular Bushing Oil Seals,* College Station, Texas: Texas A&M University.

[20] Glienicke, J., 1966-67, "Experimental Investigation of the Stiffness and Damping Coefficients of Turbine Bearings and Their Application to Instability Prediction," in *Proceedings of IMechE 1966-67*, **181**, pp. 116-129.

[21] Zirkelback, N., San Andrés, L., 1996, "Bulk-Flow Model for the Transition to Turbulence Regime in Annular Pressure Seals," Tribology Transactions, **39**, pp. 835-842

[22] Rouvas, C., and Childs, D.W., 1993, "A Parameter Identification Method for the Rotordynamic Coefficients of a High Reynolds Number Hydrostatic Bearing," Jounal of Vibration and Acoustics, 115, pp. 264-270.

[23] Childs, D., and Hale, K., 1994, "A Test Apparatus and Facility to Identify the Rotordynamic Coefficients of High-Speed Hydrostatic Bearings," *Journal of Tribology,* **116**, pp. 337-343.

[24] San Andrés, L., 1991, "Analysis of Variable Fluid Properties, Turbulent Annular Seals," *Transactions of the ASME*, **113**, 694-702.

[25] Moreland, J.A., 2016 "Influence of Pre-Swirl and Eccentricity in Smooth

Stator/Grooved Rotor Liquid Annular Seals, Measured Static and Rotordynamic

Characteristics," M.S. Thesis, Texas A&M University

APPENDIX A

TEST CONDITIONS TABLE

Table A.1 gives the reference for the test point number in the left column for the test condition corresponding to ω, ΔP, and ε_0. This test point number is used for test point in the left hand column for reference in Appendix B.

Table A.1. Test Condition Matrix

Test Point	Target ω	Target ΔP	Target ε_0
	[rpm]	[bar]	[-]
1	2000	2.068	0.00
2	2000	2.068	0.27
3	2000	2.068	0.53
4	2000	2.068	0.80
5	2000	4.137	0.00
6	2000	4.137	0.27
7	2000	4.137	0.53
8	2000	4.137	0.80
9	2000	6.205	0.00
10	2000	6.205	0.27
11	2000	6.205	0.53
12	2000	6.205	0.80
13	2000	8.274	0.00
14	2000	8.274	0.27
15	2000	8.274	0.53
16	2000	8.274	0.80
17	4000	2.068	0.00
18	4000	2.068	0.27
19	4000	2.068	0.53
20	4000	2.068	0.80
21	4000	4.137	0.00
22	4000	4.137	0.27
23	4000	4.137	0.53
24	4000	4.137	0.80
25	4000	6.205	0.00
26	4000	6.205	0.27
27	4000	6.205	0.53
28	4000	6.205	0.80

Test Point	Target ω	Target ΔP	Target ε_0
	[rpm]	[bar]	[-]
29	4000	8.274	0.00
30	4000	8.274	0.27
31	4000	8.274	0.53
32	4000	8.274	0.80
33	6000	2.068	0.00
34	6000	2.068	0.27
35	6000	2.068	0.53
36	6000	2.068	0.80
37	6000	4.137	0.00
38	6000	4.137	0.27
39	6000	4.137	0.53
40	6000	4.137	0.80
41	6000	6.205	0.00
42	6000	6.205	0.27
43	6000	6.205	0.53
44	6000	6.205	0.80
45	6000	8.274	0.00
46	6000	8.274	0.27
47	6000	8.274	0.53
48	6000	8.274	0.80
49	8000	2.068	0.00
50	8000	2.068	0.27
51	8000	2.068	0.53
52	8000	2.068	0.80
53	8000	4.137	0.00
54	8000	4.137	0.27
55	8000	4.137	0.53
56	8000	4.137	0.80
57	8000	6.205	0.00
58	8000	6.205	0.27
59	8000	6.205	0.53
60	8000	6.205	0.80
61	8000	8.274	0.00
62	8000	8.274	0.27
63	8000	8.274	0.53
64	8000	8.274	0.80

APPENDIX B

SB TABULATED RESULTS

Assembly 1 – High Pre-Swirl Insert

Table B.2. Measured Pressure Drop, Leakage, Static Force, Eccentricity and Attitude Angle of the SB seal with the high pre-swirl insert

Measured ω	$u\omega$	Measured ΔP	$u\Delta P$	$\dot{Q}$	$u\dot{Q}$	F_s	uF_s	Measured ε_0	φ
[rpm]	[rpm]	[bar]	[bar]	[LPM]	[LPM]	[N]	[N]	[-]	[deg]
2000.03	0.25	2.05	0.01	16.86	0.01	-4.17	27.12	0.01	-1.13
2000.49	0.39	2.05	0.01	16.86	0.01	85.00	0.65	0.26	-0.05
2000.66	0.47	2.09	0.01	17.43	0.01	141.54	1.40	0.53	-0.07
2000.67	0.19	2.05	0.04	19.38	0.01	181.03	4.19	0.8	0.02
2002.41	0.21	4.07	0.01	27.35	0.01	-16.71	3.02	0.01	0.89
2002.13	0.45	4.10	0.01	28.14	0.02	120.64	6.26	0.28	0.18
2001.62	0.46	4.07	0.02	29.22	0.02	229.24	7.00	0.53	0.15
2001.24	0.46	4.14	0.01	32.34	0.02	412.03	29.35	0.86	0.50
2001.22	0.41	6.21	0.01	36.98	0.01	-6.97	6.38	0.05	0.56
2001.34	0.57	6.21	0.01	37.37	0.01	119.45	15.79	0.28	0.10
2001.01	0.24	6.18	0.01	39.76	0.02	317.42	13.48	0.54	0.10
2000.99	0.27	6.23	0.02	42.69	0.03	443.40	8.98	0.79	0.11
2002.72	0.49	8.42	0.01	45.15	0.02	-29.72	2.25	0.03	-0.12
2002.40	0.43	8.35	0.01	45.37	0.02	109.41	26.49	0.27	0.07
2001.49	0.18	8.30	0.01	47.87	0.03	392.27	18.86	0.54	0.27
2001.00	0.27	8.29	0.01	51.06	0.06	586.06	10.27	0.80	0.22
4004.42	0.27	2.10	0.02	14.99	0.02	12.29	0.39	0.02	0.84
4005.18	0.09	2.03	0.01	14.74	0.02	55.95	1.64	0.28	0.18
4005.65	0.18	2.12	0.02	15.83	0.02	127.05	6.35	0.52	0.16
4006.13	0.19	2.02	0.22	17.99	0.01	303.67	51.29	0.82	0.30
4009.52	0.37	4.10	0.00	27.37	0.02	-31.46	3.51	0.05	-1.56
4008.59	0.08	4.12	0.02	28.24	0.03	59.85	8.34	0.27	0.37
4008.23	0.21	4.16	0.01	29.18	0.02	201.66	11.36	0.53	0.21
4007.57	0.54	4.11	0.02	31.62	0.01	405.19	13.28	0.79	0.39
4005.79	0.26	6.21	0.02	35.89	0.01	-38.60	1.07	0.06	-0.60
4005.95	0.18	6.14	0.02	36.54	0.02	60.92	3.99	0.29	0.05
4006.57	0.17	6.17	0.01	38.84	0.03	257.10	2.11	0.53	0.07
4006.62	0.47	6.23	0.01	42.40	0.02	458.02	9.22	0.81	0.15
4010.16	0.65	8.20	0.02	44.07	0.02	-38.21	5.48	0.03	-0.89

Table B.2. Measured static characteristics of the SB seal with the high pre-swirl insert

Measured ω	$u\omega$	Measured ΔP	$u\Delta P$	$\dot{Q}$	$u\dot{Q}$	F_s	uF_s	Measured ε_0	φ
[rpm]	[rpm]	[bar]	[bar]	[LPM]	[LPM]	[N]	[N]	[-]	[deg]
4009.34	0.38	8.38	0.01	45.05	0.01	91.23	14.81	0.28	0.29
4009.76	0.11	8.25	0.01	47.23	0.01	348.78	5.47	0.54	0.18
4008.75	0.25	8.22	0.01	50.44	0.06	550.26	27.12	0.81	0.09
5999.53	0.25	2.12	0.01	16.70	0.01	25.89	5.00	0.03	1.16
6000.31	0.51	2.02	0.03	16.75	0.02	87.00	0.94	0.26	0.26
6000.60	0.48	2.07	0.02	18.89	0.02	155.08	5.56	0.55	0.21
6001.11	0.31	2.11	0.02	21.58	0.02	355.91	13.51	0.79	0.27
6005.98	0.44	4.14	0.01	28.30	0.02	-23.06	13.73	0.11	-1.29
6004.88	0.33	4.19	0.01	29.00	0.00	152.77	4.32	0.29	0.38
6003.79	0.42	4.08	0.01	30.64	0.02	254.70	7.42	0.54	0.35
6002.92	0.45	4.17	0.02	34.33	0.05	476.76	74.06	0.78	0.39
5999.34	0.38	6.21	0.02	39.51	0.01	2.08	3.93	0.03	1.07
6000.82	0.14	6.12	0.01	39.74	0.03	159.51	5.60	0.28	0.26
6001.40	0.33	6.27	0.02	43.00	0.01	282.31	9.57	0.52	0.24
6001.22	0.30	6.19	0.01	46.29	0.02	542.99	22.02	0.80	0.29
6002.69	0.49	8.63	0.01	50.82	0.02	-14.88	14.35	0.03	1.18
6002.34	0.27	8.32	0.01	50.42	0.01	189.66	8.77	0.27	0.29
6002.60	0.45	8.29	0.02	52.77	0.03	340.23	16.51	0.53	0.30
6002.88	0.28	8.39	0.01	56.20	0.03	581.61	47.32	0.76	0.22
7999.05	0.34	2.07	0.02	13.95	0.02	-9.37	33.82	0.05	-0.19
7999.54	0.07	2.01	0.04	14.00	0.01	57.72	7.82	0.27	0.22
7999.73	1.10	2.12	0.02	15.63	0.01	187.05	8.77	0.52	0.36
8002.71	1.67	2.10	0.01	17.66	0.01	729.84	32.04	0.80	0.42
8003.64	0.64	4.07	0.01	24.74	0.02	57.98	5.18	0.04	0.75
8004.09	0.12	4.22	0.02	26.83	0.01	174.85	8.90	0.29	0.21
8004.64	0.67	4.17	0.02	28.70	0.02	322.42	14.09	0.52	0.33
8004.85	0.66	4.13	0.05	32.59	0.02	800.25	55.77	0.79	0.48
7998.04	0.59	6.28	0.02	36.07	0.04	3.34	7.10	0.03	-1.17
7999.01	0.18	6.15	0.01	36.40	0.01	178.53	7.29	0.28	0.14
7998.89	0.33	6.21	0.01	38.88	0.03	350.59	11.64	0.52	0.29
7999.31	0.26	6.26	0.03	43.15	0.04	761.23	33.45	0.79	0.48
8000.44	0.34	8.28	0.02	45.39	0.01	-3.23	5.07	0.03	-0.50
8000.73	0.56	8.20	0.01	45.90	0.02	203.58	19.71	0.29	0.07
8001.04	0.32	8.29	0.01	48.43	0.02	408.25	18.65	0.52	0.20
8000.83	0.25	8.22	0.01	53.10	0.01	771.93	5.00	0.82	0.28

Table B.3. PSR, OSR, Inlet and Outlet Temperature, and Reynolds Number of the SB seal with the high pre-swirl insert

Test Point	PSR	OSR	T_i	uT_i	T_e	uT_e	Re_z	Re_θ	Re
	[-]	[-]	[°C]	[°C]	[°C]	[°C]	[-]	[-]	[-]
1	0.512	0.281	46.38	0.05	46.13	0.05	1.10E+03	8.62E+02	1.40E+03
2	0.519	0.307	46.40	0.05	46.22	0.05	1.10E+03	8.63E+02	1.40E+03
3	0.481	0.309	46.34	0.05	46.19	0.05	1.15E+03	8.63E+02	1.44E+03
4	0.423	0.324	46.45	0.05	46.25	0.05	1.21E+03	8.64E+02	1.49E+03
5	0.607	0.292	46.43	0.05	46.38	0.05	1.70E+03	8.67E+02	1.91E+03
6	0.579	0.324	46.45	0.05	46.42	0.05	1.70E+03	8.67E+02	1.91E+03
7	0.513	0.329	46.15	0.05	46.19	0.05	1.69E+03	8.63E+02	1.90E+03
8	0.409	0.357	45.91	0.05	45.94	0.05	1.83E+03	8.59E+02	2.03E+03
9	0.680	0.326	45.97	0.05	46.09	0.05	2.19E+03	8.62E+02	2.35E+03
10	0.634	0.316	45.88	0.05	46.03	0.05	2.18E+03	8.61E+02	2.35E+03
11	0.513	0.320	45.91	0.05	46.01	0.05	2.19E+03	8.60E+02	2.36E+03
12	0.452	0.335	45.86	0.05	45.94	0.05	2.31E+03	8.59E+02	2.46E+03
13	0.846	0.301	46.26	0.05	46.43	0.05	2.62E+03	8.68E+02	2.76E+03
14	0.823	0.335	46.30	0.05	46.48	0.05	2.64E+03	8.68E+02	2.77E+03
15	0.749	0.370	46.39	0.05	46.54	0.05	2.65E+03	8.69E+02	2.79E+03
16	0.747	0.347	46.43	0.05	46.60	0.05	2.77E+03	8.69E+02	2.90E+03
17	0.420	0.235	46.01	0.05	46.48	0.05	8.98E+02	1.74E+03	1.94E+03
18	0.409	0.265	46.00	0.05	46.43	0.05	9.01E+02	1.74E+03	1.94E+03
19	0.405	0.266	46.27	0.05	46.61	0.05	9.94E+02	1.74E+03	2.00E+03
20	0.389	0.269	46.57	0.05	46.91	0.05	9.90E+02	1.75E+03	2.00E+03
21	0.507	0.248	46.53	0.05	46.80	0.05	1.57E+03	1.75E+03	2.34E+03
22	0.487	0.289	46.49	0.05	46.80	0.05	1.57E+03	1.75E+03	2.34E+03
23	0.474	0.295	46.04	0.05	46.28	0.05	1.59E+03	1.73E+03	2.35E+03
24	0.488	0.298	46.41	0.05	46.64	0.05	1.69E+03	1.74E+03	2.42E+03
25	0.577	0.274	45.73	0.05	46.08	0.05	2.04E+03	1.72E+03	2.66E+03
26	0.559	0.278	45.73	0.05	46.09	0.05	2.05E+03	1.72E+03	2.67E+03
27	0.481	0.295	45.83	0.05	46.20	0.05	2.09E+03	1.73E+03	2.70E+03
28	0.467	0.306	45.87	0.05	46.28	0.05	2.22E+03	1.73E+03	2.81E+03
29	0.445	0.274	45.35	0.05	45.95	0.05	2.40E+03	1.72E+03	2.95E+03
30	0.481	0.292	46.38	0.05	46.15	0.05	2.04E+03	1.73E+03	3.03E+03
31	0.468	0.312	46.40	0.05	46.41	0.05	2.11E+03	1.74E+03	3.06E+03
32	0.465	0.291	46.34	0.05	46.57	0.05	2.25E+03	1.74E+03	3.16E+03

Table B.4. PSR, OSR, Inlet and Outlet Temperature, and Reynolds Number of the SB seal with the high pre-swirl insert

Test Point	PSR	OSR	T_i	uT_i	T_e	uT_e	Re_z	Re_θ	Re
	[-]	[-]	[°C]	[°C]	[°C]	[°C]	[-]	[-]	[-]
33	0.449	0.200	46.11	0.05	47.82	0.05	7.52E+02	2.66E+03	2.69E+03
34	0.432	0.207	46.40	0.05	48.10	0.05	7.58E+02	2.68E+03	2.71E+03
35	0.408	0.231	46.74	0.05	48.32	0.05	8.60E+02	2.69E+03	2.75E+03
36	0.388	0.257	46.59	0.05	48.07	0.05	9.80E+02	2.68E+03	2.79E+03
37	0.421	0.221	46.49	0.05	47.76	0.05	1.28E+03	2.66E+03	2.90E+03
38	0.409	0.266	45.82	0.05	47.08	0.05	1.30E+03	2.63E+03	2.88E+03
39	0.397	0.265	46.35	0.05	47.48	0.05	1.39E+03	2.65E+03	2.94E+03
40	0.392	0.271	46.39	0.05	47.51	0.05	1.55E+03	2.65E+03	3.03E+03
41	0.456	0.238	45.82	0.05	46.88	0.05	1.77E+03	2.62E+03	3.12E+03
42	0.439	0.273	45.89	0.05	46.99	0.05	1.78E+03	2.63E+03	3.13E+03
43	0.432	0.282	46.27	0.05	47.17	0.05	1.94E+03	2.63E+03	3.24E+03
44	0.431	0.308	46.54	0.05	47.41	0.05	2.10E+03	2.65E+03	3.35E+03
45	0.407	0.245	45.84	0.05	46.80	0.05	2.28E+03	2.62E+03	3.44E+03
46	0.391	0.294	46.55	0.05	47.50	0.05	2.29E+03	2.65E+03	3.47E+03
47	0.386	0.310	45.28	0.05	46.15	0.05	2.34E+03	2.59E+03	3.46E+03
48	0.420	0.288	46.32	0.05	47.32	0.05	2.54E+03	2.64E+03	3.63E+03
49	0.498	0.211	44.61	0.05	49.10	0.05	6.12E+02	3.64E+03	3.41E+03
50	0.498	0.231	44.66	0.05	49.06	0.05	6.14E+02	3.64E+03	3.42E+03
51	0.461	0.206	45.31	0.05	49.28	0.05	6.94E+02	3.65E+03	3.47E+03
52	0.422	0.192	46.49	0.05	49.99	0.05	8.00E+02	3.70E+03	3.56E+03
53	0.429	0.198	46.34	0.05	49.12	0.05	1.12E+03	3.64E+03	3.64E+03
54	0.410	0.226	47.11	0.05	49.85	0.05	1.23E+03	3.69E+03	3.72E+03
55	0.396	0.253	45.21	0.05	48.05	0.05	1.27E+03	3.57E+03	3.62E+03
56	0.379	0.254	46.22	0.05	48.56	0.05	1.47E+03	3.60E+03	3.75E+03
57	0.416	0.233	45.20	0.05	47.56	0.05	1.60E+03	3.54E+03	3.75E+03
58	0.396	0.262	45.73	0.05	48.00	0.05	1.63E+03	3.57E+03	3.79E+03
59	0.380	0.260	46.28	0.05	48.50	0.05	1.76E+03	3.60E+03	3.88E+03
60	0.368	0.264	45.64	0.05	47.80	0.05	1.93E+03	3.55E+03	3.92E+03
61	0.349	0.232	45.73	0.05	47.90	0.05	2.03E+03	3.56E+03	3.98E+03
62	0.341	0.263	46.02	0.05	48.07	0.05	2.06E+03	3.57E+03	4.01E+03
63	0.336	0.271	46.22	0.05	48.20	0.05	2.18E+03	3.58E+03	4.09E+03
64	0.335	0.279	46.09	0.05	47.97	0.05	2.39E+03	3.56E+03	4.19E+03

Table B.5. Stiffness coefficients and uncertainties for the SB seal with the high pre-swirl insert.

Test Point	K_{XX} [MN/m]	$u_{K_{XX}}$ [MN/m]	K_{YY} [MN/m]	$u_{K_{YY}}$ [MN/m]	K_{XY} [MN/m]	$u_{K_{XY}}$ [MN/m]	K_{YX} [MN/m]	$u_{K_{YX}}$ [MN/m]
1	1.72	0.09	1.60	0.69	0.39	0.25	-0.11	0.11
2	1.54	0.13	0.58	0.61	0.74	0.30	-0.50	0.08
3	1.27	0.11	-0.12	0.30	0.87	0.29	-0.76	0.09
4	0.92	0.21	-1.23	3.55	6.72	1.20	-1.27	0.71
5	1.82	0.12	1.53	0.25	1.13	0.17	-0.92	0.06
6	2.33	0.11	2.34	0.23	0.80	0.43	-0.58	0.09
7	2.18	0.15	1.29	0.20	1.41	0.19	-0.74	0.09
8	-0.61	1.19	11.03	11.16	6.09	4.43	-4.44	3.84
9	1.62	0.43	1.44	0.37	0.72	0.36	-0.87	0.26
10	2.39	0.19	4.08	0.36	0.59	0.28	-0.76	0.12
11	3.00	0.18	2.90	0.28	1.40	0.55	-0.83	0.17
12	2.47	0.17	1.12	0.75	5.05	0.60	-1.17	0.16
13	2.21	0.24	2.22	0.31	0.71	0.45	-0.81	0.06
14	2.78	0.25	4.13	0.28	0.87	0.59	-0.79	0.19
15	4.05	0.15	4.80	0.41	0.64	0.38	-0.91	0.09
16	2.73	0.39	1.81	4.16	6.10	2.06	-0.96	0.61
17	-0.32	0.14	-0.50	0.28	1.69	0.17	-1.58	0.10
18	0.24	0.13	0.53	0.26	1.25	0.27	-1.68	0.11
19	0.62	0.12	0.85	0.51	2.70	0.23	-1.79	0.22
20	-1.68	1.44	7.36	7.45	12.46	3.92	-6.08	4.97
21	-0.76	0.26	-1.52	0.20	1.70	0.28	-1.94	0.31
22	0.77	0.22	2.02	0.17	0.81	0.28	-1.77	0.18
23	1.28	0.15	1.88	0.38	2.57	0.19	-1.86	0.17
24	-1.44	0.21	4.02	1.03	9.26	0.66	-4.03	0.53
25	-0.24	0.23	-0.58	0.23	1.91	0.15	-1.44	0.19
26	1.06	0.16	3.52	0.28	1.95	0.15	-1.66	0.10
27	2.43	0.11	3.01	0.31	2.42	0.17	-1.55	0.15
28	1.47	0.56	3.18	1.35	11.51	3.17	-3.19	0.39
29	0.70	0.11	0.59	0.37	1.55	0.36	-1.49	0.14
30	1.54	0.12	3.15	0.36	2.14	0.37	-1.96	0.18
31	3.23	0.13	4.95	0.43	2.33	0.51	-1.97	0.14
32	3.77	0.30	4.02	3.51	12.39	1.41	-3.58	0.44

Table B.6. Stiffness coefficients and uncertainties for the SB seal with the high pre-swirl insert.

Test Point	K_{XX} [MN/m]	$u_{K_{XX}}$ [MN/m]	K_{YY} [MN/m]	$u_{K_{YY}}$ [MN/m]	K_{XY} [MN/m]	$u_{K_{XY}}$ [MN/m]	K_{YX} [MN/m]	$u_{K_{YX}}$ [MN/m]
33	0.49	0.18	0.41	0.19	2.46	0.28	-2.57	0.13
34	0.22	0.25	-0.02	0.48	3.07	0.36	-2.41	0.39
35	-0.04	0.26	0.14	0.31	5.21	0.27	-3.18	0.32
36	-1.85	0.82	9.19	5.68	14.73	1.22	-7.68	2.08
37	1.67	0.24	1.83	0.27	2.32	0.42	-2.57	0.26
38	1.01	0.24	1.24	0.35	2.92	0.43	-2.50	0.26
39	0.63	0.25	0.43	0.38	5.02	0.48	-2.99	0.31
40	-2.10	0.54	5.76	3.25	13.91	1.37	-6.55	1.88
41	2.95	0.24	2.75	0.48	2.07	0.37	-2.17	0.40
42	2.67	0.19	2.10	0.18	2.67	0.13	-2.29	0.24
43	1.79	0.22	1.36	0.75	4.39	0.37	-2.60	0.54
44	-0.58	0.25	5.88	3.03	15.81	0.69	-5.96	0.89
45	4.01	0.44	3.93	0.95	2.34	1.14	-2.09	0.33
46	3.41	0.25	2.94	0.25	2.86	0.45	-2.12	0.15
47	2.64	0.35	4.65	0.75	3.10	0.61	-3.69	0.40
48	2.42	0.65	4.36	2.03	12.29	1.58	-4.85	0.79
49	0.03	0.40	-0.28	0.39	3.87	0.55	-3.82	0.24
50	-0.34	0.17	-0.58	0.29	4.33	0.36	-3.92	0.19
51	-0.90	0.27	0.46	0.31	7.55	0.43	-5.18	0.29
52	1.76	0.66	24.00	2.51	10.05	0.83	-18.22	1.13
53	1.62	0.40	1.38	0.44	3.91	0.83	-3.72	0.23
54	0.97	0.62	0.69	0.42	4.83	0.89	-3.85	0.20
55	0.10	0.64	0.58	0.42	7.70	0.83	-4.84	0.35
56	-0.99	0.55	16.58	1.06	14.17	1.67	-16.01	0.69
57	2.64	0.20	2.03	0.31	3.30	0.44	-3.53	0.30
58	2.11	0.19	1.49	0.37	4.39	0.35	-3.72	0.40
59	1.17	0.40	1.25	0.78	7.51	0.41	-4.57	0.58
60	-3.74	1.15	11.21	1.42	18.34	1.99	-11.91	0.54
61	3.49	0.54	3.18	0.54	3.40	0.92	-3.30	0.48
62	3.64	0.41	2.79	0.93	4.01	0.50	-3.52	0.63
63	3.02	0.39	1.27	0.70	7.11	0.69	-4.01	0.65
64	-2.14	0.87	13.11	2.94	21.44	1.60	-11.71	1.15

Table B.7. Damping coefficients and uncertainties for the SB seal with the high pre-swirl insert.

Test Point	C_{XX} [kN-s/m]	$u_{C_{XX}}$ [kN-s/m]	C_{YY} [kN-s/m]	$u_{C_{YY}}$ [kN-s/m]	C_{XY} [kN-s/m]	$u_{C_{XY}}$ [kN-s/m]	C_{YX} [kN-s/m]	$u_{C_{YX}}$ [kN-s/m]
1	8.32	0.28	7.85	1.55	2.6	0.64	-1.63	0.37
2	8.66	0.33	8.83	1.78	2.3	0.77	-1.53	0.24
3	10.12	0.37	14.62	1.35	3.56	0.92	-1.22	0.56
4	16.58	0.66	65.18	8.72	4.01	5.26	-1.08	1.24
5	12.07	0.29	11.75	0.52	2.64	0.95	-1.53	0.31
6	11.61	0.32	11.01	0.57	2.91	1.13	-1.76	0.32
7	12.45	0.22	15.63	0.66	2.64	0.58	-2.08	0.28
8	33.48	7.43	79.35	26.49	-27.27	19.19	-27.81	10.65
9	14.88	1.10	13.77	0.72	3.65	1.09	-2.24	0.82
10	14.23	0.47	13.04	0.83	3.13	0.93	-1.89	0.35
11	14.58	0.26	17.34	1.99	3.44	2.04	-1.98	0.27
12	19.86	0.42	54.77	3.25	1.38	2.32	-5.57	0.70
13	16.05	0.56	14.88	0.71	3.73	1.14	-2.22	0.39
14	16.3	0.41	15.55	1.09	2.75	1.28	-2.16	0.25
15	16.52	0.47	18.09	1.2	2.99	0.99	-2.39	0.27
16	22.81	0.99	57.74	4.75	-4.11	2.28	-8.49	0.94
17	9.52	0.39	8.79	1.29	3.12	0.56	-2.63	0.37
18	9.48	0.46	9.13	0.81	3.33	1.13	-2.99	0.44
19	10.34	0.48	14.56	1.65	4.42	0.62	-3.91	0.61
20	25.63	5.08	46.75	86	-20.6	13.96	-8.93	30.57
21	13.13	0.55	13.42	0.57	4.12	0.68	-3.56	0.73
22	12.4	0.51	11.62	0.46	4.85	0.77	-3.08	0.52
23	12.57	0.29	15.94	0.48	4.92	1.05	-3.77	0.28
24	22.5	0.55	53.79	3.60	-6.68	1.57	-18.28	1.36
25	14.81	0.42	14.67	0.78	5.05	0.89	-4.07	0.62
26	14.74	0.38	13.67	0.83	4.8	0.81	-3.72	0.55
27	14.82	0.36	17.08	0.46	5.78	0.62	-3.49	0.46
28	20.86	0.72	63.84	4.73	4.11	3.28	-8.83	1.34
29	16.22	0.32	15.52	0.96	5.08	0.77	-4.03	0.57
30	16.48	0.37	16.18	0.82	4.63	0.83	-4.38	0.30
31	16.42	0.35	18.83	1.08	5.41	1.05	-3.93	0.29
32	23.69	0.77	65.36	4.17	4.03	3.51	-2.17	0.59

Table B.8. Damping coefficients and uncertainties for the SB seal with the high pre-swirl insert.

Test Point	C_{XX} [kN-s/m]	$u_{C_{XX}}$ [kN-s/m]	C_{YY} [kN-s/m]	$u_{C_{YY}}$ [kN-s/m]	C_{XY} [kN-s/m]	$u_{C_{XY}}$ [kN-s/m]	C_{YX} [kN-s/m]	$u_{C_{YX}}$ [kN-s/m]
33	9.44	0.96	8.93	0.89	5.44	1.91	-4.29	0.33
34	10.41	0.71	10.47	1.42	4.87	1.10	-4.82	0.71
35	12.26	0.75	17.56	1.40	5.78	0.93	-5.91	0.85
36	20.4	1.57	64.38	17.4	-1.46	5.14	-17.35	5.93
37	12.61	0.59	12.09	2.12	5.20	1.37	-4.99	0.94
38	12.26	0.45	12.70	1.13	5.40	0.74	-5.04	0.77
39	14.17	0.77	17.36	1.01	4.89	1.61	-6.66	0.81
40	23.00	2.21	52.66	10.29	-4.01	3.54	-18.11	3.99
41	12.97	0.50	12.21	0.77	5.8	0.53	-4.98	0.90
42	13.2	0.39	13.88	0.57	6.03	0.75	-5.64	0.77
43	14.47	0.45	17.23	1.22	5.57	1.18	-7.02	0.57
44	21.25	1.75	55.16	4.28	3.25	3.40	-15.48	2.23
45	15.05	1.02	14.44	2.11	6.49	2.21	-5.28	0.82
46	14.64	0.54	15.27	1.03	6.33	0.7	-5.78	0.60
47	16.55	1.19	19.04	2.16	6.4	1.65	-6.87	0.98
48	20.67	1.15	44.81	6.39	5.32	3.55	-8.55	2.27
49	10.31	0.77	9.47	0.66	6.57	1.16	-6.17	0.59
50	10.43	1.17	11.45	0.72	7.19	1.26	-6.88	0.55
51	13.17	0.46	18.42	0.51	6.52	1.07	-8.39	0.28
52	18.58	2.04	58.07	4.77	-2.31	3.80	-16.46	3.76
53	12.24	0.83	12.38	2.56	6.49	1.21	-6.07	0.90
54	13.41	0.99	13.77	1.16	5.65	0.87	-6.39	0.98
55	15.44	0.83	19.95	1.02	5.85	1.59	-8.33	0.83
56	25.62	3.53	57.59	3.19	-4.39	5.91	-20.84	1.82
57	14.8	0.90	14.04	1.45	7.03	1.37	-6.20	1.05
58	15.15	0.93	15.29	1.79	6.9	1.64	-6.67	0.98
59	16.62	1.05	20.59	0.92	7.23	1.52	-8.56	0.62
60	27.28	2.01	52.46	4.97	-2.14	3.81	-23.29	2.87
61	15.00	1.48	14.29	2.03	8.13	2.68	-6.77	1.02
62	15.53	1.25	15.97	1.34	8.33	2.62	-7.01	1.11
63	16.84	1.03	22.69	2.40	8.28	1.72	-9.07	1.16
64	26.07	2.41	69.58	6.32	1.75	6.99	-25.92	3.75

Table B.9. Virtual Mass coefficients and uncertainties for the SB seal with the high pre-swirl insert.

Test Point	M_{XX} [kg]	$u_{M_{XX}}$ [kg]	M_{YY} [kg]	$u_{M_{YY}}$ [kg]	M_{XY} [kg]	$u_{M_{XY}}$ [kg]	M_{YX} [kg]	$u_{M_{YX}}$ [kg]
1	14.49	0.26	13.67	2.00	-0.09	0.71	0.79	0.32
2	14.49	0.38	13.14	1.75	0.45	0.87	0.30	0.23
3	15.29	0.33	16.21	0.86	-0.88	0.82	0.25	0.25
4	17.69	0.61	16.96	10.23	4.24	3.47	1.08	2.05
5	15.15	0.33	13.70	0.72	0.53	0.49	0.31	0.17
6	16.21	0.32	15.91	0.65	0.21	1.24	0.47	0.27
7	17.11	0.44	16.75	0.58	0.17	0.55	-0.03	0.25
8	21.94	3.44	48.39	32.16	-5.61	12.77	-9.00	11.06
9	17.12	1.23	15.80	1.06	-0.68	1.03	0.89	0.75
10	16.54	0.54	16.99	1.04	-0.04	0.81	0.62	0.34
11	17.13	0.53	17.94	0.80	0.13	1.60	-0.15	0.48
12	19.51	0.50	25.95	2.17	-1.25	1.73	-0.28	0.47
13	17.18	0.70	16.03	0.89	-0.01	1.31	0.50	0.17
14	17.51	0.72	16.00	0.80	-0.25	1.71	0.56	0.55
15	17.89	0.44	18.62	1.20	-1.07	1.08	0.09	0.27
16	19.58	1.12	21.72	11.99	0.60	5.95	-0.35	1.77
17	11.85	0.39	11.63	0.81	0.28	0.49	-0.37	0.28
18	12.82	0.37	12.67	0.76	-1.00	0.77	-0.60	0.31
19	14.51	0.34	16.33	1.47	-0.79	0.66	-1.08	0.62
20	12.00	4.16	19.39	21.48	6.52	11.30	-4.60	14.32
21	14.35	0.75	13.38	0.58	-1.02	0.82	1.17	0.90
22	14.96	0.63	14.15	0.48	-1.19	0.81	0.34	0.51
23	16.35	0.43	16.56	1.08	-0.45	0.53	-0.27	0.50
24	20.17	0.61	26.71	2.96	-3.62	1.90	-4.07	1.54
25	16.36	0.66	14.41	0.66	-1.32	0.42	1.20	0.54
26	16.32	0.47	16.08	0.80	-0.42	0.45	0.88	0.29
27	17.48	0.32	17.01	0.88	-0.21	0.50	1.07	0.43
28	21.03	1.62	29.37	3.88	-4.33	9.14	-1.49	1.12
29	16.75	0.32	14.39	1.07	-1.26	1.05	1.26	0.40
30	16.69	0.34	16.18	1.04	0.99	1.07	0.93	0.52
31	17.67	0.37	18.73	1.24	0.66	1.47	0.42	0.41
32	20.71	0.87	29.42	10.13	-0.65	4.06	-1.25	1.27

Table B.10. Virtual Mass coefficients and uncertainties for the SB seal with the high pre-swirl insert.

Test Point	M_{XX} [kg]	$u_{M_{XX}}$ [kg]	M_{YY} [kg]	$u_{M_{YY}}$ [kg]	M_{XY} [kg]	$u_{M_{XY}}$ [kg]	M_{YX} [kg]	$u_{M_{YX}}$ [kg]
33	11.10	0.52	10.72	0.54	0.88	0.81	-0.87	0.37
34	12.26	0.73	10.96	1.39	1.07	1.04	-0.29	1.11
35	13.90	0.76	14.51	0.90	-0.21	0.77	-0.84	0.91
36	12.05	2.36	35.33	16.35	0.96	3.51	-2.91	5.99
37	14.85	0.69	14.69	0.77	-1.15	1.21	0.67	0.76
38	14.22	0.69	13.84	1.02	-0.56	1.24	0.39	0.74
39	15.87	0.73	16.13	1.09	-0.70	1.38	0.25	0.89
40	18.82	1.55	22.57	9.38	-2.27	3.94	-1.97	5.42
41	16.63	0.68	15.20	1.38	-0.79	1.07	0.66	1.14
42	16.74	0.54	14.90	0.53	-0.35	0.38	0.50	0.70
43	16.56	0.62	17.37	2.16	-0.19	1.05	0.77	1.56
44	21.77	0.73	27.02	8.73	-4.80	1.98	-2.89	2.58
45	16.91	1.28	15.63	2.75	-0.40	3.28	1.35	0.96
46	16.82	0.73	16.58	0.72	-0.33	1.29	0.69	0.44
47	17.80	1.00	18.93	2.15	-1.65	1.75	-0.27	1.14
48	20.14	1.88	18.34	5.85	-2.18	4.55	-0.05	2.28
49	11.66	1.16	10.82	1.11	0.73	1.59	-0.86	0.70
50	12.63	0.49	11.50	0.84	0.76	1.04	-0.34	0.54
51	13.49	0.77	14.26	0.89	0.71	1.25	-1.42	0.85
52	10.01	1.91	26.86	7.24	-0.91	2.39	-4.43	3.25
53	12.74	1.17	12.04	1.27	1.24	2.41	-0.47	0.66
54	12.68	1.80	12.25	1.22	1.53	2.56	-0.80	0.58
55	13.87	1.84	13.90	1.21	0.84	2.39	-1.62	1.01
56	14.88	1.60	17.26	3.05	-2.65	4.82	-0.52	2.00
57	16.05	0.56	13.18	0.88	-1.54	1.26	1.67	0.86
58	15.37	0.54	14.51	1.06	-1.33	1.01	0.84	1.14
59	17.19	1.15	17.05	2.26	-1.95	1.17	-0.15	1.67
60	19.36	3.31	25.50	4.09	-4.01	5.75	-3.10	1.56
61	16.84	1.56	13.71	1.56	-0.43	2.65	1.00	1.38
62	17.40	1.18	15.03	2.67	-0.59	1.45	1.11	1.80
63	18.23	1.12	15.29	2.00	-0.83	1.99	1.39	1.87
64	21.36	2.51	37.96	8.47	-6.44	4.61	-6.14	3.33

Table B.11. WFR, C_{eff}, and uncertainties for the SB seal with the high pre-swirl insert.

Test Point	WFR, Lund [10]	u_{WFR}, Lund [10]	WFR, San Andrés [11]	u_{WFR}, San Andrés [11]	C_{eff} [kN-s/m]	$u_{C_{eff}}$ [kN-s/m]
1	0.12	0.10	0.12	0.10	6.89	1.02
2	0.21	0.23	0.21	0.23	N/A	N/A
3	0.20	0.12	0.20	0.12	N/A	N/A
4	0.41	0.14	0.41	0.14	N/A	N/A
5	0.40	0.04	0.40	0.04	7.02	0.52
6	0.29	0.08	0.29	0.08	N/A	N/A
7	0.32	0.04	0.32	0.04	N/A	N/A
8	0.00	0.00	0.00	0.00	N/A	N/A
9	0.26	0.08	0.26	0.08	10.54	1.24
10	0.00	0.00	0.00	0.00	N/A	N/A
11	0.32	0.07	0.32	0.07	N/A	N/A
12	0.35	0.04	0.35	0.04	N/A	N/A
13	0.23	0.08	0.23	0.08	11.85	1.18
14	0.15	0.17	0.15	0.17	N/A	N/A
15	0.18	0.08	0.18	0.08	N/A	N/A
16	0.33	0.12	0.33	0.12	N/A	N/A
17	0.42	0.04	0.42	0.04	5.26	0.71
18	0.37	0.05	0.37	0.05	N/A	N/A
19	0.43	0.04	0.42	0.04	N/A	N/A
20	0.57	0.69	0.54	0.61	N/A	N/A
21	0.32	0.04	0.32	0.04	8.95	0.64
22	0.21	0.05	0.21	0.05	N/A	N/A
23	0.36	0.02	0.36	0.02	N/A	N/A
24	0.40	0.05	0.39	0.05	N/A	N/A
25	0.27	0.02	0.27	0.02	10.75	0.53
26	0.23	0.03	0.23	0.03	N/A	N/A
27	0.29	0.02	0.29	0.02	N/A	N/A
28	0.39	0.06	0.39	0.06	N/A	N/A
29	0.23	0.03	0.23	0.03	12.25	0.69
30	0.28	0.03	0.28	0.03	N/A	N/A
31	0.27	0.04	0.27	0.04	N/A	N/A
32	0.40	0.04	0.40	0.04	N/A	N/A

Table B.12. WFR, C_{eff}, and uncertainties for the SB seal with the high pre-swirl insert.

Test Point	WFR, Lund [10]	u_{WFR}, Lund [10]	WFR, San Andrés [11]	u_{WFR}, San Andrés [11]	C_{eff} [kN-s/m]	$u_{C_{eff}}$ [kN-s/m]
33	0.44	0.04	0.43	0.04	5.18	0.70
34	0.42	0.05	0.41	0.05	N/A	N/A
35	0.44	0.03	0.44	0.03	N/A	N/A
36	0.40	0.12	0.40	0.12	N/A	N/A
37	0.31	0.04	0.32	0.05	8.46	1.17
38	0.34	0.04	0.35	0.04	N/A	N/A
39	0.40	0.03	0.40	0.03	N/A	N/A
40	0.42	0.10	0.41	0.10	N/A	N/A
41	0.27	0.04	0.27	0.04	9.22	0.63
42	0.29	0.02	0.29	0.02	N/A	N/A
43	0.34	0.04	0.35	0.04	N/A	N/A
44	0.43	0.05	0.42	0.05	N/A	N/A
45	0.24	0.06	0.24	0.07	11.22	1.51
46	0.26	0.03	0.26	0.03	N/A	N/A
47	0.29	0.04	0.29	0.04	N/A	N/A
48	0.40	0.05	0.40	0.06	N/A	N/A
49	0.46	0.04	0.45	0.04	5.30	0.62
50	0.45	0.04	0.44	0.04	N/A	N/A
51	0.48	0.02	0.46	0.02	N/A	N/A
52	0.32	0.07	0.32	0.07	N/A	N/A
53	0.37	0.06	0.36	0.06	7.76	1.44
54	0.38	0.04	0.37	0.04	N/A	N/A
55	0.42	0.03	0.41	0.03	N/A	N/A
56	0.39	0.05	0.40	0.06	N/A	N/A
57	0.28	0.03	0.29	0.03	10.34	0.91
58	0.32	0.03	0.32	0.03	N/A	N/A
59	0.38	0.03	0.39	0.03	N/A	N/A
60	0.42	0.05	0.42	0.05	N/A	N/A
61	0.27	0.05	0.28	0.05	10.64	1.40
62	0.28	0.04	0.29	0.04	N/A	N/A
63	0.33	0.04	0.33	0.04	N/A	N/A
64	0.39	0.05	0.39	0.05	N/A	N/A

Assembly 2 – Tangential Injection: Medium Pre-swirl

Table B.13. Measured Pressure Drop, Leakage, Static Force, Eccentricity and Attitude Angle of the SB seal with the medium pre-swirl insert

Measured ω	$u\omega$	Measured ΔP	$u\Delta P$	$\dot{Q}$	$u\dot{Q}$	F_s	uF_s	Measured ε_0	φ
[rpm]	[rpm]	[bar]	[bar]	[LPM]	[LPM]	[N]	[N]	[-]	[deg]
1999.71	0.43	2.12	0.01	26.91	0.01	18.19	15.96	0.02	-0.88
2000.74	0.47	2.02	0.01	26.03	0.01	103.66	10.96	0.25	-0.03
2001.20	0.74	2.07	0.08	26.78	0.06	141.38	81.27	0.62	-0.25
2002.03	0.30	2.11	0.01	29.64	0.01	241.51	12.16	0.82	0.09
2023.75	0.69	4.14	0.01	41.79	0.01	-39.04	31.62	0.06	2.56
2023.76	0.29	4.19	0.01	41.69	0.01	120.75	6.79	0.28	0.17
2002.19	0.12	4.08	0.01	41.81	0.01	247.23	2.05	0.54	0.09
2002.14	0.29	4.17	0.05	44.46	0.02	354.39	27.84	0.80	0.16
2022.77	0.28	6.21	0.01	52.37	0.02	-31.05	2.09	0.03	2.35
2002.52	0.61	6.12	0.01	52.15	0.02	152.77	2.32	0.29	0.02
2002.18	0.24	6.27	0.02	52.41	0.03	351.34	14.09	0.53	0.02
2002.41	0.65	6.19	0.01	56.86	0.05	515.69	3.88	0.80	0.10
2002.00	0.33	8.63	0.02	61.22	0.01	-42.29	0.59	0.05	2.41
2002.19	0.48	8.32	0.01	61.63	0.02	141.92	13.63	0.28	0.12
2001.96	0.42	8.29	0.01	62.76	0.02	435.71	6.17	0.54	0.05
2001.61	0.31	8.39	0.01	65.51	0.07	617.68	7.57	0.78	0.08
3351.60	876.31	2.07	0.02	26.00	0.03	-9.69	21.75	0.11	-1.74
4003.56	0.18	2.01	0.02	23.13	0.01	69.63	41.74	0.27	0.03
4003.62	0.09	2.12	0.01	23.27	0.01	105.80	1.71	0.56	-0.14
4003.24	0.28	2.10	0.01	26.12	0.01	327.75	20.08	0.81	0.11
4012.69	0.30	4.07	0.01	37.24	0.02	10.86	1.26	0.02	2.57
4011.86	0.45	4.22	0.01	37.18	0.01	89.22	19.24	0.28	0.16
4011.27	0.12	4.17	0.01	38.92	0.02	226.45	7.48	0.52	0.13
4010.11	0.35	4.13	0.01	40.90	0.02	444.13	17.19	0.80	0.27
4007.95	0.19	6.28	0.01	48.64	0.02	-9.04	0.83	0.02	0.01
4008.26	0.36	6.15	0.01	50.85	0.02	96.95	21.57	0.27	0.09
4008.36	0.48	6.21	0.01	51.30	0.01	336.31	4.73	0.55	0.12
4008.12	0.04	6.26	0.02	54.67	0.04	560.39	25.62	0.79	0.23
4007.19	0.20	8.28	0.01	58.31	0.01	-22.04	6.96	0.01	-0.26
4007.17	0.51	8.20	0.01	58.92	0.03	103.70	8.93	0.28	0.07
4007.39	0.40	8.29	0.01	60.28	0.02	392.02	1.36	0.55	0.05
4007.24	0.43	8.22	0.01	64.02	0.01	638.05	15.96	0.78	0.14

Table B.14. Measured Pressure Drop, Leakage, Static Force, Eccentricity and Attitude Angle of the SB seal with the medium pre-swirl insert

Measured ω	$u\omega$	Measured ΔP	$u\Delta P$	$\dot{Q}$	$u\dot{Q}$	F_s	uF_s	Measured ε_0	φ
[rpm]	[rpm]	[bar]	[bar]	[LPM]	[LPM]	[N]	[N]	[-]	[deg]
5999.53	0.54	2.12	0.02	17.29	0.01	43.22	2.00	0.03	3.02
6000.31	0.33	2.02	0.01	17.37	0.02	138.19	1.27	0.26	0.39
6000.60	0.69	2.07	0.03	20.12	0.03	215.87	2.73	0.55	0.30
6001.11	0.22	2.11	0.02	23.19	0.02	724.91	11.25	0.79	0.47
6005.98	0.25	4.14	0.01	30.12	0.00	53.97	12.35	0.11	1.35
6004.88	0.16	4.19	0.01	31.41	0.01	170.76	3.20	0.29	0.31
6003.79	0.47	4.08	0.02	33.60	0.00	299.16	9.13	0.54	0.34
6002.92	0.28	4.17	0.01	37.03	0.02	726.42	9.20	0.78	0.44
5999.34	0.52	6.21	0.01	43.10	0.01	8.53	5.92	0.03	2.78
6000.82	0.36	6.12	0.02	43.48	0.02	201.04	9.69	0.28	0.21
6001.40	0.21	6.27	0.02	47.10	0.05	351.20	31.59	0.52	0.27
6001.22	0.24	6.19	0.01	51.45	0.02	789.10	7.85	0.80	0.42
6002.69	0.73	8.63	0.02	52.17	0.01	20.37	9.74	0.03	0.10
6002.34	0.35	8.32	0.02	53.70	0.07	206.08	8.07	0.27	0.15
6002.60	0.68	8.29	0.01	56.41	0.01	382.68	10.30	0.53	0.23
6002.88	0.11	8.39	0.01	60.92	0.04	889.08	47.86	0.76	0.39
7999.05	1.08	2.07	0.01	15.28	0.01	70.70	9.93	0.05	1.34
7999.54	0.27	2.01	0.01	16.39	0.02	174.11	2.78	0.27	0.50
7999.73	0.47	2.12	0.01	18.27	0.02	356.43	4.14	0.52	0.54
8002.71	0.27	2.10	0.01	20.05	0.02	1142.70	15.21	0.80	0.50
8003.64	0.21	4.07	0.01	26.91	0.01	73.89	9.75	0.04	2.93
8004.09	0.79	4.22	0.01	27.86	0.02	235.51	6.10	0.29	0.34
8004.64	0.26	4.17	0.01	31.52	0.03	427.39	3.52	0.52	0.44
8004.85	0.19	4.13	0.03	35.21	0.01	1172.25	19.45	0.79	0.52
7998.04	0.78	6.28	0.01	38.20	0.01	75.18	9.05	0.03	1.70
7999.01	0.19	6.15	0.01	38.52	0.02	254.07	18.40	0.28	0.32
7998.89	0.20	6.21	0.02	41.60	0.03	463.85	9.73	0.52	0.40
7999.31	0.23	6.26	0.02	47.09	0.00	1239.05	9.31	0.79	0.54
8000.44	0.05	8.28	0.01	48.01	0.02	57.83	13.90	0.03	2.09
8000.73	0.26	8.20	0.01	50.23	0.05	303.07	30.40	0.29	0.29
8001.04	0.16	8.29	0.01	52.43	0.02	555.02	5.63	0.52	0.35
8000.83	0.54	8.22	0.02	56.54	0.01	1204.11	2.00	0.82	0.52

Table B.15. PSR, OSR, Inlet and Outlet Temperature, and Reynolds Number of the SB seal with the medium pre-swirl insert

Test Point	PSR	OSR	T_i	uT_i	T_e	uT_e	Re_z	Re_θ	Re
	[-]	[-]	[°C]	[°C]	[°C]	[°C]	[-]	[-]	[-]
1	0.449	0.302	45.33	0.05	45.07	0.05	1.19E+03	8.57E+02	1.47E+03
2	0.398	0.333	45.39	0.05	45.03	0.05	1.15E+03	8.59E+02	1.44E+03
3	0.376	0.313	45.58	0.05	45.23	0.05	1.19E+03	8.62E+02	1.47E+03
4	0.370	0.318	45.99	0.05	45.73	0.05	1.33E+03	8.68E+02	1.59E+03
5	0.460	0.301	46.19	0.05	45.95	0.05	1.88E+03	8.81E+02	2.08E+03
6	0.405	0.344	46.31	0.05	46.12	0.05	1.88E+03	8.83E+02	2.08E+03
7	0.329	0.316	45.82	0.05	45.52	0.05	1.86E+03	8.66E+02	2.06E+03
8	0.273	0.312	46.40	0.05	46.08	0.05	2.00E+03	8.75E+02	2.19E+03
9	0.552	0.294	45.37	0.05	45.15	0.05	2.32E+03	8.68E+02	2.48E+03
10	0.509	0.348	46.02	0.05	45.64	0.05	2.33E+03	8.69E+02	2.50E+03
11	0.392	0.307	46.07	0.05	45.67	0.05	2.34E+03	8.70E+02	2.51E+03
12	0.392	0.324	46.04	0.05	45.89	0.05	2.55E+03	8.69E+02	2.70E+03
13	0.623	0.298	45.48	0.05	45.55	0.05	2.73E+03	8.61E+02	2.86E+03
14	0.529	0.344	45.49	0.05	45.37	0.05	2.74E+03	8.61E+02	2.88E+03
15	0.425	0.367	45.58	0.05	45.44	0.05	2.79E+03	8.62E+02	2.93E+03
16	0.359	0.352	45.55	0.05	45.48	0.05	2.92E+03	8.61E+02	3.04E+03
17	0.307	0.215	46.40	0.05	46.19	0.05	1.17E+03	1.46E+03	1.88E+03
18	0.303	0.255	46.57	0.05	46.63	0.05	1.05E+03	1.75E+03	2.04E+03
19	0.278	0.263	46.84	0.05	46.91	0.05	1.06E+03	1.76E+03	2.06E+03
20	0.286	0.274	47.18	0.05	47.35	0.05	1.20E+03	1.77E+03	2.14E+03
21	0.359	0.248	44.80	0.05	44.87	0.05	1.64E+03	1.70E+03	2.36E+03
22	0.343	0.277	44.92	0.05	44.97	0.05	1.64E+03	1.71E+03	2.37E+03
23	0.335	0.275	45.20	0.05	45.16	0.05	1.72E+03	1.72E+03	2.43E+03
24	0.320	0.275	45.32	0.05	45.35	0.05	1.82E+03	1.72E+03	2.50E+03
25	0.458	0.265	45.87	0.05	45.92	0.05	2.18E+03	1.73E+03	2.79E+03
26	0.452	0.280	45.87	0.05	45.94	0.05	2.28E+03	1.73E+03	2.86E+03
27	0.416	0.304	45.75	0.05	45.84	0.05	2.30E+03	1.73E+03	2.87E+03
28	0.407	0.313	45.61	0.05	45.79	0.05	2.45E+03	1.73E+03	2.99E+03
29	0.564	0.271	45.69	0.05	45.87	0.05	2.61E+03	1.73E+03	3.13E+03
30	0.542	0.282	45.73	0.05	45.90	0.05	2.64E+03	1.73E+03	3.15E+03
31	0.517	0.298	45.95	0.05	46.09	0.05	2.71E+03	1.74E+03	3.22E+03
32	0.478	0.288	46.16	0.05	46.30	0.05	2.89E+03	1.74E+03	3.37E+03

Table B.16. PSR, OSR, Inlet and Outlet Temperature, and Reynolds Number of the SB seal with the medium pre-swirl insert

Test Point	PSR	OSR	T_i	uT_i	T_e	uT_e	Re_z	Re_θ	Re
	[-]	[-]	[°C]	[°C]	[°C]	[°C]	[-]	[-]	[-]
33	0.325	0.241	46.86	0.05	48.22	0.05	8.09E+02	2.64E+03	2.76E+03
34	0.318	0.208	46.92	0.05	48.35	0.05	8.14E+02	2.65E+03	2.76E+03
35	0.307	0.238	43.83	0.05	46.13	0.05	9.06E+02	2.51E+03	2.65E+03
36	0.286	0.256	45.63	0.05	46.74	0.05	1.06E+03	2.59E+03	2.79E+03
37	0.304	0.232	44.57	0.05	45.54	0.05	1.34E+03	2.54E+03	2.86E+03
38	0.293	0.264	44.72	0.05	45.64	0.05	1.40E+03	2.55E+03	2.90E+03
39	0.283	0.266	45.10	0.05	45.71	0.05	1.50E+03	2.57E+03	2.96E+03
40	0.271	0.265	44.78	0.05	45.69	0.05	1.65E+03	2.55E+03	3.03E+03
41	0.363	0.232	45.49	0.05	46.22	0.05	1.94E+03	2.58E+03	3.22E+03
42	0.354	0.279	45.49	0.05	46.24	0.05	1.96E+03	2.58E+03	3.23E+03
43	0.348	0.296	45.58	0.05	46.27	0.05	2.13E+03	2.58E+03	3.33E+03
44	0.335	0.319	45.89	0.05	46.57	0.05	2.34E+03	2.60E+03	3.48E+03
45	0.389	0.243	45.85	0.05	46.61	0.05	2.37E+03	2.60E+03	3.50E+03
46	0.380	0.287	46.05	0.05	46.76	0.05	2.45E+03	2.61E+03	3.55E+03
47	0.372	0.293	46.01	0.05	46.69	0.05	2.57E+03	2.61E+03	3.64E+03
48	0.356	0.281	45.99	0.05	46.72	0.05	2.77E+03	2.60E+03	3.78E+03
49	0.340	0.179	45.44	0.05	49.12	0.05	7.27E+02	3.44E+03	3.51E+03
50	0.331	0.246	45.44	0.05	48.91	0.05	7.76E+02	3.44E+03	3.52E+03
51	0.315	0.204	45.63	0.05	48.84	0.05	8.65E+02	3.45E+03	3.55E+03
52	0.301	0.203	45.59	0.05	48.56	0.05	9.44E+02	3.45E+03	3.57E+03
53	0.306	0.224	45.70	0.05	48.08	0.05	1.26E+03	3.46E+03	3.66E+03
54	0.295	0.223	45.76	0.05	48.18	0.05	1.30E+03	3.46E+03	3.68E+03
55	0.280	0.263	45.87	0.05	48.24	0.05	1.47E+03	3.47E+03	3.75E+03
56	0.282	0.258	45.14	0.05	47.53	0.05	1.63E+03	3.43E+03	3.76E+03
57	0.330	0.221	45.99	0.05	47.85	0.05	1.77E+03	3.46E+03	3.87E+03
58	0.321	0.257	45.27	0.05	47.21	0.05	1.77E+03	3.43E+03	3.83E+03
59	0.315	0.259	45.59	0.05	47.58	0.05	1.92E+03	3.45E+03	3.92E+03
60	0.306	0.265	45.88	0.05	47.74	0.05	2.18E+03	3.47E+03	4.06E+03
61	0.343	0.236	46.11	0.05	47.90	0.05	2.23E+03	3.48E+03	4.10E+03
62	0.334	0.264	46.28	0.05	48.00	0.05	2.34E+03	3.49E+03	4.16E+03
63	0.325	0.272	46.44	0.05	48.14	0.05	2.45E+03	3.50E+03	4.23E+03
64	0.317	0.274	45.35	0.05	46.96	0.05	2.58E+03	3.43E+03	4.26E+03

Table B.17. Stiffness coefficients and uncertainties for the SB seal with the medium pre-swirl insert.

Test Point	K_{XX} [MN/m]	$u_{K_{XX}}$ [MN/m]	K_{YY} [MN/m]	$u_{K_{YY}}$ [MN/m]	K_{XY} [MN/m]	$u_{K_{XY}}$ [MN/m]	K_{YX} [MN/m]	$u_{K_{YX}}$ [MN/m]
1	1.85	-0.41	0.44	0.17	0.13	0.17	0.27	1.76
2	1.53	-0.64	1.00	1.00	0.17	0.14	0.50	1.07
3	0.84	-0.24	3.81	8.89	0.27	0.86	2.22	-3.06
4	-0.47	0.20	8.68	17.87	1.04	1.67	9.69	-3.44
5	1.71	-1.05	0.12	0.32	0.27	0.27	1.06	1.75
6	2.12	-0.79	2.87	1.73	0.37	0.26	-0.13	2.05
7	1.98	-0.67	0.61	2.13	0.21	0.25	1.59	0.95
8	0.46	-1.13	6.00	18.81	1.04	2.19	8.20	-1.37
9	1.13	-1.07	0.33	0.37	0.28	0.28	0.82	1.21
10	2.57	-1.08	0.43	0.58	0.17	0.23	0.14	4.48
11	3.47	-0.76	2.33	1.24	0.33	0.15	0.50	2.70
12	2.21	-1.47	6.25	12.72	0.76	0.98	7.23	3.27
13	2.59	-1.10	0.32	0.34	0.30	0.44	0.94	2.74
14	3.23	-1.39	0.67	0.42	0.22	0.20	0.19	5.86
15	4.53	-0.81	1.32	0.71	0.15	0.17	1.84	4.68
16	3.54	-0.98	2.38	9.43	0.36	1.60	6.61	1.04
17	1.19	-0.76	1.10	0.75	0.90	0.62	1.58	1.16
18	-0.63	-0.87	0.42	0.31	1.11	0.88	0.80	0.87
19	1.77	-2.15	1.09	1.82	1.13	0.83	3.42	0.78
20	-0.33	-2.65	9.86	18.21	2.82	4.94	15.64	2.20
21	-0.97	-1.84	0.35	0.21	0.40	0.17	1.83	-1.18
22	1.32	-2.25	0.51	0.45	0.59	0.33	0.92	2.53
23	1.73	-1.83	0.32	0.42	0.27	0.13	2.27	1.84
24	-6.82	0.51	14.06	15.09	7.41	7.46	24.03	-5.61
25	-0.63	-1.89	0.76	0.58	0.84	0.71	1.33	-0.35
26	1.96	-2.31	2.57	2.37	0.44	0.24	0.67	4.41
27	2.85	-1.96	0.62	0.77	0.27	0.12	2.62	3.05
28	0.15	-3.87	5.33	8.44	1.36	1.56	14.90	3.73
29	1.82	-1.42	0.24	0.41	0.50	0.34	1.42	1.85
30	2.43	-2.11	0.55	1.10	0.43	0.15	1.55	4.49
31	3.90	-1.96	0.39	0.28	0.28	0.18	2.59	4.53
32	2.27	-3.56	2.43	3.27	0.60	0.66	14.16	5.01

Table B.18. Stiffness coefficients and uncertainties for the SB seal with the medium pre-swirl insert.

Test Point	K_{XX} [MN/m]	$u_{K_{XX}}$ [MN/m]	K_{YY} [MN/m]	$u_{K_{YY}}$ [MN/m]	K_{XY} [MN/m]	$u_{K_{XY}}$ [MN/m]	K_{YX} [MN/m]	$u_{K_{YX}}$ [MN/m]
33	0.42	0.39	0.47	0.18	2.31	0.26	-2.30	0.29
34	-1.94	2.30	0.78	0.66	3.36	0.94	-1.35	1.46
35	-1.89	2.15	-1.32	3.25	6.64	3.70	-1.87	2.31
36	0.28	1.18	21.02	3.28	9.11	2.03	-16.73	2.25
37	1.18	0.31	1.62	0.78	2.85	0.72	-2.27	0.21
38	1.34	0.21	1.52	0.53	2.45	0.78	-2.80	0.34
39	-3.17	4.80	-0.86	4.35	7.42	4.25	-0.47	3.93
40	-1.58	2.45	22.88	12.38	13.66	4.14	-16.62	6.61
41	3.25	0.67	3.43	0.99	1.87	0.59	-2.41	0.70
42	2.51	0.41	1.73	0.86	3.32	0.57	-2.05	0.22
43	2.00	0.50	3.70	0.69	4.62	0.83	-3.65	0.27
44	-4.13	1.78	12.70	7.60	19.98	3.88	-9.81	3.47
45	4.25	0.49	3.92	0.68	2.34	0.55	-2.00	0.26
46	2.98	0.41	0.59	0.44	4.33	0.66	-1.46	0.20
47	3.66	0.65	4.96	0.39	3.26	0.72	-3.91	0.26
48	-3.30	1.85	14.90	6.25	22.33	5.18	-10.47	2.90
49	-0.22	0.29	0.36	0.48	3.59	0.28	-3.60	0.25
50	-0.79	0.89	-0.03	0.88	5.02	1.69	-3.79	0.72
51	-3.32	1.97	-0.25	1.68	9.43	1.90	-4.48	1.61
52	7.70	0.67	35.57	1.82	5.33	0.86	-29.65	1.28
53	1.30	0.55	1.34	0.44	3.91	0.49	-3.71	0.28
54	1.06	0.51	1.92	2.01	3.34	2.48	-4.06	0.44
55	-3.10	2.49	0.13	1.84	9.90	2.66	-3.56	1.93
56	5.33	0.70	33.11	1.44	8.34	1.15	-28.72	1.12
57	2.97	0.76	2.55	0.96	3.18	0.83	-3.74	0.44
58	2.70	0.84	2.20	1.17	3.96	1.28	-4.34	0.54
59	0.00	0.91	2.29	0.86	8.18	0.87	-4.79	0.60
60	5.18	1.23	37.25	2.62	9.42	2.27	-31.46	1.79
61	4.44	0.63	3.50	0.68	2.99	0.70	-3.58	0.41
62	3.89	0.50	4.00	0.65	3.39	0.98	-3.63	0.45
63	2.30	0.89	3.52	1.15	7.83	1.11	-4.80	0.60
64	-0.29	0.93	28.20	0.96	17.28	1.80	-23.52	1.12

Table B.19. Damping coefficients and uncertainties for the SB seal with the medium pre-swirl insert.

Test Point	C_{XX} [kN-s/m]	$u_{C_{XX}}$ [kN-s/m]	C_{YY} [kN-s/m]	$u_{C_{YY}}$ [kN-s/m]	C_{XY} [kN-s/m]	$u_{C_{XY}}$ [kN-s/m]	C_{YX} [kN-s/m]	$u_{C_{YX}}$ [kN-s/m]
1	8.56	0.89	7.71	0.72	1.37	1.35	-1.35	0.27
2	8.72	0.74	8.67	2.27	1.32	4.08	-0.92	0.41
3	10.71	1.27	23.44	17.01	8.29	6.70	-0.51	2.36
4	22.95	3.46	78.52	72.34	-1.76	17.36	-13.44	9.29
5	12.40	0.79	11.51	0.51	1.87	0.90	-1.36	0.37
6	12.23	1.02	11.39	0.79	2.91	1.54	-1.01	0.37
7	13.26	0.66	16.56	1.00	2.65	1.42	-1.58	0.58
8	24.09	3.32	66.92	45.30	-2.38	17.06	-12.27	9.08
9	15.25	1.12	13.89	0.91	2.15	1.03	-1.72	0.46
10	14.36	0.60	13.99	3.48	2.65	1.39	-0.92	0.40
11	14.89	1.47	17.35	1.24	2.86	2.40	-1.42	0.45
12	24.61	1.63	72.42	25.13	-2.64	7.04	-9.17	3.68
13	16.28	1.22	15.16	1.04	1.92	1.75	-1.59	0.50
14	16.43	0.73	14.95	0.85	3.07	0.56	-1.18	0.42
15	17.07	0.70	19.05	1.17	3.55	0.52	-1.38	0.34
16	24.33	1.80	65.80	30.22	0.08	11.35	-7.37	3.66
17	10.10	1.48	9.30	2.28	1.22	2.14	-2.47	1.33
18	11.03	1.55	9.55	1.84	2.31	2.31	-4.41	1.58
19	10.09	1.69	16.32	1.97	4.63	2.53	-1.91	1.42
20	18.62	7.03	87.65	16.92	-4.38	21.52	-12.59	7.09
21	13.76	0.89	12.45	0.75	3.99	0.81	-3.83	0.36
22	12.83	1.20	11.52	1.18	4.56	1.13	-3.02	0.57
23	13.22	0.62	15.50	0.85	4.32	1.00	-3.48	0.36
24	41.20	14.37	106.06	14.91	-34.13	17.62	-38.57	12.22
25	17.27	2.48	14.65	0.92	2.27	2.67	-4.56	1.30
26	15.74	1.19	15.66	4.34	3.01	5.23	-3.30	0.36
27	15.55	0.62	18.53	0.73	5.24	0.58	-3.36	0.32
28	27.96	2.37	84.51	5.66	-11.62	6.76	-21.07	1.83
29	17.22	1.43	15.27	0.55	3.70	1.74	-3.55	0.23
30	17.08	0.90	15.52	0.98	4.52	1.99	-3.84	0.29
31	17.09	0.56	19.46	0.96	5.62	0.94	-3.17	0.29
32	26.27	1.32	81.67	10.23	-4.32	3.93	-14.45	2.11

Table B.20. Damping coefficients and uncertainties for the SB seal with the medium pre-swirl insert.

Test Point	C_{XX} [kN-s/m]	$u_{C_{XX}}$ [kN-s/m]	C_{YY} [kN-s/m]	$u_{C_{YY}}$ [kN-s/m]	C_{XY} [kN-s/m]	$u_{C_{XY}}$ [kN-s/m]	C_{YX} [kN-s/m]	$u_{C_{YX}}$ [kN-s/m]
33	9.03	0.47	7.90	0.73	4.50	0.64	-4.90	0.82
34	12.41	3.14	11.81	3.26	1.86	4.53	-8.30	3.96
35	12.56	3.93	16.30	3.00	2.70	2.77	-7.19	2.05
36	32.18	5.35	82.30	11.45	-27.58	11.81	-30.78	5.68
37	12.42	0.76	12.37	1.58	4.29	1.26	-4.49	0.72
38	12.95	0.90	12.63	1.17	4.80	0.96	-5.21	0.84
39	19.70	7.16	22.68	6.29	-1.66	6.63	-11.28	5.05
40	40.89	8.49	98.04	20.16	-34.56	16.82	-40.07	8.96
41	14.18	1.23	12.28	1.11	5.53	1.39	-5.49	1.09
42	13.53	0.45	13.10	1.34	4.57	1.37	-4.93	0.31
43	17.21	2.12	19.99	1.22	4.47	1.60	-7.95	1.22
44	41.07	5.81	95.82	15.78	-25.54	10.67	-41.12	8.37
45	15.05	0.64	13.74	0.87	5.02	1.68	-4.86	0.40
46	15.61	0.63	14.95	2.60	5.40	1.92	-5.25	0.36
47	17.57	1.29	18.98	1.96	6.21	1.50	-6.55	0.60
48	40.59	3.71	98.70	13.52	-25.75	5.79	-37.71	7.24
49	10.06	0.72	9.10	0.92	6.48	0.86	-6.81	1.23
50	11.01	1.62	11.56	1.00	5.47	1.75	-8.06	1.24
51	16.03	5.33	22.28	4.42	2.12	4.50	-12.75	5.02
52	25.83	2.02	74.76	3.45	-16.89	3.07	-28.11	2.57
53	12.43	1.22	11.26	1.05	6.25	1.57	-6.11	1.13
54	14.50	3.17	12.97	1.51	6.95	3.55	-8.05	2.65
55	19.97	3.42	23.35	2.81	-0.16	5.43	-11.91	2.30
56	32.60	2.26	75.08	3.53	-19.51	3.62	-29.52	2.24
57	15.52	2.08	13.31	1.09	7.30	1.18	-6.47	0.87
58	16.41	2.31	15.20	0.94	6.34	1.53	-7.50	1.30
59	25.29	9.44	25.52	3.63	0.52	6.82	-14.65	5.54
60	37.09	2.71	78.65	4.19	-19.88	4.48	-34.84	2.26
61	15.40	0.81	13.39	1.47	7.59	0.79	-6.66	0.79
62	16.91	1.66	16.12	0.94	7.11	1.66	-7.93	0.87
63	20.20	2.00	24.91	1.41	5.44	1.41	-12.00	1.29
64	40.63	3.38	79.23	5.18	-22.11	5.01	-35.41	2.87

Table B.21. Virtual Mass coefficients and uncertainties for the SB seal with the medium pre-swirl insert.

Test Point	M_{XX} [kg]	$u_{M_{XX}}$ [kg]	M_{YY} [kg]	$u_{M_{YY}}$ [kg]	M_{XY} [kg]	$u_{M_{XY}}$ [kg]	M_{YX} [kg]	$u_{M_{YX}}$ [kg]
1	13.30	0.46	0.59	0.23	0.18	0.23	0.38	12.73
2	13.44	0.74	1.35	1.35	0.23	0.19	-0.41	12.83
3	14.21	1.57	5.16	12.02	0.37	1.16	0.30	8.05
4	16.46	2.33	11.73	24.16	1.41	2.26	2.64	27.65
5	13.79	0.51	0.16	0.43	0.37	0.36	0.76	13.34
6	13.87	0.61	3.88	2.33	0.49	0.35	-2.52	12.10
7	15.21	0.56	0.82	2.88	0.29	0.34	0.55	14.24
8	19.64	0.39	8.12	25.44	1.40	2.96	-0.55	11.15
9	14.86	0.59	0.45	0.49	0.38	0.38	0.54	14.69
10	14.60	0.74	0.58	0.79	0.23	0.31	-0.38	14.81
11	15.68	0.73	3.14	1.67	0.45	0.20	0.21	15.61
12	19.33	-0.60	8.45	17.21	1.03	1.33	-2.08	29.00
13	15.41	0.63	0.43	0.46	0.40	0.59	1.29	15.14
14	15.40	0.90	0.91	0.56	0.30	0.28	1.11	15.89
15	16.70	0.93	1.78	0.96	0.21	0.24	2.05	16.71
16	19.40	-0.26	3.22	12.76	0.49	2.17	-0.72	27.99
17	11.26	1.68	1.48	1.01	1.22	0.84	2.03	11.59
18	9.51	2.51	0.57	0.43	1.50	1.19	-1.25	12.70
19	12.27	2.32	1.47	2.46	1.53	1.13	4.50	14.06
20	6.97	9.55	13.33	24.62	3.82	6.68	23.43	9.46
21	13.89	0.80	0.47	0.29	0.54	0.23	-0.52	12.76
22	15.02	-0.42	0.69	0.61	0.80	0.45	-0.08	13.67
23	15.58	-0.36	0.43	0.57	0.37	0.18	-0.13	15.38
24	6.42	9.06	19.01	20.41	10.03	10.09	23.73	4.03
25	14.94	0.09	1.03	0.78	1.14	0.96	-0.01	14.75
26	15.99	0.36	3.48	3.20	0.60	0.33	-2.66	16.45
27	16.64	-0.08	0.84	1.05	0.37	0.16	-0.22	15.89
28	21.59	-3.03	7.21	11.41	1.84	2.12	-2.25	28.59
29	16.35	0.58	0.32	0.56	0.68	0.46	-0.09	14.78
30	16.38	0.85	0.74	1.49	0.59	0.20	-0.08	14.53
31	17.19	0.38	0.53	0.38	0.38	0.25	-0.09	16.88
32	21.35	-1.53	3.28	4.42	0.81	0.90	-3.92	31.64

Table B.22. Virtual Mass coefficients and uncertainties for the SB seal with the medium pre-swirl insert.

Test Point	M_{XX} [kg]	$u_{M_{XX}}$ [kg]	M_{YY} [kg]	$u_{M_{YY}}$ [kg]	M_{XY} [kg]	$u_{M_{XY}}$ [kg]	M_{YX} [kg]	$u_{M_{YX}}$ [kg]
33	10.32	-0.07	0.35	0.25	0.53	0.39	1.11	9.96
34	4.30	3.53	1.27	0.90	3.12	1.97	1.44	12.06
35	8.42	2.04	5.00	4.39	2.91	3.13	2.59	10.36
36	6.23	2.27	2.75	4.43	1.60	3.04	-0.93	16.08
37	11.62	0.75	0.97	1.05	0.42	0.29	1.76	12.68
38	13.78	-0.69	1.05	0.71	0.28	0.46	-1.63	13.26
39	3.82	7.96	5.74	5.88	6.49	5.31	4.57	11.44
40	11.49	1.43	5.60	16.75	3.31	8.94	-0.12	25.22
41	15.01	-0.50	0.80	1.34	0.91	0.94	-0.08	15.44
42	15.24	0.17	0.76	1.17	0.55	0.29	0.67	12.93
43	17.02	-1.22	1.12	0.93	0.68	0.37	-0.32	18.48
44	23.93	-3.47	5.25	10.28	2.41	4.69	-10.32	29.31
45	15.01	0.68	0.75	0.92	0.67	0.35	1.95	13.86
46	15.43	0.86	0.89	0.60	0.56	0.27	1.51	13.91
47	18.02	-0.89	0.97	0.53	0.88	0.35	-0.24	16.92
48	23.30	-2.33	7.01	8.45	2.50	3.92	-6.07	25.29
49	10.16	0.14	0.38	0.65	0.39	0.33	1.02	11.03
50	8.97	1.37	2.29	1.18	1.21	0.98	2.76	10.84
51	6.19	4.46	2.56	2.28	2.67	2.18	5.59	8.52
52	6.45	-1.10	1.16	2.47	0.90	1.72	0.32	19.61
53	9.84	0.14	0.67	0.59	0.74	0.37	1.76	9.70
54	10.97	-0.76	3.35	2.72	0.68	0.59	-2.66	13.75
55	3.90	4.34	3.60	2.49	3.37	2.61	4.54	9.83
56	6.98	-0.25	1.55	1.94	0.95	1.52	1.23	18.02
57	14.74	0.63	1.12	1.30	1.03	0.60	-0.78	13.15
58	15.68	-0.32	1.74	1.58	1.13	0.72	-2.03	13.56
59	15.11	0.21	1.18	1.17	1.23	0.81	-2.11	17.05
60	14.65	-3.42	3.07	3.55	1.67	2.42	-3.16	27.24
61	15.84	0.09	0.95	0.92	0.86	0.56	0.15	12.63
62	16.08	0.04	1.33	0.88	0.67	0.61	-1.98	15.26
63	18.98	-1.70	1.50	1.56	1.20	0.82	-3.10	19.61
64	13.81	0.76	2.43	1.29	1.26	1.52	-1.54	23.45

Table B.23. WFR, C_{eff}, and uncertainties for the SB seal with the medium pre-swirl insert.

Test Point	WFR, Lund [10]	u_{WFR}, Lund [10]	WFR, San Andrés [11]	u_{WFR}, San Andrés [11]	C_{eff} [kN-s/m]	$u_{C_{eff}}$ [kN-s/m]
1	0.19	0.17	0.19	0.17	6.53	1.26
2	0.29	0.36	0.29	0.36	5.96	2.69
3	0.00	0.00	0.00	0.00	11.20	12.64
4	0.05	2.16	0.05	2.17	27.14	41.90
5	0.42	0.06	0.42	0.06	6.96	0.83
6	0.00	0.00	0.00	0.00	9.62	6.82
7	0.29	0.21	0.29	0.21	9.53	1.68
8	0.39	0.41	0.39	0.41	23.24	27.34
9	0.30	0.07	0.30	0.07	10.10	1.25
10	0.00	0.00	0.00	0.00	11.27	2.11
11	0.15	0.55	0.15	0.55	13.12	5.64
12	0.37	0.27	0.37	0.27	27.76	19.64
13	0.31	0.08	0.31	0.08	10.87	1.52
14	0.00	0.00	0.00	0.00	11.91	1.76
15	0.32	0.12	0.32	0.12	11.74	3.24
16	0.30	0.32	0.30	0.32	26.94	16.61
17	0.33	0.18	0.33	0.18	6.36	2.25
18	0.11	0.28	0.11	0.28	8.30	1.67
19	0.50	0.14	0.50	0.14	6.56	2.09
20	0.38	0.43	0.39	0.43	31.32	16.03
21	0.33	0.04	0.34	0.04	8.74	0.75
22	0.27	0.09	0.27	0.09	8.40	1.11
23	0.34	0.03	0.34	0.03	9.48	0.67
24	0.22	0.75	0.22	0.77	44.41	21.59
25	0.24	0.08	0.24	0.08	12.12	1.81
26	0.06	1.36	0.06	1.38	12.14	3.81
27	0.32	0.04	0.32	0.04	11.59	0.89
28	0.39	0.14	0.39	0.14	33.87	7.29
29	0.21	0.03	0.21	0.03	12.86	0.91
30	0.22	0.08	0.22	0.08	11.93	0.95
31	0.29	0.03	0.29	0.03	12.85	0.76
32	0.37	0.06	0.37	0.06	32.86	5.97

Table B.24. WFR, C_{eff}, and uncertainties for the SB seal with the medium pre-swirl insert.

Test Point	WFR, Lund	u_{WFR}, Lund	WFR, San Andrés	u_{WFR}, San Andrés	C_{eff}	$u_{C_{eff}}$
	[10]	[10]	[11]	[11]	[kN-s/m]	[kN-s/m]
33	0.43	0.04	0.43	0.04	4.79	0.53
34	0.26	0.21	0.27	0.21	N/A	N/A
35	0.42	0.27	0.43	0.28	N/A	N/A
36	0.34	0.14	0.34	0.14	N/A	N/A
37	0.33	0.05	0.32	0.05	8.33	1.06
38	0.33	0.06	0.33	0.06	N/A	N/A
39	0.18	0.50	0.19	0.53	N/A	N/A
40	0.32	0.29	0.32	0.29	N/A	N/A
41	0.26	0.06	0.26	0.06	9.82	1.10
42	0.31	0.04	0.31	0.04	N/A	N/A
43	0.35	0.04	0.34	0.04	N/A	N/A
44	0.33	0.15	0.33	0.15	N/A	N/A
45	0.24	0.03	0.24	0.03	10.94	0.72
46	0.24	0.04	0.24	0.04	N/A	N/A
47	0.31	0.04	0.30	0.04	N/A	N/A
48	0.35	0.13	0.36	0.13	N/A	N/A
49	0.45	0.04	0.44	0.04	5.29	0.63
50	0.47	0.10	0.46	0.10	N/A	N/A
51	0.43	0.13	0.43	0.13	N/A	N/A
52	0.26	0.08	0.26	0.08	N/A	N/A
53	0.38	0.04	0.38	0.04	7.31	0.87
54	0.32	0.13	0.33	0.13	N/A	N/A
55	0.35	0.11	0.35	0.12	N/A	N/A
56	0.30	0.06	0.30	0.06	N/A	N/A
57	0.29	0.05	0.29	0.05	10.28	1.30
58	0.31	0.06	0.32	0.06	N/A	N/A
59	0.31	0.07	0.31	0.08	N/A	N/A
60	0.26	0.10	0.27	0.10	N/A	N/A
61	0.27	0.04	0.27	0.04	10.48	0.97
62	0.25	0.04	0.26	0.04	N/A	N/A
63	0.33	0.04	0.33	0.04	N/A	N/A
64	0.36	0.05	0.36	0.05	N/A	N/A

Assembly 3 – Radial Injection Insert

Table B.25. Measured Pressure Drop, Leakage, Static Force, Eccentricity and Attitude Angle of the SB seal with the radial injection insert

Measured ω	$u\omega$	Measured ΔP	$u\Delta P$	$\dot{Q}$	$u\dot{Q}$	F_s	uF_s	Measured ε_0	φ
[rpm]	[rpm]	[bar]	[bar]	[LPM]	[LPM]	[N]	[N]	[-]	[deg]
2002.47	0.38	2.06	0.01	26.22	0.00	-10.86	10.83	0.03	1.98
2002.63	0.24	2.05	0.01	26.18	0.02	86.08	21.20	0.32	-0.44
2002.58	0.58	2.04	0.01	26.53	0.01	140.97	17.12	0.47	0.17
2002.39	0.41	2.14	0.02	30.18	0.03	262.60	23.84	0.78	0.47
2004.91	0.25	4.22	0.02	42.45	0.07	-10.71	45.31	0.04	-1.34
2005.27	0.97	4.23	0.01	42.39	0.02	118.80	16.54	0.26	0.01
2005.15	0.24	4.20	0.01	42.48	0.01	252.98	7.58	0.53	0.10
2004.85	0.18	4.10	0.10	44.87	0.12	327.21	122.30	0.81	0.00
2004.91	0.11	6.11	0.02	53.20	0.02	-11.04	15.47	0.05	-1.03
2004.69	0.33	6.35	0.01	54.52	0.05	124.80	38.33	0.27	0.03
2004.64	0.88	6.32	0.01	54.71	0.05	348.28	21.72	0.53	0.02
2004.45	0.22	6.12	0.02	57.30	0.04	495.80	14.06	0.80	0.15
2004.59	0.34	8.30	0.01	63.05	0.02	-31.89	9.80	0.01	1.48
2004.07	0.14	8.31	0.01	63.98	0.02	98.03	27.39	0.25	0.28
2003.96	0.21	8.23	0.01	64.36	0.02	401.25	26.08	0.52	0.01
2003.66	0.19	8.22	0.01	67.98	0.05	631.47	7.86	0.80	0.20
4007.22	0.36	2.11	0.01	22.05	0.00	11.92	4.02	0.02	-2.42
4007.70	0.43	2.04	0.01	22.09	0.01	43.97	3.88	0.27	-0.06
4008.30	0.33	2.04	0.02	23.38	0.03	124.23	7.00	0.54	0.02
4008.53	0.28	2.06	0.01	26.22	0.01	271.60	20.72	0.81	0.13
4013.67	0.31	4.20	0.02	37.63	0.01	-5.90	4.22	0.02	0.06
4013.18	0.29	4.24	0.01	37.65	0.01	67.20	11.47	0.26	0.45
4013.19	0.27	4.14	0.01	37.78	0.01	218.69	13.19	0.53	0.24
4012.80	0.38	4.17	0.01	41.40	0.02	466.03	22.14	0.82	0.33
4011.51	0.22	6.33	0.01	50.34	0.02	-6.66	2.11	0.01	-1.67
4011.83	0.56	6.21	0.01	50.62	0.01	72.39	19.97	0.26	0.09
4011.68	0.49	6.11	0.02	51.10	0.03	294.99	18.02	0.54	0.05
4011.54	0.46	6.27	0.01	55.53	0.02	547.30	24.87	0.80	0.20
4016.03	0.34	8.29	0.01	58.87	0.03	-37.27	4.01	0.04	-1.77
4014.57	0.28	8.28	0.01	60.85	0.04	83.02	20.03	0.27	-0.14
4013.86	0.32	8.35	0.01	62.62	0.03	393.05	22.38	0.53	0.23
4012.91	0.38	8.27	0.01	65.80	0.00	659.19	10.83	0.79	0.21

Table B.26. Measured Pressure Drop, Leakage, Static Force, Eccentricity and Attitude Angle of the SB seal with the radial injection insert

Measured ω	$u\omega$	Measured ΔP	$u\Delta P$	$\dot{Q}$	$u\dot{Q}$	F_s	uF_s	Measured ε_0	φ
[rpm]	[rpm]	[bar]	[bar]	[LPM]	[LPM]	[N]	[N]	[-]	[deg]
6002.69	0.27	2.07	0.01	16.35	0.02	22.29	7.28	0.01	2.65
6003.99	0.61	2.07	0.01	16.90	0.03	95.29	6.42	0.27	0.20
6004.53	0.25	2.09	0.02	18.70	0.02	253.62	10.16	0.52	0.57
6004.66	0.09	2.05	0.02	22.26	0.01	701.45	11.96	0.79	0.54
6010.19	0.63	4.09	0.01	28.63	0.02	30.09	12.19	0.02	0.04
6009.44	0.34	4.22	0.01	30.49	0.00	135.11	7.66	0.27	0.11
6008.62	0.32	4.15	0.02	32.47	0.01	236.14	35.39	0.52	0.20
6008.43	0.69	4.24	0.01	37.51	0.01	625.45	21.33	0.80	0.39
6006.05	0.39	6.20	0.01	42.87	0.01	0.26	26.71	0.05	-1.09
6007.39	0.33	6.13	0.01	43.27	0.01	185.04	7.70	0.28	0.22
6008.08	0.34	6.29	0.02	47.58	0.03	313.41	7.26	0.53	0.22
6007.61	0.39	6.24	0.02	51.59	0.02	693.90	22.41	0.80	0.34
6009.17	0.49	8.30	0.02	54.03	0.08	-10.81	26.81	0.11	-1.19
6009.49	0.28	8.39	0.05	55.30	0.16	59.37	26.07	0.24	-0.82
6009.48	0.49	8.24	0.01	58.12	0.03	383.59	30.37	0.53	0.30
6009.69	0.52	8.23	0.02	62.46	0.04	877.61	52.70	0.80	0.46
8003.83	0.17	2.05	0.01	13.93	0.02	0.18	9.78	0.04	-0.74
8006.61	0.57	2.07	0.02	14.51	0.01	97.51	7.54	0.27	0.26
8007.33	0.61	2.06	0.02	15.57	0.01	257.40	52.93	0.54	0.41
8008.31	0.70	2.02	0.02	17.26	0.01	1058.78	6.66	0.81	0.50
8008.41	0.18	4.15	0.01	26.31	0.01	48.14	14.59	0.05	-0.67
8009.73	0.34	4.09	0.03	26.89	0.03	180.16	58.53	0.27	0.15
8009.04	0.17	4.17	0.02	30.02	0.01	353.93	20.80	0.54	0.26
8009.39	0.71	4.25	0.04	34.77	0.01	935.13	65.38	0.79	0.46
7994.55	1.17	6.20	0.01	37.49	0.01	32.09	9.08	0.04	-0.88
7996.92	0.29	6.14	0.01	38.78	0.02	140.12	9.44	0.33	-0.32
7996.99	0.20	6.33	0.01	41.85	0.01	267.46	14.29	0.50	-0.06
7997.57	0.42	6.29	0.02	47.02	0.02	691.03	20.43	0.79	0.25
7997.61	0.43	8.29	0.00	48.36	0.02	4.43	17.82	0.02	2.64
7997.88	0.48	8.40	0.03	50.08	0.10	235.49	64.77	0.30	-0.05
7999.17	0.33	8.19	0.03	51.87	0.06	436.85	17.95	0.54	0.09
7999.39	0.27	8.31	0.01	57.83	0.02	984.36	7.28	0.79	0.49

Table B.27. PSR, OSR, Inlet and Outlet Temperature, and Reynolds Number of the SB seal with the radial injection insert

Test Point	PSR	OSR	T_i	uT_i	T_e	uT_e	Re_z	Re_θ	Re
	[-]	[-]	[°C]	[°C]	[°C]	[°C]	[-]	[-]	[-]
1	0.221	0.286	46.40	0.05	45.91	0.05	1.18E+03	8.78E+02	1.48E+03
2	0.197	0.304	46.36	0.05	46.03	0.05	1.18E+03	8.78E+02	1.47E+03
3	0.172	0.328	45.84	0.05	45.41	0.05	1.18E+03	8.70E+02	1.47E+03
4	0.000	0.335	46.16	0.05	45.77	0.05	1.35E+03	8.74E+02	1.62E+03
5	0.059	0.307	45.28	0.05	44.97	0.05	1.87E+03	8.62E+02	2.07E+03
6	0.000	0.310	45.87	0.05	45.64	0.05	1.89E+03	8.71E+02	2.09E+03
7	0.000	0.327	46.49	0.05	46.21	0.05	1.92E+03	8.81E+02	2.12E+03
8	0.000	0.315	44.34	0.05	44.49	0.05	1.96E+03	8.48E+02	2.13E+03
9	0.000	0.315	45.17	0.05	45.01	0.05	2.35E+03	8.60E+02	2.51E+03
10	0.000	0.321	45.11	0.05	45.03	0.05	2.41E+03	8.59E+02	2.56E+03
11	0.000	0.334	45.21	0.05	45.10	0.05	2.42E+03	8.61E+02	2.57E+03
12	0.000	0.354	45.39	0.05	45.24	0.05	2.54E+03	8.64E+02	2.69E+03
13	0.159	0.271	45.45	0.05	45.45	0.05	2.81E+03	8.64E+02	2.94E+03
14	0.064	0.317	45.47	0.05	45.45	0.05	2.85E+03	8.65E+02	2.98E+03
15	0.000	0.345	45.49	0.05	45.47	0.05	2.87E+03	8.65E+02	2.99E+03
16	0.178	0.351	45.42	0.05	45.42	0.05	3.02E+03	8.64E+02	3.14E+03
17	0.314	0.248	46.21	0.05	46.17	0.05	9.94E+02	1.75E+03	2.01E+03
18	0.302	0.254	46.24	0.05	46.22	0.05	9.97E+02	1.75E+03	2.02E+03
19	0.292	0.264	45.89	0.05	46.12	0.05	1.05E+03	1.74E+03	2.03E+03
20	0.264	0.271	45.94	0.05	46.00	0.05	1.18E+03	1.74E+03	2.10E+03
21	0.265	0.256	45.98	0.05	46.24	0.05	1.70E+03	1.75E+03	2.43E+03
22	0.247	0.275	45.69	0.05	45.77	0.05	1.68E+03	1.74E+03	2.42E+03
23	0.228	0.287	45.82	0.05	45.90	0.05	1.69E+03	1.74E+03	2.43E+03
24	0.199	0.269	45.88	0.05	46.04	0.05	1.86E+03	1.74E+03	2.55E+03
25	0.200	0.265	45.57	0.05	45.67	0.05	2.25E+03	1.73E+03	2.84E+03
26	0.181	0.268	45.53	0.05	45.65	0.05	2.26E+03	1.73E+03	2.84E+03
27	0.171	0.290	45.63	0.05	45.75	0.05	2.29E+03	1.74E+03	2.87E+03
28	0.127	0.305	45.69	0.05	45.84	0.05	2.49E+03	1.74E+03	3.03E+03
29	0.226	0.254	46.66	0.05	46.89	0.05	2.69E+03	1.77E+03	3.21E+03
30	0.231	0.267	45.69	0.05	45.89	0.05	2.73E+03	1.74E+03	3.23E+03
31	0.199	0.294	45.73	0.05	45.93	0.05	2.81E+03	1.74E+03	3.30E+03
32	0.152	0.273	45.72	0.05	45.93	0.05	2.95E+03	1.74E+03	3.42E+03

Table B.28. PSR, OSR, Inlet and Outlet Temperature, and Reynolds Number of the SB seal with the radial injection insert

Test Point	PSR	OSR	T_i	uT_i	T_e	uT_e	Re_z	Re_θ	Re
	[-]	[-]	[°C]	[°C]	[°C]	[°C]	[-]	[-]	[-]
33	0.417	0.290	46.08	0.05	47.39	0.05	7.53E+02	2.62E+03	2.72E+03
34	0.383	0.249	46.46	0.05	47.65	0.05	7.82E+02	2.64E+03	2.74E+03
35	0.343	0.249	45.82	0.05	47.04	0.05	8.56E+02	2.61E+03	2.74E+03
36	0.310	0.241	46.47	0.05	47.62	0.05	1.03E+03	2.64E+03	2.82E+03
37	0.324	0.246	44.36	0.05	45.58	0.05	1.28E+03	2.54E+03	2.83E+03
38	0.305	0.259	45.44	0.05	46.28	0.05	1.38E+03	2.59E+03	2.93E+03
39	0.289	0.259	45.97	0.05	46.86	0.05	1.48E+03	2.62E+03	2.99E+03
40	0.261	0.266	46.46	0.05	47.31	0.05	1.73E+03	2.64E+03	3.14E+03
41	0.277	0.232	45.76	0.05	46.55	0.05	1.94E+03	2.60E+03	3.23E+03
42	0.261	0.272	45.89	0.05	46.68	0.05	1.97E+03	2.61E+03	3.25E+03
43	0.238	0.296	46.30	0.05	46.96	0.05	2.18E+03	2.63E+03	3.40E+03
44	0.201	0.310	46.46	0.05	47.17	0.05	2.37E+03	2.64E+03	3.52E+03
45	0.000	0.240	45.73	0.05	46.46	0.05	2.45E+03	2.60E+03	3.55E+03
46	0.000	0.257	46.16	0.05	46.86	0.05	2.52E+03	2.62E+03	3.62E+03
47	0.000	0.282	46.23	0.05	46.87	0.05	2.65E+03	2.63E+03	3.71E+03
48	0.000	0.273	46.36	0.05	47.07	0.05	2.86E+03	2.63E+03	3.86E+03
49	0.435	0.154	45.61	0.05	49.61	0.05	6.69E+02	3.46E+03	3.52E+03
50	0.475	0.319	45.72	0.05	49.29	0.05	6.93E+02	3.47E+03	3.53E+03
51	0.422	0.239	47.04	0.05	50.55	0.05	7.61E+02	3.55E+03	3.62E+03
52	0.372	0.232	46.62	0.05	49.73	0.05	8.30E+02	3.53E+03	3.61E+03
53	0.349	0.272	46.37	0.05	48.77	0.05	1.24E+03	3.51E+03	3.71E+03
54	0.340	0.243	46.34	0.05	48.72	0.05	1.27E+03	3.51E+03	3.71E+03
55	0.320	0.262	45.71	0.05	48.19	0.05	1.40E+03	3.47E+03	3.72E+03
56	0.294	0.248	46.56	0.05	48.69	0.05	1.64E+03	3.52E+03	3.86E+03
57	0.297	0.241	44.99	0.05	46.96	0.05	1.71E+03	3.42E+03	3.80E+03
58	0.279	0.250	45.71	0.05	47.66	0.05	1.80E+03	3.46E+03	3.87E+03
59	0.263	0.266	46.00	0.05	47.96	0.05	1.95E+03	3.48E+03	3.96E+03
60	0.240	0.258	46.09	0.05	47.99	0.05	2.19E+03	3.49E+03	4.08E+03
61	0.197	0.235	46.15	0.05	47.90	0.05	2.25E+03	3.49E+03	4.12E+03
62	0.151	0.274	46.41	0.05	48.14	0.05	2.34E+03	3.51E+03	4.18E+03
63	0.131	0.271	45.92	0.05	47.66	0.05	2.40E+03	3.48E+03	4.19E+03
64	0.015	0.265	46.32	0.05	47.95	0.05	2.69E+03	3.50E+03	4.37E+03

Table B.29. Stiffness coefficients and uncertainties for the SB seal with the radial injection insert.

Test Point	K_{XX} [MN/m]	K_{XY} [MN/m]	K_{YX} [MN/m]	K_{YY} [MN/m]	$u_{K_{XX}}$ [MN/m]	$u_{K_{XY}}$ [MN/m]	$u_{K_{YX}}$ [MN/m]	$u_{K_{YY}}$ [MN/m]
1	1.76	0.04	-0.17	1.68	0.15	0.13	0.08	0.14
2	1.43	0.28	-0.38	0.72	0.09	0.14	0.13	0.16
3	0.75	1.02	-0.27	0.31	0.23	0.21	0.23	0.23
4	-1.26	4.60	-1.74	3.01	1.00	0.88	0.96	1.08
5	2.06	0.63	-0.57	1.91	0.15	0.17	0.08	0.18
6	2.28	0.23	-0.41	2.38	0.15	0.10	0.09	0.23
7	2.30	1.04	-0.57	1.58	0.19	0.12	0.21	0.21
8	1.41	5.85	-0.75	0.76	0.20	0.41	1.04	1.89
9	0.85	0.70	-0.79	0.78	0.22	0.19	0.13	0.16
10	2.49	0.20	-0.69	4.48	0.08	0.08	0.11	0.16
11	3.50	0.89	-0.45	3.05	0.07	0.13	0.18	0.17
12	2.11	6.76	-0.91	3.42	0.25	0.65	1.18	2.87
13	3.37	0.59	-0.53	3.07	0.31	0.19	0.16	0.17
14	3.03	0.31	-0.70	3.58	0.39	0.25	0.29	0.24
15	4.44	0.80	-0.45	4.69	0.19	0.14	0.13	0.34
16	3.36	6.11	-1.04	3.31	0.34	1.05	0.56	2.54
17	-0.78	1.76	-1.80	-0.85	0.07	0.15	0.09	0.07
18	0.30	1.24	-1.50	0.81	0.18	0.17	0.21	0.16
19	0.53	2.69	-1.37	0.57	0.18	0.27	0.46	0.27
20	-1.58	16.19	-2.23	0.38	0.53	1.58	2.53	7.49
21	-1.54	1.33	-1.77	-1.61	0.27	0.33	0.18	0.15
22	1.30	0.33	-2.23	2.01	0.12	0.11	0.14	0.14
23	1.42	2.25	-1.58	1.96	0.07	0.16	0.26	0.17
24	-2.19	14.04	-4.40	5.97	1.08	1.66	1.99	3.04
25	-0.24	1.18	-1.42	-0.32	0.23	0.21	0.35	0.11
26	1.46	1.08	-1.76	3.24	0.19	0.26	0.31	0.19
27	2.81	2.11	-1.46	3.26	0.08	0.12	0.14	0.25
28	0.66	12.48	-2.82	4.35	0.37	0.62	1.24	1.58
29	2.34	1.12	-1.08	2.03	0.28	0.27	0.46	0.15
30	2.47	1.65	-1.04	3.00	0.22	0.13	0.16	0.17
31	4.03	1.77	-1.58	5.25	0.12	0.15	0.12	0.25
32	2.25	11.10	-2.38	4.21	0.35	0.68	0.86	1.65

Table B.30. Stiffness coefficients and uncertainties for the SB seal with the radial injection insert.

Test Point	K_{XX} [MN/m]	K_{XY} [MN/m]	K_{YX} [MN/m]	K_{YY} [MN/m]	$u_{K_{XX}}$ [MN/m]	$u_{K_{XY}}$ [MN/m]	$u_{K_{YX}}$ [MN/m]	$u_{K_{YY}}$ [MN/m]
33	0.54	2.01	-2.37	0.61	0.15	0.31	0.17	0.13
34	0.31	2.79	-2.07	0.20	0.15	0.18	0.36	0.21
35	-1.04	4.42	-3.06	0.83	0.48	0.35	0.42	0.36
36	0.58	6.81	-15.37	17.61	0.89	1.51	2.02	2.54
37	1.78	1.87	-2.62	1.49	0.64	0.60	0.64	0.29
38	1.95	1.97	-2.66	1.60	0.58	0.65	0.55	0.65
39	1.01	4.22	-2.38	0.80	0.66	0.61	1.16	0.66
40	-1.98	14.46	-9.32	12.15	1.08	1.48	3.55	5.70
41	2.99	1.71	-1.63	2.77	0.32	0.30	0.42	0.37
42	2.79	2.28	-1.83	2.39	0.16	0.17	0.23	0.19
43	2.46	3.28	-3.04	3.41	0.34	0.17	0.30	0.26
44	-2.00	18.08	-7.31	9.85	0.76	1.63	1.43	3.07
45	4.00	1.66	-1.48	3.84	0.33	0.57	0.28	0.27
46	4.39	1.20	-1.34	2.78	0.45	0.51	0.30	0.47
47	3.21	2.71	-3.26	5.03	0.22	0.32	0.15	0.18
48	-2.25	16.69	-8.72	12.96	0.77	1.21	1.09	0.72
49	0.27	3.35	-3.45	0.23	0.18	0.37	0.14	0.19
50	0.08	4.21	-3.63	0.02	0.22	0.33	0.11	0.18
51	-1.41	7.49	-4.60	0.86	0.31	0.36	0.81	0.46
52	7.17	4.81	-26.87	32.63	0.48	0.54	1.24	1.36
53	1.60	3.36	-3.21	1.54	0.37	0.41	0.40	0.40
54	1.46	4.12	-3.54	1.07	0.33	0.36	0.24	0.28
55	-0.18	8.04	-4.30	0.99	0.49	0.62	0.61	0.48
56	1.23	12.29	-19.73	23.60	0.60	1.13	1.44	1.93
57	2.62	3.32	-2.83	2.01	0.60	0.87	0.48	0.69
58	2.84	4.00	-3.76	1.53	0.31	0.35	0.34	0.33
59	2.59	6.63	-4.06	1.15	0.44	0.72	0.50	0.47
60	-3.45	26.00	-6.68	6.85	2.25	4.46	3.66	7.53
61	3.96	2.60	-2.55	3.68	0.34	0.32	0.34	0.34
62	3.99	3.59	-2.81	3.37	0.15	0.34	0.30	0.18
63	3.50	7.42	-3.81	2.24	0.41	0.47	0.29	0.44
64	-2.87	19.27	-12.75	15.34	0.64	1.18	0.78	1.08

Table B.31. Damping coefficients and uncertainties for the SB seal with the radial injection insert.

Test Point	C_{XX} [kN-s/m]	$u_{C_{XX}}$ [kN-s/m]	C_{YY} [kN-s/m]	$u_{C_{YY}}$ [kN-s/m]	C_{XY} [kN-s/m]	$u_{C_{XY}}$ [kN-s/m]	C_{YX} [kN-s/m]	$u_{C_{YX}}$ [kN-s/m]
1	7.68	0.38	7.42	0.22	1.40	0.26	-1.44	0.20
2	8.04	0.49	8.20	0.60	1.82	0.18	-1.22	0.18
3	9.37	0.66	11.55	0.67	1.62	0.34	-3.03	0.32
4	27.03	1.74	55.92	2.64	-20.94	1.95	-22.81	2.10
5	12.35	0.21	11.48	0.45	1.56	0.47	-1.74	0.23
6	11.72	0.35	10.93	0.32	1.82	0.24	-1.35	0.23
7	12.24	0.48	14.75	0.40	1.92	0.23	-1.49	0.58
8	18.99	0.29	66.71	3.51	-1.95	1.38	-7.08	1.33
9	14.62	0.25	13.91	0.26	1.68	0.41	-1.51	0.32
10	14.40	0.17	12.95	0.32	1.98	0.16	-1.22	0.31
11	14.62	0.12	16.89	0.41	2.34	0.25	-1.33	0.13
12	22.82	0.41	78.09	2.51	-6.79	1.16	-11.09	1.45
13	15.51	0.54	14.71	0.37	1.67	0.77	-1.47	0.46
14	16.34	0.70	15.75	0.38	1.54	0.29	-1.39	0.59
15	16.39	0.20	17.82	0.55	2.35	0.45	-1.48	0.31
16	23.86	0.67	66.20	4.83	-5.80	1.43	-10.38	1.15
17	9.20	0.55	8.97	0.49	2.19	0.31	-2.78	0.30
18	9.28	0.29	9.13	0.27	2.59	0.56	-3.88	0.91
19	10.56	0.47	15.55	0.51	3.10	0.74	-4.50	0.91
20	21.10	0.85	90.70	7.11	-9.56	2.56	-17.25	3.21
21	13.06	0.38	12.32	0.32	3.61	0.34	-3.76	0.37
22	11.72	0.39	11.16	0.47	3.45	0.32	-2.90	0.25
23	12.13	0.34	15.24	0.68	3.42	0.19	-3.61	0.22
24	27.21	1.23	81.66	5.62	-17.16	3.09	-24.98	3.27
25	14.68	0.22	13.86	0.47	3.11	0.49	-2.86	0.50
26	14.48	0.22	13.75	0.43	3.33	0.23	-3.17	0.31
27	14.56	0.27	17.25	0.45	4.55	0.37	-2.79	0.21
28	22.85	0.87	70.63	4.39	-3.68	2.46	-14.97	1.57
29	16.22	0.95	15.30	0.42	2.21	1.24	-3.05	0.61
30	16.23	0.40	15.86	0.54	3.02	0.63	-3.30	0.43
31	16.40	0.39	18.75	0.57	4.13	0.34	-3.17	0.22
32	22.91	0.72	60.60	4.32	-1.28	1.74	-11.77	1.37

Table B.32. Damping coefficients and uncertainties for the SB seal with the radial injection insert.

Test Point	C_{XX} [kN-s/m]	$u_{C_{XX}}$ [kN-s/m]	C_{YY} [kN-s/m]	$u_{C_{YY}}$ [kN-s/m]	C_{XY} [kN-s/m]	$u_{C_{XY}}$ [kN-s/m]	C_{YX} [kN-s/m]	$u_{C_{YX}}$ [kN-s/m]
33	8.70	0.39	8.24	0.35	4.45	0.42	-5.24	0.68
34	9.75	0.31	10.26	0.32	3.95	0.68	-6.02	0.94
35	13.78	0.81	14.85	0.54	2.20	0.72	-9.05	1.32
36	30.06	1.71	62.77	4.61	-18.52	2.81	-28.84	3.80
37	11.95	0.30	11.43	0.39	4.27	0.40	-4.79	0.79
38	13.03	2.14	13.09	2.70	3.47	3.41	-5.86	2.69
39	14.29	1.65	17.54	1.95	3.92	1.53	-7.55	2.15
40	29.24	2.64	74.89	7.01	-16.41	4.74	-27.41	4.21
41	13.49	0.45	12.62	0.58	4.60	0.51	-5.74	1.06
42	12.70	0.49	12.79	0.46	5.00	0.37	-4.60	0.40
43	14.10	0.54	17.02	0.65	5.64	0.39	-5.95	0.23
44	27.38	1.34	73.82	4.30	-9.65	2.12	-25.33	2.59
45	15.65	0.60	14.49	0.40	3.68	1.34	-5.40	0.55
46	15.87	0.67	15.00	0.98	4.21	1.00	-5.55	0.70
47	16.03	0.57	19.20	0.51	5.24	0.41	-5.85	0.23
48	32.56	2.08	67.42	3.41	-12.78	3.44	-27.87	2.28
49	9.21	0.65	8.79	0.49	6.20	0.60	-6.92	0.75
50	10.21	0.60	10.18	0.68	6.28	0.53	-7.64	0.77
51	14.26	0.49	19.57	0.82	4.07	0.94	-10.70	1.35
52	23.22	1.06	68.51	2.61	-12.25	2.11	-26.20	1.99
53	12.00	0.64	11.17	0.91	5.00	1.17	-6.91	1.55
54	12.39	0.71	12.50	0.51	5.72	0.57	-6.84	1.05
55	16.46	0.82	22.02	0.87	4.29	0.76	-10.20	1.62
56	29.53	2.86	69.88	4.45	-13.07	4.22	-27.58	3.42
57	14.97	0.94	13.51	1.29	5.33	0.92	-6.77	0.77
58	15.95	0.96	15.82	0.80	6.99	0.88	-6.47	0.85
59	16.74	1.34	21.37	1.16	7.87	1.47	-7.58	1.21
60	28.01	3.83	74.22	14.09	-6.35	8.34	-22.24	7.07
61	15.04	0.49	14.10	0.61	6.77	0.62	-7.23	0.79
62	14.78	0.55	15.37	0.35	7.05	0.63	-6.44	0.49
63	16.56	0.73	22.37	0.62	7.79	1.34	-7.67	0.52
64	31.67	1.37	61.15	2.67	-8.42	1.86	-27.91	2.05

Table B.33. Virtual Mass coefficients and uncertainties for the SB seal with the radial injection insert.

Test Point	M_{XX} [kg]	$u_{M_{XX}}$ [kg]	M_{YY} [kg]	$u_{M_{YY}}$ [kg]	M_{XY} [kg]	$u_{M_{XY}}$ [kg]	M_{YX} [kg]	$u_{M_{YX}}$ [kg]
1	14.60	0.20	13.61	0.18	-0.46	0.18	0.16	0.10
2	14.51	0.12	13.50	0.21	-0.17	0.18	0.40	0.17
3	15.25	0.30	14.64	0.30	-0.05	0.28	-0.41	0.31
4	19.79	1.33	24.46	1.44	-5.19	1.17	-3.15	1.27
5	15.34	0.19	14.16	0.24	-0.31	0.23	0.35	0.10
6	15.39	0.20	14.63	0.30	-0.44	0.13	0.23	0.12
7	16.55	0.25	16.34	0.28	-0.59	0.16	-0.06	0.28
8	19.10	0.27	27.81	2.51	-2.22	0.54	-0.06	1.38
9	16.41	0.29	15.61	0.21	-0.44	0.25	0.01	0.18
10	16.63	0.11	15.92	0.22	-0.39	0.10	0.33	0.15
11	17.46	0.09	17.40	0.23	-0.45	0.18	0.49	0.24
12	20.39	0.33	32.81	3.81	-2.51	0.86	-0.80	1.56
13	18.11	0.41	16.70	0.23	-0.14	0.25	0.38	0.21
14	17.69	0.52	16.20	0.32	-0.30	0.34	1.30	0.39
15	18.09	0.25	18.10	0.45	-0.27	0.19	0.65	0.17
16	21.14	0.45	29.94	3.37	-2.88	1.39	-1.59	0.75
17	12.31	0.09	11.48	0.09	-0.06	0.20	-0.91	0.12
18	13.46	0.24	13.18	0.21	-0.43	0.23	-0.62	0.28
19	14.47	0.24	15.59	0.36	-0.39	0.35	-0.23	0.61
20	14.80	0.71	18.22	9.94	5.43	2.09	3.24	3.35
21	15.20	0.36	13.85	0.20	-1.69	0.44	-0.34	0.24
22	15.66	0.16	14.43	0.18	-0.92	0.14	-0.83	0.19
23	16.10	0.09	16.21	0.23	-0.73	0.21	-0.84	0.35
24	20.81	1.44	26.72	4.04	-4.73	2.20	-2.81	2.64
25	16.57	0.31	15.16	0.15	-0.61	0.29	-0.67	0.46
26	16.99	0.25	15.45	0.26	-0.88	0.34	-0.49	0.41
27	17.11	0.10	17.12	0.33	-0.52	0.16	-0.10	0.18
28	20.27	0.49	28.49	2.09	-3.14	0.82	-1.34	1.65
29	17.76	0.37	16.13	0.20	-0.44	0.36	-0.42	0.61
30	17.99	0.29	15.92	0.23	-0.75	0.17	0.21	0.21
31	18.07	0.16	17.73	0.33	-0.24	0.20	0.08	0.16
32	20.30	0.47	27.40	2.18	-2.04	0.90	-0.92	1.14

Table B.34. Virtual Mass coefficients and uncertainties for the SB seal with the radial injection insert.

Test Point	M_{XX}	$u_{M_{XX}}$	M_{YY}	$u_{M_{YY}}$	M_{XY}	$u_{M_{XY}}$	M_{YX}	$u_{M_{YX}}$
	[kg]	[kg]	[kg]	[kg]	[kg]	[kg]	[kg]	[kg]
33	11.86	0.20	11.61	0.17	-0.18	0.42	-1.31	0.22
34	11.74	0.20	11.04	0.28	0.07	0.24	0.06	0.47
35	12.81	0.64	13.45	0.48	-0.90	0.46	-1.48	0.55
36	12.36	1.18	20.57	3.37	-6.23	2.00	-2.00	2.68
37	14.44	0.86	13.47	0.39	-1.45	0.80	-1.74	0.85
38	16.02	0.77	15.35	0.86	-2.83	0.86	-1.91	0.73
39	16.07	0.87	17.16	0.87	-2.10	0.81	-0.37	1.54
40	17.69	1.43	20.69	7.56	-4.52	1.97	1.02	4.72
41	15.73	0.42	14.92	0.50	-0.12	0.40	-0.16	0.56
42	15.98	0.21	14.44	0.26	-0.10	0.23	-0.35	0.31
43	17.77	0.45	17.91	0.34	-1.44	0.23	-1.51	0.40
44	22.50	1.01	27.37	4.08	-5.98	2.16	-4.04	1.89
45	15.89	0.43	15.10	0.36	0.37	0.75	0.43	0.37
46	17.21	0.60	14.85	0.63	-0.81	0.67	0.64	0.39
47	17.38	0.30	17.28	0.24	-0.79	0.43	-0.34	0.20
48	22.64	1.02	27.92	0.96	-5.70	1.61	-3.81	1.45
49	12.32	0.24	11.87	0.25	-0.04	0.49	-1.12	0.18
50	12.71	0.29	12.19	0.24	0.04	0.44	-0.99	0.15
51	12.64	0.41	13.61	0.61	-0.84	0.48	-0.64	1.07
52	11.11	0.64	22.37	1.81	-5.04	0.72	-2.98	1.64
53	12.08	0.49	11.82	0.52	0.28	0.54	-0.81	0.53
54	12.25	0.44	12.09	0.37	0.39	0.48	-0.68	0.32
55	13.26	0.65	14.78	0.64	-0.47	0.83	-1.15	0.81
56	14.34	0.79	24.92	2.57	-5.57	1.50	-3.66	1.91
57	14.84	0.79	13.26	0.92	0.08	1.15	1.13	0.64
58	16.12	0.42	15.54	0.44	-1.34	0.47	0.14	0.46
59	17.25	0.58	18.31	0.63	-1.80	0.95	-0.27	0.67
60	15.25	2.98	13.75	10.00	2.87	5.92	6.20	4.86
61	16.40	0.45	15.08	0.45	-0.40	0.43	0.37	0.45
62	16.57	0.20	15.53	0.24	0.13	0.45	-0.20	0.40
63	18.54	0.55	18.33	0.59	-0.42	0.62	-0.79	0.39
64	22.65	0.84	26.39	1.44	-5.44	1.57	-4.62	1.03

Table B.35. WFR, C_{eff}, and uncertainties for the SB seal with the radial injection insert.

Test Point	WFR, Lund [10]	u_{WFR}, Lund [10]	WFR, San Andrés [11]	u_{WFR}, San Andrés [11]	C_{eff} [kN-s/m]	$u_{C_{eff}}$ [kN-s/m]
1	0.04	0.11	0.04	0.11	7.05	0.43
2	0.00	0.00	0.00	0.00	N/A	N/A
3	0.23	0.12	0.23	0.12	N/A	N/A
4	0.28	0.23	0.28	0.22	N/A	N/A
5	0.24	0.04	0.24	0.04	9.06	0.51
6	0.13	0.03	0.13	0.03	N/A	N/A
7	0.24	0.07	0.24	0.07	N/A	N/A
8	0.29	0.19	0.29	0.19	N/A	N/A
9	0.25	0.04	0.25	0.04	10.73	0.58
10	0.00	0.00	0.00	0.00	N/A	N/A
11	0.18	0.04	0.18	0.04	N/A	N/A
12	0.28	0.20	0.28	0.20	N/A	N/A
13	0.17	0.04	0.17	0.04	12.46	0.68
14	0.11	0.09	0.11	0.09	N/A	N/A
15	0.16	0.03	0.16	0.03	N/A	N/A
16	0.32	0.09	0.32	0.09	N/A	N/A
17	0.47	0.03	0.46	0.03	4.84	0.42
18	0.35	0.04	0.35	0.04	N/A	N/A
19	0.36	0.06	0.36	0.06	N/A	N/A
20	0.35	0.20	0.35	0.20	N/A	N/A
21	0.29	0.04	0.29	0.04	9.00	0.51
22	0.18	0.03	0.18	0.03	N/A	N/A
23	0.33	0.03	0.33	0.03	N/A	N/A
24	0.38	0.13	0.38	0.14	N/A	N/A
25	0.22	0.03	0.22	0.03	11.17	0.55
26	0.18	0.05	0.18	0.05	N/A	N/A
27	0.26	0.02	0.26	0.02	N/A	N/A
28	0.34	0.09	0.34	0.09	N/A	N/A
29	0.16	0.04	0.16	0.04	13.14	0.82
30	0.19	0.02	0.19	0.02	N/A	N/A
31	0.21	0.02	0.21	0.02	N/A	N/A
32	0.33	0.06	0.33	0.06	N/A	N/A

Table B.36. WFR, C_{eff}, and uncertainties for the SB seal with the radial injection insert.

Test Point	WFR, Lund [10]	u_{WFR}, Lund [10]	WFR, San Andrés [11]	u_{WFR}, San Andrés [11]	C_{eff} [kN-s/m]	$u_{C_{eff}}$ [kN-s/m]
33	0.41	0.04	0.40	0.04	4.99	0.38
34	0.39	0.04	0.39	0.04	N/A	N/A
35	0.41	0.04	0.41	0.04	N/A	N/A
36	0.30	0.10	0.31	0.11	N/A	N/A
37	0.30	0.06	0.30	0.06	8.12	0.74
38	0.28	0.07	0.28	0.07	N/A	N/A
39	0.33	0.08	0.33	0.08	N/A	N/A
40	0.35	0.14	0.36	0.15	N/A	N/A
41	0.20	0.03	0.20	0.03	10.40	0.55
42	0.25	0.02	0.25	0.02	N/A	N/A
43	0.32	0.02	0.32	0.02	N/A	N/A
44	0.37	0.07	0.37	0.07	N/A	N/A
45	0.17	0.03	0.17	0.03	12.58	0.62
46	0.10	0.05	0.10	0.05	N/A	N/A
47	0.26	0.02	0.26	0.02	N/A	N/A
48	0.35	0.05	0.35	0.05	N/A	N/A
49	0.45	0.03	0.44	0.03	4.94	0.47
50	0.46	0.03	0.45	0.03	N/A	N/A
51	0.42	0.04	0.42	0.04	N/A	N/A
52	0.21	0.06	0.22	0.07	N/A	N/A
53	0.34	0.03	0.33	0.03	7.67	0.65
54	0.37	0.02	0.36	0.02	N/A	N/A
55	0.38	0.03	0.37	0.03	N/A	N/A
56	0.33	0.05	0.34	0.05	N/A	N/A
57	0.26	0.04	0.26	0.04	10.56	0.99
58	0.29	0.02	0.29	0.02	N/A	N/A
59	0.33	0.03	0.33	0.03	N/A	N/A
60	0.34	0.13	0.35	0.14	N/A	N/A
61	0.21	0.02	0.21	0.02	11.50	0.48
62	0.25	0.02	0.25	0.02	N/A	N/A
63	0.33	0.02	0.33	0.02	N/A	N/A
64	0.37	0.03	0.37	0.03	N/A	N/A

APPENDIX C

TEST STAND DESCRIPTION

C1. Process Fluid Supply System

There are two tanks that move the process fluid to the test stand by a motor-pump system, the sump and main tanks. The sump tank was supplied by process fluid that exited from the collection chambers and flowed via gravity to the tank. The sump tank has a nominal capacity of 227 L and a maximum capacity of 303 L. The sump tank moved fluid out of the main holding area by means of a Viking external spur gear pump driven by a 11.2 kW, 1750 rpm motor. A continuous output pressure of 34 bar can be achieved with this configuration. A maximum output of 265 LPM can be reached. A Masoneilan Camflex II valve regulated by a Magtech flow level system controlled the capacities between the sump tank and the main tank. After moving through the control valve, the process fluid moved into the main tank. The main tank has a nominal capacity of 473 L and a maximum capacity of 681 L. While the process fluid was in the main tank, the fluid was either heated or cooled by the heat exchanger or the circulation heater. The circulation heater is a 15.8 kW, 23 WSI heater that was driven by a 373 W motor and a 30 LPM pump. The process fluid was then moved from the main tank into the test section by the same model Viking pump and motor configuration as the sump pump. The target inlet temperature is 46.1 °C measured at the inlet of the stator with thermocouples.

C2. Excitation Element

Excitation force was created by a Zonic Hydraulic Shaker Unit, seen in Fig. C1. There were two main elements to the shaker; the pumps themselves and the shaker heads. The hydraulic pumps gave a 207 bar supply pressure to the shaker heads. The pumps were two different models. The Y Zonic unit operated up to 4450 N in tension and 1125 N in compression. The X Zonic unit operated at 4450 N in tension and compression. The shaker heads are orthogonally mounted on to the stator housing, displayed in Fig. C1. The shaker head assembly consists of a shaker head unit, a load cell, and a stinger , which is attached to the stator housing itself. An excitation frequency of up to 10 kHz could be reached. The load cell was used as a measurement device to determine the amount of load that the Zonic unit imparts upon the stator housing at any given ε_0. The stinger was meant to isolate the stator from the dynamics of the shaker head. Each individual Zonic unit, pump and shaker head assembly are controlled by a dual-loop master controller fabricated by Xcite.
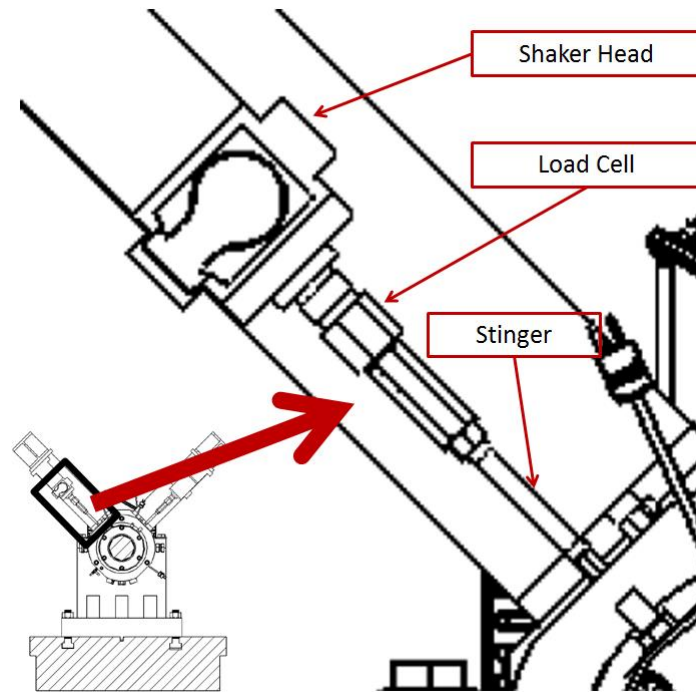
Figure C1. Zonic Head Unit Assembly

C3. Instrumentation and Measurement Devices

Visible in Fig. C2, the test assembly had an array of instrumentation to aid in the acquisition of data. Proximity probes, accelerometers, load cells and a tachometer were mounted to the stator housing. Lion Precision eddy current proximity probes work in two planes and were mounted in pairs on the X and Y planes of the stator housing. The probes have a 1mm range, 1 kHz bandwidth and .06 μm resolution. These proximity probes operated in a linear range of 0.2 percent with an error band of 0.4 percent. The accelerometers located on the X and Y planes were constructed by PCB and utilized a piezoelectric material that measured the acceleration of the stator housing. The tachometer was a PHILTEC fiber-optic displacement sensor.
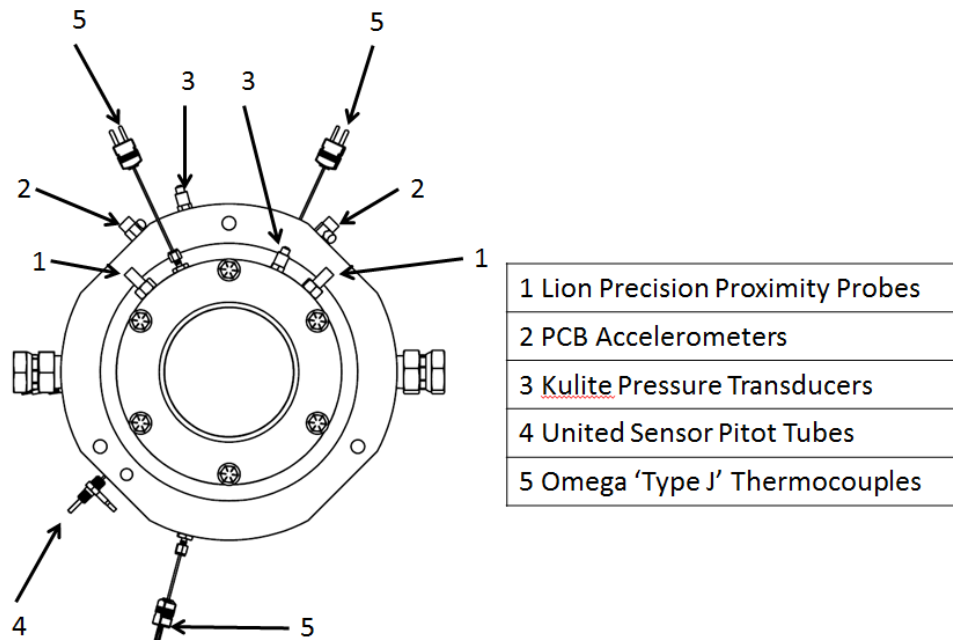
Figure C2. Instrumentation on stator housing

1	Lion Precision Proximity Probes
2	PCB Accelerometers
3	Kulite Pressure Transducers
4	United Sensor Pitot Tubes
5	Omega 'Type J' Thermocouples

The pressure and velocity of the process fluid were measured by a set of three Kulite pressure probes and a pair of United Sensor pitot tubes. The miniature pressure transducers have a max measurement of 17 bar. One transducer was placed upstream of the pre-swirl insert and the other two were placed downstream of the seal exits. The pitot tubes were custom built for the test stand and measure static and dynamic pressure. One was placed at the inlet chamber of the stator before the fluid enters the seals while the other was placed directly downstream the outlet of the coupling side seal. The pitot tubes were mounted tangentially to the rotor with gauge blocks. Data from the pitot tubes was processed through a Rosemount differential pressure transducer. The transducer could run up to a maximum pressure of 21 bar. Omega 'Type J' thermocouples were used on the stator assembly to acquire inlet and outlet temperatures for data processing. Omega

'Type K' thermocouples were used on the main tank, sump tank, piping and ball to regulate proper static conditions for testing. 'Type K' thermocouple data was not recorded. To acquire and process the data, a National Instruments PCI 6229 and PCI 4472 cards were utilized. A LabVIEW virtual interface was used to facilitate data acquisition.

APPENDIX D

UNCERTAINTY ANALYSIS

The uncertainty analysis is only for the measure of repeatability following Moreland [25]. A 95% confidence interval was utilized. Meaning a true mean (β) for a sample set of measurements (x_i) lies within the confidence interval. The confidence interval contains the mean of the sample ($\bar{x}$), the t-distribution value ($t_{\alpha/2,v}$), level of significance ($\alpha = 0.05$), degrees of freedom ($f = 1 - n$) and standard deviation (σ_x). The resulting interval is represented by

$$\bar{x} - t_{\alpha/2,f} \frac{\sigma_x}{\sqrt{n}} < \beta < \bar{x} + t_{\alpha/2,f} \frac{\sigma_x}{\sqrt{n}} \tag{C.1}$$

where the number of samples is represented by n and the σ_x is described as

$$\sigma_x = \sqrt{\frac{(\sum_{i=1}^{n} x_i^2) - n\bar{x}^2}{n - 1}} \tag{C.2}$$

From the curve fitting presented in Section 4, the true slope of a least squares regression lies within the confidence interval presented by

$$b \pm t_{\alpha/2,f} \frac{s_{y/x}}{\sigma_{xx}} \tag{C.3}$$

where the standard error ($s_{y/x}$) of the y-data from the curve fit is

$$s_{y/x} = \left(\frac{1}{n-2} \sum_{i=1}^{n} [y_i - y(x_i)]^2 \right)^{1/2} \tag{C.4}$$

to which the total variation squared (σ_{xx}^2) in Eq. (C.3) of the independent variable (x_i) is

$$\sigma_{xx}^2 = \sum_{i=1}^{n} (x_i - \bar{x})^2 \tag{C.5}$$

From the curve fitting presented in Section 4, the true intercept falls within the interval of

$$a \pm t_{\alpha/2,f} s_{y/x} \sqrt{\frac{1}{n} + \frac{\bar{x}^2}{\sigma_{xx}^2}} \tag{C.6}$$

When calculating the WFR and C_{eff} repeatability, the confidence intervals of the rotordynamic coefficients are propagated into the confidence intervals of WFR and C_{eff}. The propagation that results is

$$u_y = \sqrt{\left(\frac{\partial y}{\partial x_1} u_1\right)^2 + \left(\frac{\partial y}{\partial x_2} u_2\right)^2 + \cdots + \left(\frac{\partial y}{\partial x_n} u_n\right)^2} \tag{C.7}$$